

9950-1206

JPL

7N-63-CP

266005

1988

FINAL REPORT
UNIFIED CONTROL/STRUCTURE DESIGN AND MODELING RESEARCH
Report No. 957114-6
Oct. 31, 1986

Volume III

Appendix III

Integrated Control/Structure Design and Robustness

NAS 7-918

A. Adamian

Mechanical, Aerospace and Nuclear Engineering Department
University of California
Los Angeles, CA 90024

(NASA-CR-166553) UNIFIED CONTROL/STRUCTURE
DESIGN AND MODELING RESEARCH. VOLUME 3,
APPENDIX 3: INTEGRATED CONTROL/STRUCTURE
DESIGN AND ROBUSTNESS Final Report
(California Univ.) 198 p

N90-70891

Unclass

00/63 0266005

FINAL REPORT
UNIFIED CONTROL/STRUCTURE DESIGN AND MODELING RESEARCH
Report No. 957114-6
Oct. 31, 1986

Volume III

Appendix III

Integrated Control/Structure Design and Robustness

A. Adamian

Mechanical, Aerospace and Nuclear Engineering Department
University of California
Los Angeles, CA 90024

Appendix III
(Volume III of Report)

Integrated Control/Structure Design and Robustness

A. Adamian

CONTENTS

LIST OF FIGURES	vi
LIST OF TABLES	ix
LIST OF NOTATION	xii
ACKNOWLEDGEMENTS	xxi
VITA	xxii
ABSTRACT	xxiii
 I. Introduction	 1
II. Finite Element Model	5
2.1 Hermite Splines	10
2.2 B-Splines	14
2.3 Normal Modes	20
III. Control Design	23
3.1 Time-Invariant Optimal Linear-Quadratic Regulator Problem	23
3.2 Time-Invariant Optimal Observer Problem	26
3.3 Time-Invariant Stochastic Optimal Linear-Quadratic Regulator Problem	28
3.4 Eigenvalues and Eigenvectors of the Closed-Loop System	32
3.5 Determining Right and Left Eigenvectors of the Closed-Loop System with Real Arithmetic	36
IV. Functional Gains	39
4.1 Functional Control Gains	39
4.2 Numerical Results	41
V. Sensitivity of Closed-Loop Eigenvalues and Robustness	50
5.1 First-Order Sensitivity of the Closed-Loop Eigenvalues	50
5.2 Sensitive and Insensitive Control Designs	54
5.3 Example	62

VI.	Sensitivity Optimization for Fixed Structure	71
6.1	First-Order Sensitivity Optimization	72
6.2	Second-Order Sensitivity Optimization	74
6.3	Example	76
VII.	Sensitivity and Structural Weight Optimization	106
7.1	First-Order and Structural Weight Optimization	106
7.2	Example	109
7.2.1	Four-Mode Compensator Example	110
7.2.1	Five-Mode Compensator Example	135
VIII.	Conclusions	159
	References	162
	Appendix A: Derivatives of Eigenvalues and Eigenvectors with Respect to a Parameter	166
	Appendix B: Comparison of analytic and finite difference gradients	170

LIST OF FIGURES

Figure		Page
2-1	(a) Flexible Structure. (b) Beam Cross Section.	7
2-2	(a) Approximation of the Beam by Finite Elements. (b) i -th Beam Element.	9
2-3	(a) Hermite Splines for Three Beam Element Model. (b) Generalized Degrees of Freedom.	13
2-4	(a) B-Splines for Three Beam Element Model. (b) Generalized Degrees of Freedom.	17
2-5	(a) B-splines for Four Beam Element Model. (b) Generalized Degrees of Freedom.	18
2-6	(a) Maximum Support B-Spline. (b) Minimum Support B-Spline.	19
2-7	First Three Natural Modes of the Ten Beam Element Model.	22
3-1	Block Diagram of the Optimal Linear-Quadratic Regulator System.	25
3-2	Block Diagram of the Stochastic Optimal Linear-Quadratic Regulator System.	31
4-1	Functional Control Gains Based on the Hermite Splines.	44
4-2	Functional Control Gains Based on the B-Splines.	46
4-3	Functional Control Gains Based on the Normal Modes.	48
5-1	Closed-Loop System.	51
5-2	Robustness Test Results.	67
6-1	Iteration History of the unconstrained minimization (BFGS).	81
6-2	Open-Loop and Closed-Loop Eigenvalues of the Initial and the Optimized Designs of the 5-Mode Compensators.	85
6-3	Time Histories of the Rigid-Body Angle and the Hub Torque. 11-mode plant, 5-mode compensator, I.C. of the structure = 1st mode, I.C. of the estimator = 1st mode.	100

Figure		Page
6-4	Time Histories of the Rigid-Body Angle and the Hub Torque. 11-mode plant, 5-mode compensator, I.C. of the structure = 1st mode, I.C. of the estimator = 0.	101
6-5	Time Histories of the Rigid-Body Angle and the Hub Torque. 11-mode plant, 5-mode compensator, I.C. of the structure = 2nd mode, I.C. of the estimator = 0.	102
6-6	Time Histories of the Rigid-Body Angle and the Hub Torque. 11-mode plant, 5-mode compensator, I.C. of the structure = 3rd mode, I.C. of the estimator = 0.	103
6-7	Time Histories of the Rigid-Body Angle and the Hub Torque. 11-mode plant, 5-mode compensator, I.C. of the structure = 4th mode, I.C. of the estimator = 0.	104
6-8	Time Histories of the Rigid-Body Angle and the Hub Torque. 11-mode plant, 5-mode compensator, I.C. of the structure = 5th mode, I.C. of the estimator = 0.	105
7-1	The Initial and Three Optimized substructures (Beams). (A) $\alpha = 2$, (B) $\alpha = 3$, (C) $\alpha = 5$.	113
7-2	Unconstrained Minimization (BFGS) Iteration History of the Objective Function. (4-mode compensator.)	116
7-3	Unconstrained Minimization (BFGS) Iteration Histories of the Control and the Structural Objective Functions. (4-mode compensator.)	117
7-4	First Three Flexible Mode-Shapes of the Initial and The Optimized structures. (A) 1st Mode, (B) 2nd Mode, (C) 3rd Mode. (4-mode compensator.)	120
7-5	Open-Loop and Closed-Loop Eigenvalues of the Initial and the Optimized Designs of 4-Mode Compensators.	122
7-6	Time Histories of the Rigid-Body Angle and the Hub Torque. 11-mode plant, 4-mode compensator, I.C. of the structure = 1st mode, I.C. of the estimator = 1st mode.	130
7-7	Time Histories of the Rigid-Body Angle and the Hub Torque. 11-mode plant, 4-mode compensator, I.C. of the structure = 1st mode, I.C. of the estimator = 0.	131
7-8	Time Histories of the Rigid-Body Angle and the Hub Torque. 11-mode plant, 4-mode compensator, I.C. of the structure = 2nd mode, I.C. of the estimator = 0.	132

Figure		Page
7-9	Time Histories of the Rigid-Body Angle and the Hub Torque. 11-mode plant, 4-mode compensator, I.C. of the structure = 3rd mode, I.C. of the estimator = 0.	133
7-10	Time Histories of the Rigid-Body Angle and the Hub Torque. 11-mode plant, 4-mode compensator, I.C. of the structure = 4th mode, I.C. of the estimator = 0.	134
7-11	The Initial and Three Optimized substructures (Beams). (A) $\alpha = 2$, (B) $\alpha = 4$, (C) $\alpha = 6$. (5-mode compensator.)	137
7-12	Unconstrained Minimization (BFGS) Iteration History of the Objective Function. (5-mode compensator.)	140
7-13	Unconstrained Minimization (BFGS) Iteration Histories of the Control and the Structural Objective Functions. (5-mode compensator.)	141
7-14	First Three Flexible Mode-Shapes of the Initial and The Optimized structures. (A) 1st Mode, (B) 2nd Mode, (C) 3rd Mode. (5-mode compensator.)	144
7-15	Open-Loop and Closed-Loop Eigenvalues of the Initial and the Optimized Designs of 5-Mode Compensators.	146
7-16	Time Histories of the Rigid-Body Angle and the Hub Torque. 11-mode plant, 5-mode compensator, I.C. of the structure = 1st mode, I.C. of the estimator = 1st mode.	153
7-17	Time Histories of the Rigid-Body Angle and the Hub Torque. 11-mode plant, 5-mode compensator, I.C. of the structure = 1st mode, I.C. of the estimator = 0.	154
7-18	Time Histories of the Rigid-Body Angle and the Hub Torque. 11-mode plant, 5-mode compensator, I.C. of the structure = 2nd mode, I.C. of the estimator = 0.	155
7-19	Time Histories of the Rigid-Body Angle and the Hub Torque. 11-mode plant, 5-mode compensator, I.C. of the structure = 3rd mode, I.C. of the estimator = 0.	156
7-20	Time Histories of the Rigid-Body Angle and the Hub Torque. 11-mode plant, 5-mode compensator, I.C. of the structure = 4th mode, I.C. of the estimator = 0.	157
7-21	Time Histories of the Rigid-Body Angle and the Hub Torque. 11-mode plant, 5-mode compensator, I.C. of the structure = 5th mode, I.C. of the estimator = 0.	158

LIST OF TABLES

Table	Page
2-1 Structural Data.	21
4-1 Structural Data.	42
5-1 Structural Data.	64
5-2 Closed-Loop Eigenvalues with Robust Compensator.	69
6-1 Structural Data.	77
6-2 Design Variables of the Initial and the Optimized Compensators.	82
6-3 Open-Loop and Closed-Loop Eigenvalues of the Initial and the Optimized Designs of the 5-Mode Compensators.	84
6-4 Robustness Test Results of the Full-State Feedback Initial Design.	86
6-5 Robustness Test Results of the Full-State Feedback Optimized Design.	88
6-6 Robustness Test Results of the Initial 5-Mode Compensator.	90
6-7 Robustness Test Results of the Optimized 5-Mode Compensator.	92
6-8 Number of Variations which Result in Unstable Designs.	94
6-9 Performance of the 5-Mode Initial Compensator Connected to the 5-Mode Plant for Various Initial Conditions.	98
6-10 Performance of the 5-Mode Initial Compensator Connected to the 11-Mode Plant for Various Initial Conditions.	98
6-11 Performance of the 5 Mode Optimized Compensator Connected to the 5-Mode Plant for Various Initial Conditions.	99
6-12 Performance of the 5-Mode Optimized Compensator Connected to the 11-Mode Plant for Various Initial Conditions.	99

Table		Page
7-1	Control Objective and Structural Weigth of the Initial and Three Optimized Designs with 4-Mode Compensators.	113
7-2	Natural Frequencies and Structural Design Variables of the Initial and the Optimized Structures. (Connected to 4-mode compensator.)	118
7-3	Controller and Observer Gains of the Initial and the Optimized 4-Mode Compensators.	119
7-4	Open-Loop and Closed-Loop Eigenvalues of the Initial and the Optimized Designs of 4-Mode Compensators.	121
7-5	Robustness Test Results of the Initial 4-Mode Plant and Compensator.	123
7-6	Robustness Test Results of the Optimized 4-Mode Plant and Compensator.	124
7-7	Performance of the 4-Mode Initial Compensator Connected to the 4-Mode Initial Plant for Various Initial Conditions.	128
7-8	Performance of the 4-Mode Initial Compensator Connected to the 11-Mode Initial Plant for Various Initial Conditions.	128
7-9	Performance of the 4-Mode Optimized Compensator Connected to the 4-Mode Optimized Plant for Various Initial Conditions.	129
7-10	Performance of the 4-Mode Optimized Compensator Connected to the 11-Mode Optimized Plant for Various Initial Conditions.	129
7-11	Control Objective and Structural Weigth of the Initial and Three Optimized Designs with 5-Mode Compensators.	137
7-12	Natural Frequencies and Structural Design Variables of the Initial and the Optimized Structures. (Connected to 5-mode compensator.)	142
7-13	Controller and Observer Gains of the Initial and the Optimized 5-Mode Compensators.	143
7-14	Open-Loop and Closed-Loop Eigenvalues of the Initial and the Optimized Designs of 5-Mode Compensators.	145

Table		Page
7-15	Robustness Test Results of the Optimized 5-Mode Compensator.	147
7-16	Performance of the 5-Mode Optimized Compensator Connected to the 5-Mode Optimized Plant for Various Initial Conditions.	152
7-17	Performance of the 5-Mode Optimized Compensator Connected to the 11-Mode Optimized Plant for Various Initial Conditions.	152

LIST OF NOTATION

		Page
Chapter II		
n	number of structural modes	20
n_e	number of beam elements	8
$\theta(t)$	rigid body angle	7
$w(t,s)$	displacement of the beam with respect to θ	7
T	kinetic energy	6
V	strain energy	6
$v(t,s)$	velocity of a point on the beam	6
ρ	density of the beam	6
l	length of the beam	6
r	radius of the hub	6
E	modulus of elasticity	6
$I(s)$	second moment of cross sectional area	6
$A(s)$	cross sectional area of the beam	6
I_o	hub moment of inertia about axis perpendicular to page through point O	6
m_1	point mass	6
c_o	damping coefficient	21
b	width of the cross-section	7
s	spacial variable along the bending axis of the beam	7
l_i	length of the i^{th} beam element	9
c_i	location of the i^{th} beam node	9

		Page
x_i	local coordinate corresponding to the i^{th} beam element	9
ξ_i	normalized local coordinate corresponding to the i^{th} beam element	8
$h_i(x_i)$	height of the cross-section at x_i	9
$I_i(x_i)$	second moment of cross sectional area at x_i	8
a_{ij}	i^{th} generalized coordinate of the j^{th} beam element	10
a_j	4×1 generalized coordinate vector corresponding to the j^{th} beam element	11
q_{ij}	i^{th} generalized coordinate of the j^{th} beam element	10
q_j	4×1 generalized coordinate vector corresponding to the j^{th} beam element	11
N_{ij}	i^{th} interpolation function of the j^{th} beam element	11
q_{HS}	$2n_e + 1$ generalized coordinate vector corresponding to the Hermite splines	15
q_{BS}	$n_e + 1$ generalized coordinate vector corresponding to the B-splines	15
U	$[2n_e + 1] \times [n_e + 1]$ linear transformation matrix	15
M_{BS}	$[n_e + 1] \times [n_e + 1]$ generalized mass matrix	16
K_{BS}	$[n_e + 1] \times [n_e + 1]$ generalized stiffness matrix	16
M_{HS}	$[2n_e + 1] \times [2n_e + 1]$ generalized mass matrix	16
K_{HS}	$[2n_e + 1] \times [2n_e + 1]$ generalized stiffness matrix	16

		Page
q	$n \times 1$ generalized coordinate vector	20
η	$n \times 1$ normal coordinate vector	20
η_i	i^{th} normal coordinate	20
M	$n \times n$ mass matrix	20
K	$n \times n$ stiffness matrix	20
ω_i	i^{th} natural frequency	20
ϕ_i	i^{th} natural mode	20
Φ	modal matrix	20

Chapter III

n	number of structural modes	23
m	number of sensors (measurement)	26
r	number of actuators	23
t	time	23
t_0	initial time	26
τ	time	26
$x(t)$	$2n \times 1$ state vector	23
$w(t)$	$2n \times 1$ state excitation noise vector	26
$y(t)$	$m \times 1$ observation or measurement vector	26
$v(t)$	$m \times 1$ observation or measurement noise vector	26
$u(t)$	$r \times 1$ control vector	23
A	$2n \times 2n$ system matrix	23
B	$2n \times r$ actuator influence matrix	23

		Page
C	$m \times 2n$ measurement matrix	26
F	$r \times 2n$ control gain matrix	24
G	$2n \times m$ observer gain matrix	27
J	quadratic performance measure	23
Q_c	$2n \times 2n$ nonnegative definite real symmetric state weighting matrix	23
R_c	$r \times r$ positive definite real symmetric input weighting matrix	23
Q_e	$2n \times 2n$ nonnegative definite real symmetric state excitation noise covariance kernel matrix	26
R_e	$m \times m$ positive definite real symmetric observation noise covariance kernel matrix	26
P	constant nonnegative definite real symmetric matrix	24
Π	$4n \times 4n$ matrix	24
W	the $4n \times 4n$ matrix whose columns are the eigenvectors of Π	25
W_{ij}	a submatrix of W	25
Λ	a $2n \times 2n$ matrix whose eigenvalues are the eigenvalues of Π with positive real part	25
$\tilde{J}[x(t t)]$	mean square error	27
$\hat{x}(t t)$	filtered estimate of the state $x(t)$	27
$\tilde{x}(t t)$	error of the filtered estimate of the state	27
\bar{P}	covariance matrix of the filtering error	27
$E[.]$	expected value	26
δ	Dirac delta function	26

		Page
A_{cl}	4nX4n closed-loop system matrix	33
X_e	the 2nX2n matrix whose columns are the eigenvectors of [A-GC]	34
X_c	the 2nX2n matrix whose columns are the eigenvectors of [A-BF]	34
Z	the 4nX4n matrix whose columns are the eigenvectors of A_{cl}	34
Λ_e	the 2nX2n diagonal matrix containing the eigenvalues of [A-GC]	34
Λ_c	the 2nX2n diagonal matrix containing the eigenvalues of [A-BF]	34
Λ_{cl}	the 4nX4n diagonal matrix containing the eigenvalues of A_{cl}	34
\bar{z}	2nX1 state vector	33
ϵ	error of the filtered estimate of the state	33
T	4nX4n transformation matrix	33
\bar{A}_{cl}	a similar matrix of A_{cl}	33
\bar{Z}	the 4nX4n matrix whose columns are the eigenvectors of \bar{A}_{cl}	34
\tilde{X}	2nX2n matrix	34
λ_{cl}	an eigenvalue of A_{cl}	36
σ	real part of λ_{cl}	36
ω	imaginary part of λ_{cl}	36
z	an eigenvector of A_{cl}	36

		Page
\Re	real part of z	36
\Im	imaginary part of z	36
T_r	$4n \times 4n$ transformation matrix	36
Λ_{cl_r}	$4n \times 4n$ block diagonal real matrix	36
Z_r	$4n \times 4n$ real matrix	36
T_{cr}	$2n \times 2n$ transformation matrix	37
T_{er}	$2n \times 2n$ transformation matrix	37
\tilde{X}_r	$2n \times 2n$ real matrix	37
X_{cr}	$2n \times 2n$ real matrix	37
X_{er}	$2n \times 2n$ real matrix	37
Λ_{cr}	$2n \times 2n$ block diagonal real matrix	38
Λ_{er}	$2n \times 2n$ block diagonal real matrix	38
C^n	the space of complex n -vectors	32
I	identity matrix	33

Chapter IV

f	functional control gain	39
g	functional control gain	39
α_f	functional control gain component (scalar)	40
ϕ_f	functional control gain component (function)	40
β_f	functional control gain component (scalar)	40

		Page
α_g	functional control gain component (scalar)	40
ϕ_g	functional control gain component (function)	40
β_g	functional control gain component (scalar)	40
f_n	n^{th} order approximation of f	40
g_n	n^{th} order approximation of g	40
α_{f_n}	n^{th} order approximation of α_f	40
ϕ_{f_n}	n^{th} order approximation of ϕ_f	40
β_{f_n}	n^{th} order approximation of β_f	40
α_{g_n}	n^{th} order approximation of α_g	40
ϕ_{g_n}	n^{th} order approximation of ϕ_g	40
β_{g_n}	n^{th} order approximation of β_g	40
$\langle \rangle_v$	strain-energy inner product	39
$\langle \rangle_H$	kinetic-energy inner product	39

Chapter V

λ_{c_i}	i^{th} eigenvalue of the $[A-BF]$ matrix	55
λ_{e_i}	i^{th} eigenvalue of the $[A-GC]$ matrix	55
λ_{cl_i}	i^{th} closed-loop eigenvalue	55
z_i	i^{th} right eigenvector of A_{cl} corresponding to λ_{cl_i}	55
λ_{ol_i}	i^{th} eigenvalue of matrix A	55

		Page
Λ_{ol}	2nx2n diagonal matrix containing the eigenvalues of the matrix A	56
α_c	controller alpha shift	63
α_e	observer alpha shift	64
β	uncertain plant parameter	50
β_0	nominal value of β	50
A_β	the derivative of A with respect to β	51
B_β	the derivative of B with respect to β	51
C_β	the derivative of C with respect to β	51
A_{cl_β}	the derivative of A_{cl} with respect to β	51
$\lambda_{cl_{j\beta}}$	the derivative of λ_{cl_j} with respect to β	54
Λ_{cl_β}	the 4nx4n diagonal matrix containing $\lambda_{cl_{j\beta}}$ ($j = 1, \dots, 4n$)	51
$\lambda_{cl_{j\beta\beta}}$	the second derivative of λ_{cl_j} with respect to β	54
Ω	diagonal matrix containing natural frequencies of a model	62
$\text{Re}(\cdot)$	real part of a complex number	54
$\text{Im}(\cdot)$	imaginary part of a complex number	55
$(\cdot)^*$	complex conjugate of a complex number	59
$ \cdot $	square of the norm	55

	Page
Chapter VI	
$J(F,G)$	objective function 72
H	hessian matrix 74
γ_i	i^{th} scalar weighting factor 72
Γ_i	i^{th} scalar weighting factor 74
∇	gradient operator 72
$\max(\cdot)$	maximum value 72
$\min(\cdot)$	minimum value 72
$ \cdot $	absolute value 72
$(\cdot)^{\ell}$	lower bound 72
$(\cdot)^u$	upper bound 72
$(\cdot)_o$	nominal value 73
Chapter VII	
$J(F,G,h)$	objective function 106
$J_c(F,G,h)$	control objective function 107
$W(h)$	structural weight 106
h	vector containing the structural design variables 107
h_i	hight of the cross-section at the i^{th} node 107
α	structural weight weighting factor 106

ACKNOWLEDGEMENTS

Many people have earned my gratitude during the preparation of this work. I wish to acknowledge specifically the efforts of my advisor, Professor J. S. Gibson, who has not only provided direction for my studies and this dissertation, but also a great deal of appreciated advice. Also, I wish to acknowledge the help and support of my committee members, Professor D. L. Mingori, Professor L. A. Schmit, Professor N. Levan and Professor H. O. Fattorini. My thanks to my office-mates, Dr. Faryar Jabbari and Dr. Paul Blelloch, who have contributed through discussions and their own researches. Finally, I wish to thank members of my family, Georgeik, Vergeik, Alenoosh and Areg, for their support and encouragement.

This research was sponsored by the Jet Propulsion Laboratory, Pasadena, California and the National Aeronautics and Space Administration under contract NAS 7-918.

VITA

August 22nd, 1957	Born, Teheran, Iran
1980	B.S., University of Portland
1982	M.S., University of California, Los Angeles
1983-1986	Research Assistant, Department of Mechanical, Aerospace and Nuclear Engineering, University of California, Los Angeles

ABSTRACT OF THE DISSERTATION

Integrated Control/Structure Design
and Robustness

by

Armen Adamian

Doctor of Philosophy in Mechanical Engineering
University of California, Los Angeles, 1986

Professor J. S. Gibson, Chair

When a flexible structure is to be controlled actively, optimum performance is obtained by integrated, or simultaneous, design of the structure and the controller, as opposed to the common practice of designing the structure independently of control considerations and then designing a controller for a fixed structure. The primary design objective from the structural point of view usually is to minimize weight, while the control design objectives depend on the application. An important requirement for a practical control system is robustness with respect to uncertain plant parameters. This dissertation discusses robust compensator design for fixed structures, and simultaneous control/structure design where the overall design objective combines the weight of the structure and the robustness of the closed-loop control system. For numerical optimization, robustness is represented

by the sensitivity of the closed-loop eigenvalues with respect to uncertain parameters. An example illustrates the closed-loop control system with robust compensator, and two examples illustrate the optimal designs of a flexible structure along with robust compensators. The dissertation also compares different finite element models to determine models most efficient for compensator design.

Chapter I

INTRODUCTION

Recent years have seen increasing research in integrated control and structural optimization. The primary motivation of this research is control of large flexible space structures, which are becoming larger and more flexible at the same time that their performance requirements are becoming more stringent. The complexity of these structures produces significant uncertainty in the parameters of such structures due to changing environments and modeling inaccuracies. Thus control/structure design methods are needed to produce high-performance, robust controllers and light, complex structures.

Among references that address integrated control/structure design are [B1], [J1], [L1], [M3], [M4], [N1] and [S2]. References [B1] and [J1] address an eigenvalue placement/optimization approach which seeks to impose specified constraints upon the closed-loop eigenvalues (without estimation) which are functions of structural and control design variables, while minimizing the control gain norm. Reference [S2] addresses the problem of minimizing a composite objective function as a linear combination of structural objective (structural mass) and control objective (standard quadratic performance index) subject to frequency constraint.

The primary objective of this dissertation is to obtain robust compensators by addressing the following two problems:

1. For a fixed structure, find controller and observer gains (design variables) that minimize the sensitivities of the closed-loop eigenvalues with respect to plant uncertainties (natural frequencies) subject to eigenvalue constraints.
2. Find structural parameters along with controller and observer gains that minimize an objective function which includes the structural weight in addition to the sensitivities of the closed-loop eigenvalues with respect to plant uncertainties, subject to eigenvalue constraints.

In this research, robustness means insensitivity of the closed-loop performance with respect to plant uncertainties. Although there is a vast literature on achieving robust designs using conventional control theory approaches, to our knowledge the proposed approach is new.

The organization of the dissertation is as follows. Chapter 2 presents a brief discussion of finite element modeling of flexible structures and presents an example in which the flexible structure consists of an Euler-Bernoulli beam attached (cantilevered) to a rigid rotating hub at one end and a point mass attached to the other end of the beam. Sections 2.2 and 2.3 discuss Hermite spline and B-Spline approximations of the structure; then Section 2.4 follows with a brief summary of the normal mode method.

The first three sections of chapter 3 summarize some of the standard results of the time-invariant linear-quadratic regulator problem (LQR), the time-invariant optimal observer problem and the time-invariant stochastic optimal linear-quadratic regulator problem (LQG). Sections 3.4 and 3.5 present equations for an efficient solution of the closed-loop eigenvalue problem, which enable one to evaluate the left and the right eigenvectors of the closed-loop system by doing numerical analysis in R^{2n} (the space of real $2n$ -vectors) instead of C^{4n} (the space of complex $4n$ -vectors) for $2n^{\text{th}}$ order plant and compensator. Chapter 4 presents an efficient method (Functional Gains) of comparing approximation schemes for control of flexible structures, and compares Hermite splines, B-splines and normal mode approximations.

Section 5.1 of Chapter 5 derives the derivatives of closed-loop eigenvalues in terms of controller and observer eigenvectors. Section 5.2 discusses some of the cases that cause the closed-loop designs to be sensitive or insensitive with respect to plant uncertainties and presents guidelines for less sensitive (i.e., more robust) control designs, which are supported by an example in Section 5.3.

Chapter 6 addresses the problem of finding controller and observer gains (design variables) that minimize the sensitivities of the closed-loop eigenvalues with respect to plant uncertainties (natural frequencies), subject to eigenvalue constraints but no side constraints on the design variables, and Section 6.3 follows with an

example which demonstrates the effectiveness of the first-order sensitivity optimization of the closed-loop eigenvalues for significantly increasing the robustness of the initial closed-loop design (LQG).

Chapter 7 addresses the problem of finding structural parameters in addition to controller and observer gains that minimize an objective function which includes the structural weight in addition to the sensitivities of the closed-loop eigenvalues with respect to plant uncertainties, subject to eigenvalue constraints and partial side constraints on the design variables. Sections 7.2.1 and 7.2.2 present examples in which optimization simultaneously reduces the structural weight and increases the robustness of the initial LQG compensator/structure designs. Chapter 8 summarizes the main conclusions of Chapters 5, 6 and 7. Appendix A summarizes some standard results involving derivatives of the eigenvalues and eigenvectors of a matrix with respect to a parameter, and appendix B compares analytic and finite difference gradients of the initial design of Section 6.3.

Chapter II

FINITE ELEMENT MODEL

In finite element modeling of structures, the continuous structure is separated by imaginary boundaries into a number of "finite elements", which are assumed to be interconnected at a finite number of nodal points located on the boundaries (nodes), then a set of functions is selected to define the state of displacement within each of the finite elements in terms of the nodal displacement. These functions can be used to obtain the kinetic and strain energies of the structure in terms of the nodal displacement. Then Lagrange's equations of motion can be used to evaluate the generalized mass and stiffness matrices of the structure. In addition, it should be clear that it is necessary to begin with an admissible displacement field (interpolation functions) for the approximation.

An admissible displacement field for an element must have the following characteristics:

1. It must have the zero strain states or the required number of rigid body modes.
2. It must have sufficient degrees of freedom to allow the kinematic continuity on the boundary of two adjacent elements.
3. It must have the constant strain state.

For more details on this topic, see [Z1].

To illustrate this method, we consider the structure shown in Figure 2-1. An Euler-Bernoulli beam is cantilevered to a rigid hub at one end and a point mass m_1 is attached to the other end of the beam. The hub can rotate about its fixed center, point 0. The kinetic and strain energies of the structure are

$$T = \frac{1}{2} I_0 \dot{\theta}^2 + \frac{1}{2} \int_0^l \rho A(s) v(s)^2 ds + \frac{1}{2} m_1 v(l)^2, \quad (2.1)$$

$$V = \frac{1}{2} \int_0^l EI(s) w_{ss}^2 ds, \quad (2.2)$$

where

T = kinetic energy,

V = strain energy,

$v(s)$ = velocity of a point on the beam,

ρ = density of the beam,

l = length of the beam,

r = radius of the hub,

E = modulus of elasticity,

$I(s)$ = second moment of cross sectional area,

$A(s)$ = cross sectional area of the beam,

I_0 = hub moment of inertia about axis perpendicular to page
through point 0,

m_1 = point mass,

and subscript s indicates partial derivative with respect to s . The square of the velocity of a point on the elastic axis of the beam is

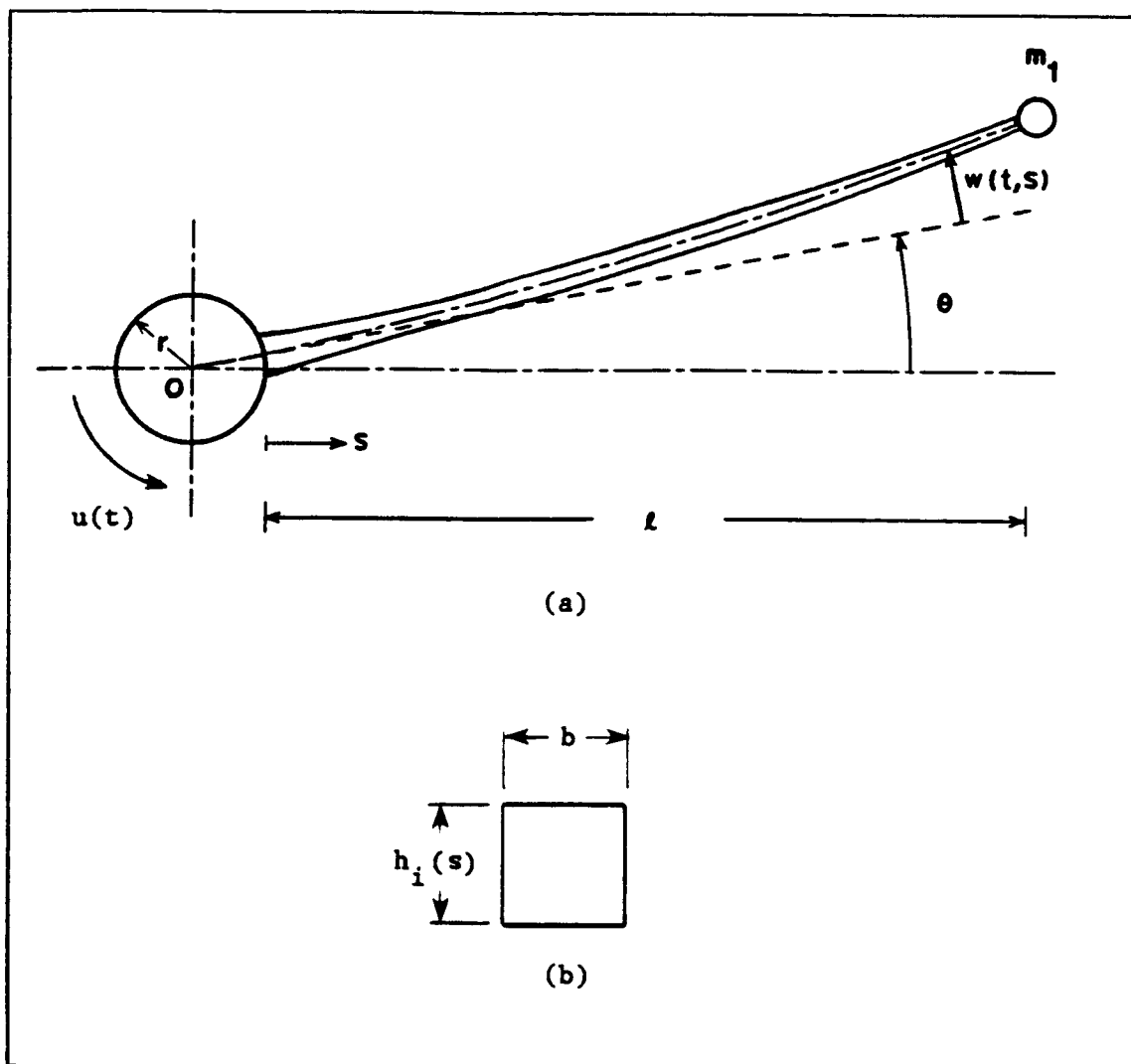


Figure 2-1. (a) Flexible Structure. (b) Beam Cross Section.

$$v(s)^2 = [\dot{w}(s) + [r+s]\dot{\theta}]^2 + [\dot{\theta}w(s)]^2. \quad (2.3)$$

Neglecting higher order terms and substituting into (2.1) yields

$$T = \frac{1}{2} I_O \dot{\theta}^2 + \frac{1}{2} m_1 [\dot{w}(\ell) + [r+\ell]\dot{\theta}]^2 + \frac{1}{2} \int_0^\ell \rho A(s) [\dot{w}(s) + [r+s]\dot{\theta}]^2 ds. \quad (2.4)$$

Next, consider the coordinate transformation shown in Figure 2-2, where

$$s = c_i + x_i. \quad (2.5)$$

From (2.2), (2.4) and (2.5), it follows that

$$T = \frac{1}{2} I_0 \dot{\theta}^2 + \frac{1}{2} m_1 [\dot{w}(\ell) + [r + \ell] \dot{\theta}]^2 + \frac{1}{2} \sum_{i=1}^{n_e} \rho b \int_0^{\ell_i} h_i(x_i) [\dot{w}(x_i) + [r + c_i + x_i] \dot{\theta}]^2 dx_i, \quad (2.6)$$

$$V = \frac{1}{2} \sum_{i=1}^{n_e} E \int_0^{\ell_i} I_i(x_i) w_{x_i x_i}^2 dx_i, \quad (2.7)$$

where n_e is the number of beam elements, and subscript x_i indicates partial derivative with respect to x_i . Next, we define

$$\xi_i = x_i / \ell_i. \quad (2.8)$$

Substituting (2.8) into (2.6) and (2.7), we obtain

$$T = \frac{1}{2} I_0 \dot{\theta}^2 + \frac{1}{2} m_1 [\dot{w}(\ell) + [r + \ell] \dot{\theta}]^2 + \frac{1}{2} \sum_{i=1}^{n_e} \rho b \ell_i \int_0^1 h_i(\xi_i) [\dot{w}(\xi_i) + [r + c_i + \ell_i \xi_i] \dot{\theta}]^2 d\xi_i, \quad (2.9)$$

$$V = \frac{1}{2} \sum_{i=1}^{n_e} [E / \ell_i^3] \int_0^1 I_i(\xi_i) w_{\xi_i \xi_i}^2 d\xi_i, \quad (2.10)$$

where

$$I_i(\xi_i) = \frac{1}{12} b h_i^3(\xi_i), \quad (2.11)$$

$$h_i(\xi_i) = h_i(0) + [h_i(1) - h_i(0)] \xi_i \quad i = 1, \dots, n_e, \quad (2.12)$$

$$h_i(1) = h_{i+1}(0) \quad i = 1, \dots, n_e - 1. \quad (2.13)$$

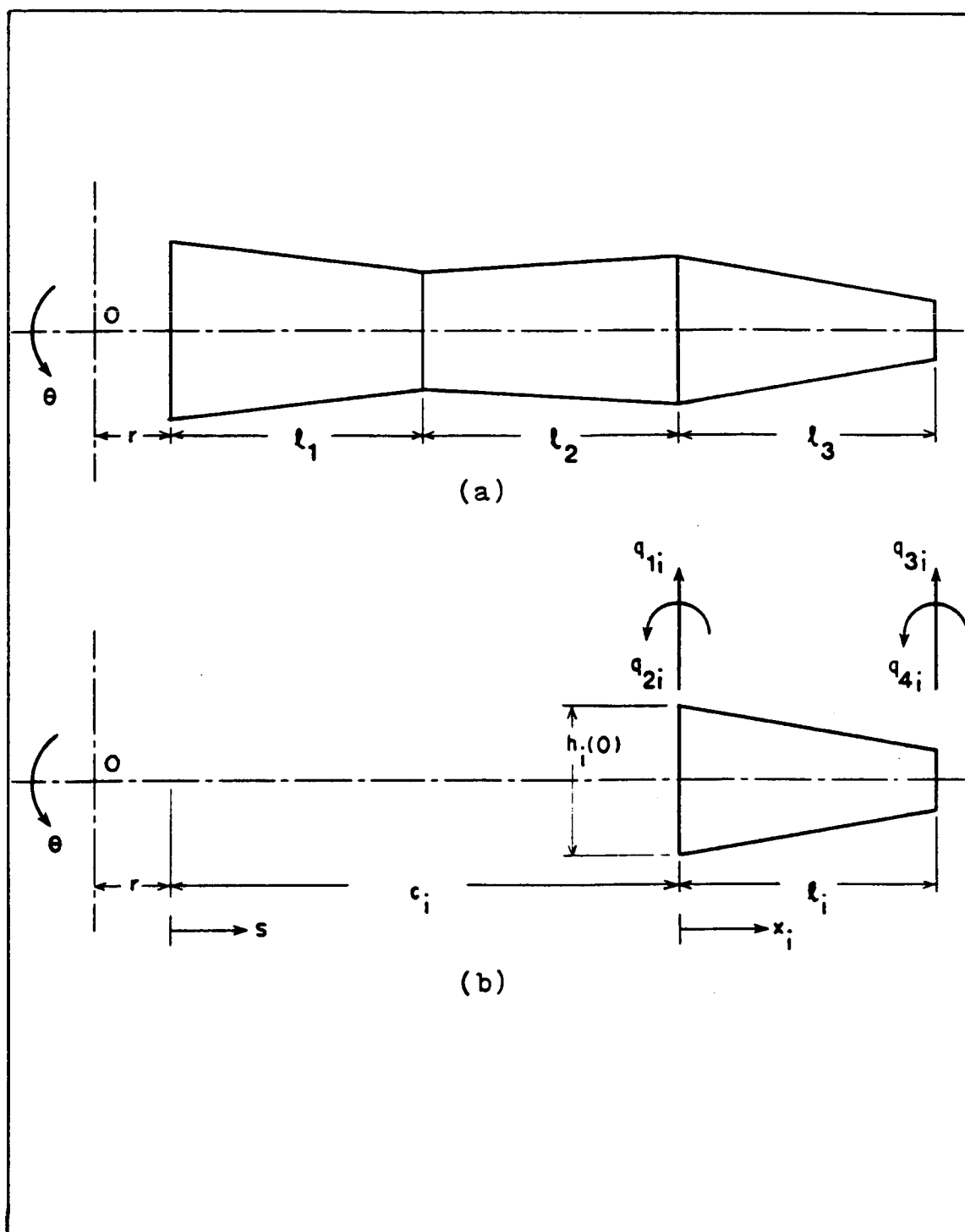


Figure 2-2. (a) Approximation of the Beam by Finite Elements.
(b) i -th Beam Element.

2.1 Hermite Splines

The displacement field for the beam element shown in Figure 2-2 is approximated as

$$w(x_i) = a_{1i} + a_{2i}x_i + a_{3i}x_i^2 + a_{4i}x_i^3, \quad (2.14)$$

where the generalized coordinate a_{1i} represents rigid body transverse translation, and a_{2i} represents rigid body rotation. There are four generalized coordinates in this case because interelement continuity in classical beam theory requires both transverse displacement and slope be continuous at the boundary of two adjacent elements. The constant strain mode in beam bending is the constant curvature change which is embedded in a_{3i} . Thus, the displacement field is seen to contain all the admissibility requirements.

It is desired to represent the displacement field in terms of the nodal displacement, so that

$$\begin{bmatrix} q_{1i} \\ q_{2i} \\ q_{3i} \\ q_{4i} \end{bmatrix} = \begin{bmatrix} w(x_i=0) \\ w_{x_i}(x_i=0) \\ w(x_i=l_i) \\ w_{x_i}(x_i=l_i) \end{bmatrix} \quad (2.15)$$

or

$$\begin{bmatrix} q_{1i} \\ q_{2i} \\ q_{3i} \\ q_{4i} \end{bmatrix} = \begin{bmatrix} 1 & 0 & 0 & 0 \\ 0 & 1 & 0 & 0 \\ 1 & l_i & l_i^2 & l_i^3 \\ 0 & 1 & 2l_i & 3l_i^2 \end{bmatrix} \begin{bmatrix} a_{1i} \\ a_{2i} \\ a_{3i} \\ a_{4i} \end{bmatrix}, \quad (2.16)$$

which implies that

$$\begin{bmatrix} a_{1i} \\ a_{2i} \\ a_{3i} \\ a_{4i} \end{bmatrix} = \frac{1}{\ell_i^3} \begin{bmatrix} \ell_i^3 & 0 & 0 & 0 \\ 0 & \ell_i^3 & 0 & 0 \\ -3\ell_i & -2\ell_i^2 & 3\ell_i & -\ell_i^2 \\ 2 & \ell_i & -2 & \ell_i \end{bmatrix} \begin{bmatrix} q_{1i} \\ q_{2i} \\ q_{3i} \\ q_{4i} \end{bmatrix}. \quad (2.17)$$

In matrix form

$$[a_i] = [B][q_i]. \quad (2.18)$$

In view of (2.8) and (2.18), (2.14) yields

$$w(\xi_i) = [N_{1i}(\xi_i) \ N_{2i}(\xi_i) \ N_{3i}(\xi_i) \ N_{4i}(\xi_i)] [q_i], \quad (2.19)$$

where

$$N_{1i}(\xi_i) = (2\xi_i^3 - 3\xi_i^2 + 1), \quad (2.20)$$

$$N_{2i}(\xi_i) = \ell_i(\xi_i^3 - 2\xi_i^2 + \xi_i), \quad (2.21)$$

$$N_{3i}(\xi_i) = (-2\xi_i^3 + 3\xi_i^2), \quad (2.22)$$

$$N_{4i}(\xi_i) = \ell_i(\xi_i^3 - \xi_i^2). \quad (2.23)$$

Substituting (2.19) into (2.9) and (2.10), and imposing the following constraints:

$$w(\xi_1=0) = 0, \quad (2.24)$$

$$w_{\xi_1}(\xi_1=0) = 0, \quad (2.25)$$

$$w(\xi_i=1) = w(\xi_{i+1}=0) \quad i = 1, \dots, n_e-1, \quad (2.26)$$

$$w_{\xi_i}(\xi_i=1) = w_{\xi_{i+1}}(\xi_{i+1}=0) \quad i = 1, \dots, n_e-1, \quad (2.27)$$

where n_e is the number of beam elements, we obtain the kinetic and strain energies of the structure in terms of the nodal displacements. Now Lagrange's equations of motion can be used to derive the generalized mass and stiffness matrices of the structure. Figure 2-3 shows the generalized degrees of freedom and the Hermite splines for three beam element model. Note that the order of the generalized mass and stiffness matrices of this structure evaluated by the Hermite splines is $[1+2n_e] \times [1+2n_e]$.

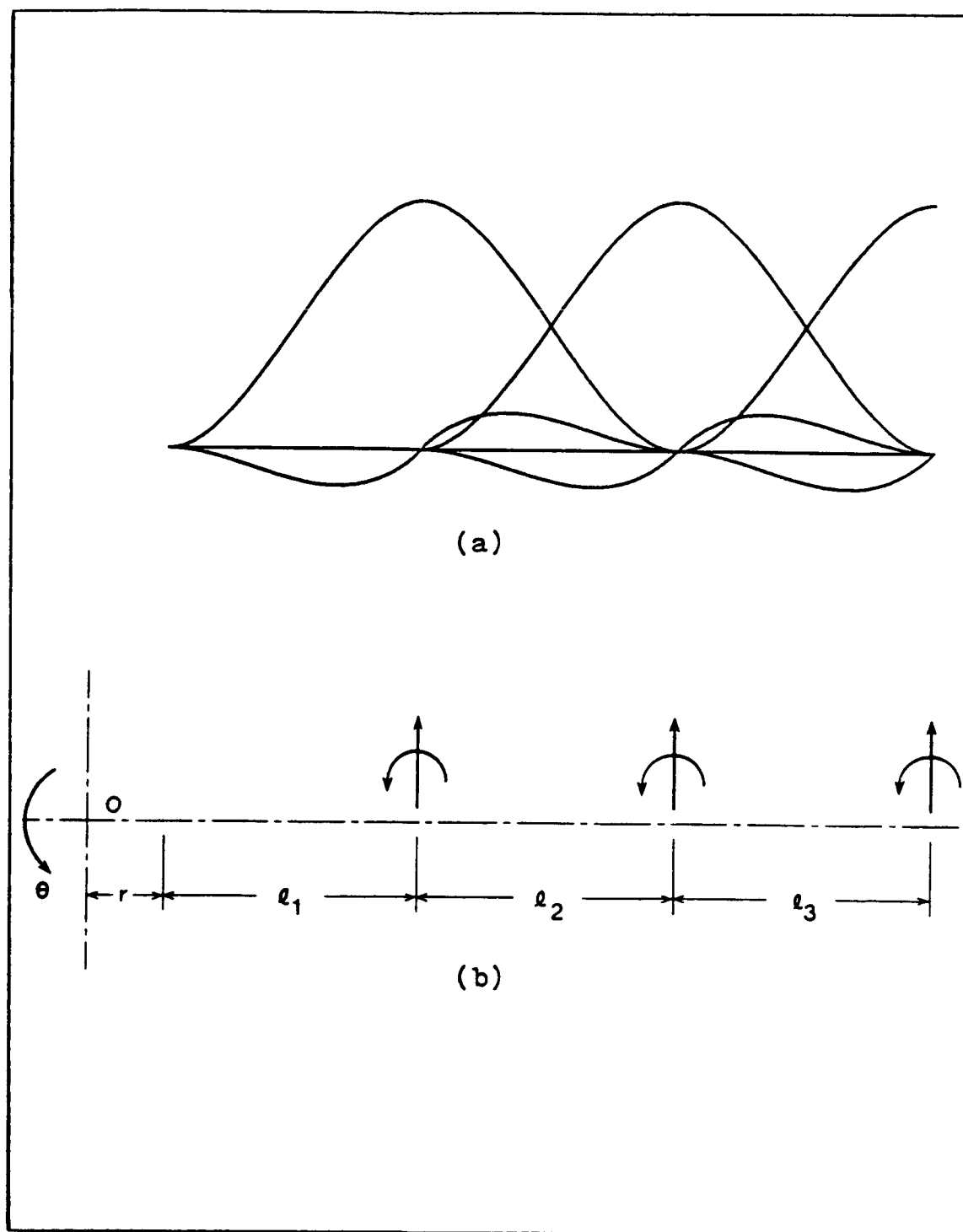


Figure 2-3. (a) Hermite Splines for Three Beam Element Model.
(b) Generalized Degrees of Freedom.

2.2 B-Splines

In the previous section we used Hermit splines to evaluate the generalized mass and stiffness matrices of the structure. Note that Hermite splines are third order polynomials which require transverse displacement and slope to be continuous at the boundary of two adjacent elements. On the other hand (cubic) B-splines do satisfy the above conditions and in addition they require that the curvature change or strain be continuous at the boundary of two adjacent elements. To approximate the displacement of the beam element shown in Figure 2-2 with the B-splines, consider equation (2.19) of the previous section

$$w(\xi_i) = [N_{1i}(\xi_i) \ N_{2i}(\xi_i) \ N_{3i}(\xi_i) \ N_{4i}(\xi_i)] [q_i], \quad (2.28)$$

where

$$N_{1i}(\xi_i) = (2\xi_i^3 - 3\xi_i^2 + 1), \quad (2.29)$$

$$N_{2i}(\xi_i) = \ell_i (\xi_i^3 - 2\xi_i^2 + \xi_i), \quad (2.30)$$

$$N_{3i}(\xi_i) = (-2\xi_i^3 + 3\xi_i^2), \quad (2.31)$$

$$N_{4i}(\xi_i) = \ell_i (\xi_i^3 - \xi_i^2). \quad (2.32)$$

Substituting (2.28) into (2.9) and (2.10), and imposing the following constraints

$$w(\xi_1=0) = 0, \quad (2.33)$$

$$w_{\xi_1}(\xi_1=0) = 0, \quad (2.34)$$

$$w(\xi_i=1) = w(\xi_{i+1}=0) \quad i = 1, \dots, n_e-1, \quad (2.35)$$

$$w_{\xi_i}(\xi_i=1) = w_{\xi_{i+1}}(\xi_{i+1}=0) \quad i = 1, \dots, n_e-1, \quad (2.36)$$

$$w_{\xi_i \xi_i}(\xi_i=1) = 0 \quad i = n_e, \quad (2.37)$$

$$w_{\xi_i \xi_i}(\xi_i=1) = w_{\xi_{i+1} \xi_{i+1}}(\xi_{i+1}=0) \quad i = 1, \dots, n_e-1, \quad (2.38)$$

where n_e is the number of beam elements, we obtain the kinetic and strain energies of the structure in terms of the nodal displacements. Now Lagrange's equations of motion can be used to derive the generalized mass and stiffness matrices of the flexible structure. Figures 2-4 and 2-5 show the generalized degrees of freedom and the B-splines for three and four beam element model. Note that the order of the generalized mass and stiffness matrices of this structure evaluated by the B-splines is $[1+n_e] \times [1+n_e]$.

These matrices can also be obtained by performing a similarity transformation on the generalized mass and stiffness matrices evaluated by the Hermite splines. Consider the linear transformation

$$q_{HS} = U q_{BS}, \quad (2.39)$$

where q_{HS} is the $[2n_e+1]$ generalized coordinate vector corresponding to the Hermite splines, q_{BS} is the $[n_e+1]$ generalized coordinate vector corresponding to the B-splines, and U is the $[2n_e+1] \times [n_e+1]$ linear transformation matrix evaluated by using the n_e constraint equations of (2.37) and (2.38). Then

$$M_{BS} = U^T M_{HS} U \quad (2.40)$$

$$K_{BS} = U^T K_{HS} U \quad (2.41)$$

where the subscript HS refers to the Hermite spline approximation scheme, and the subscript BS refers to the B-spline approximation scheme.

If one selects the transverse displacement of the nodes as the generalized coordinates then each of the B-splines will span the length of the beam (maximum support), but if one selects the linear combination of the transverse nodal displacements as the generalized coordinates then each of the B-splines will span four elements (minimum support). Figure 2-6a shows the B-spline corresponding to the generalized coordinate q_{44} which is the transverse displacement of the fourth node of an eight element beam model. Figure 2-6b shows the B-spline corresponding to the generalized coordinate $[\frac{1}{3}q_{43} + q_{44} + \frac{1}{3}q_{45}]$, which is the linear combination of the transverse displacements of the third, the fourth and the fifth nodes of an eight element beam model. For more details on this topic, see [R1] and [S1].

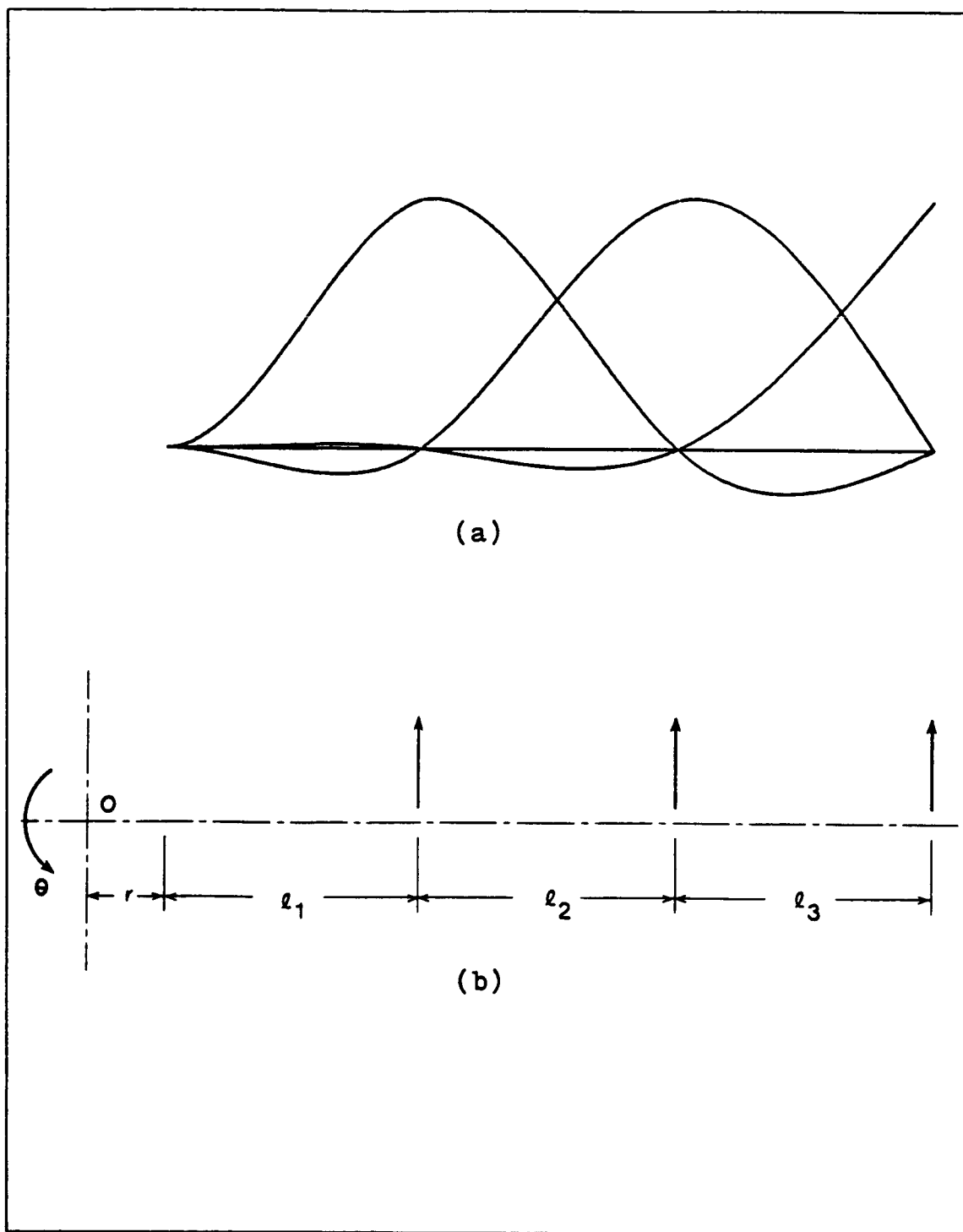


Figure 2-4. (a) B-Splines for Three Beam Element Model.
(b) Generalized Degrees of Freedom.

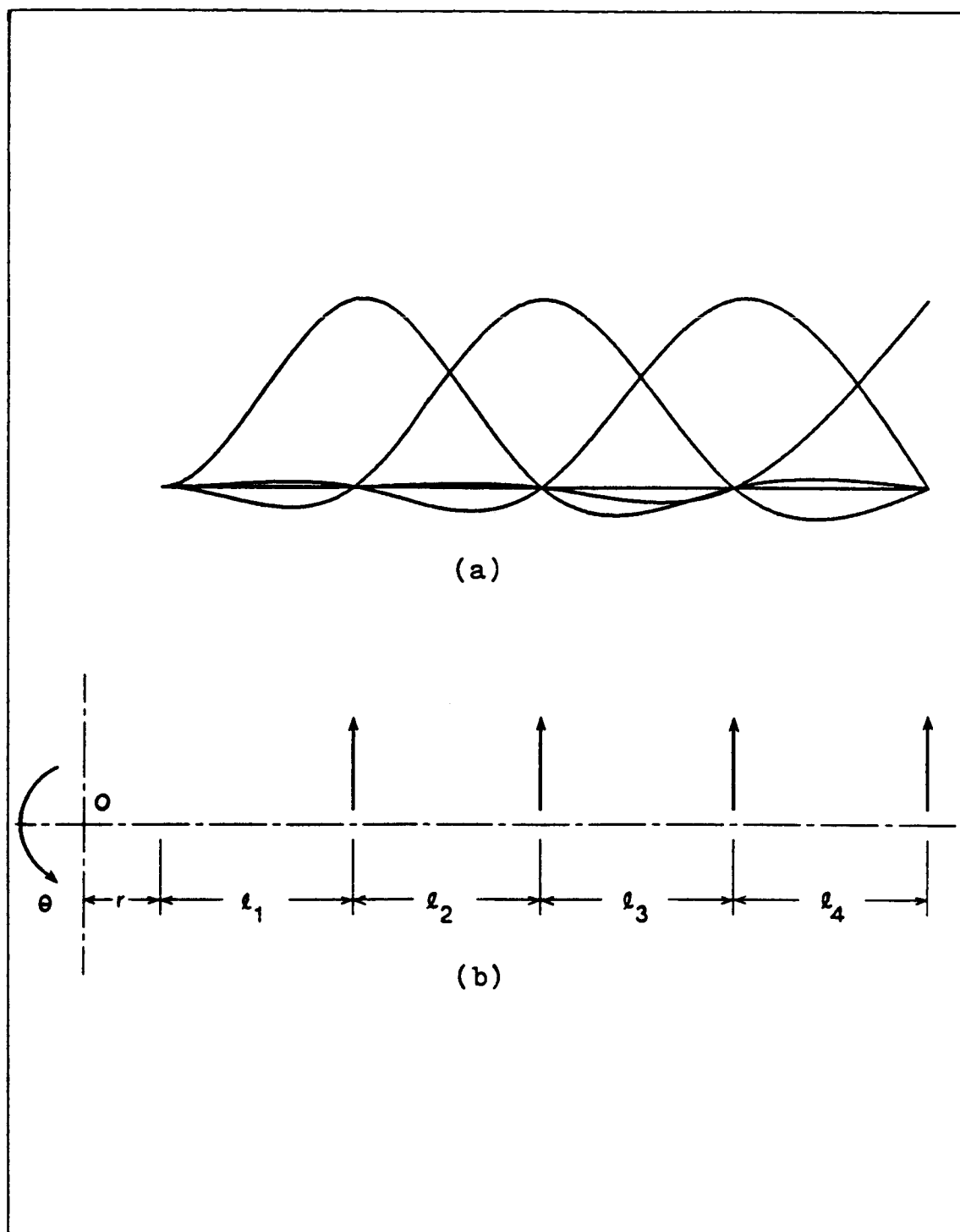


Figure 2-5. (a) B-Splines for Four Beam Element Model.
 (b) Generalized Degrees of Freedom.

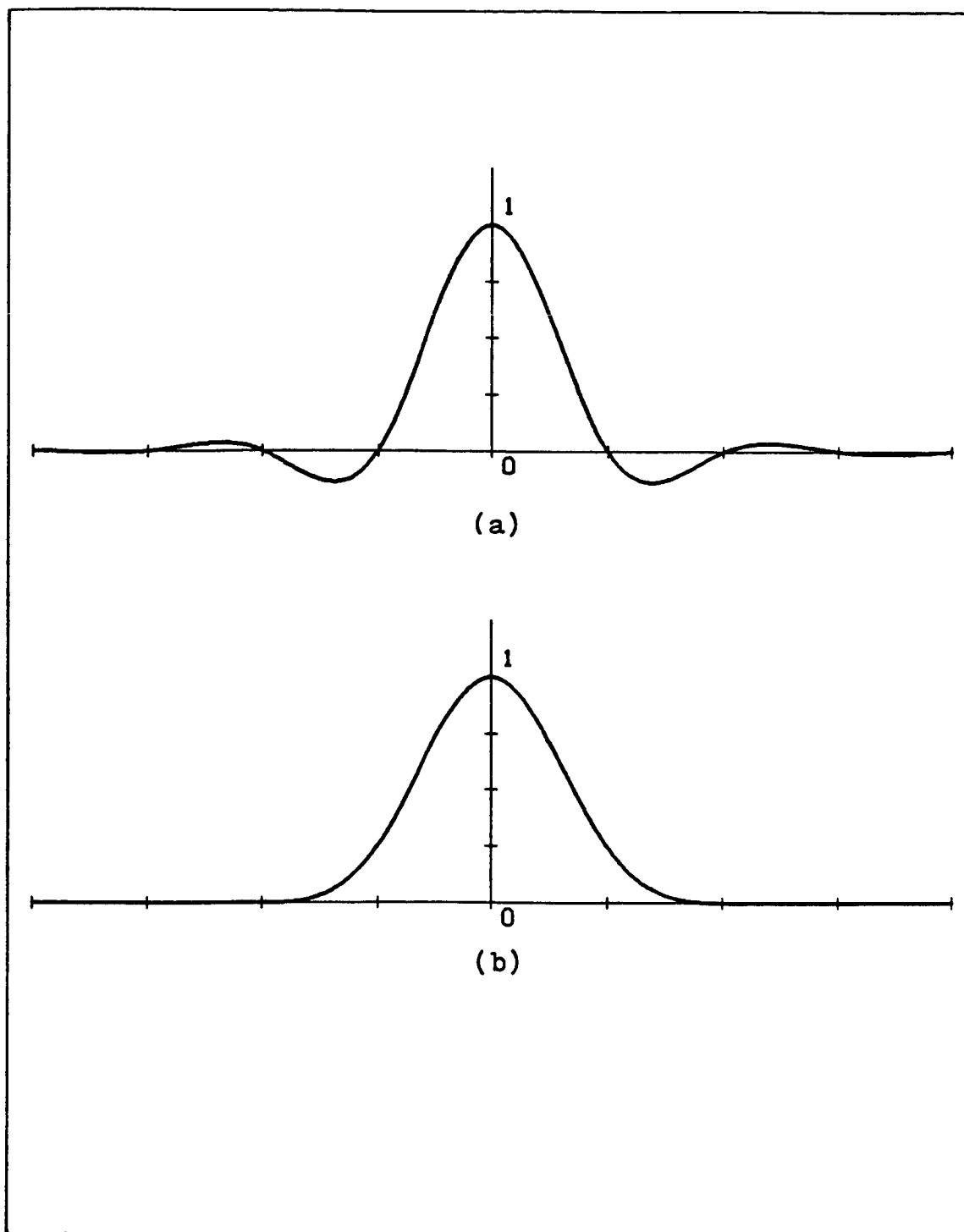


Figure 2-6. (a) Maximum Support B-Spline. (b) Minimum Support B-Spline.

2.3 Normal Modes

Consider the structural dynamic problem

$$M\ddot{q} + Kq = 0, \quad (2.42)$$

where M is a $n \times n$ mass matrix, K is a $n \times n$ stiffness matrix, and q is a generalized coordinate n -vector. Solution of (2.42) yields

$$\omega_i \quad i = 1, \dots, n,$$

$$\phi_i \quad i = 1, \dots, n,$$

where ω_i is the i^{th} natural frequency, and ϕ_i is the i^{th} natural mode.

We normalize ϕ_i so that

$$\phi_i^T M \phi_i = 1 \quad i = 1, \dots, n, \quad (2.43)$$

and impose the coordinate transformation

$$q = \Phi \eta \quad (2.44)$$

on (2.42), where

$$\Phi = [\phi_1 \phi_2 \dots \phi_n], \quad (2.45)$$

and η is the normal coordinate n -vector. Then we obtain

$$M\ddot{\Phi}\eta + K\Phi\eta = 0. \quad (2.46)$$

Premultiplying (2.46) by Φ^T yields the decoupled differential equations

$$\ddot{\eta}_i + \omega_i^2 \eta_i = 0 \quad i = 1, \dots, n. \quad (2.47)$$

PARAMETER		VALUE	UNIT
hub radius	r	10	in
hub moment of inertia	I_o	10^2	slug.in ²
beam length	l	10^2	in
beam mass per unit length	m_b	10^{-2}	slug/in
2nd moment of cross sectional area	I	$4/3$	in ⁴
modulus of elasticity	E	10^4	slug/in.sec ²
damping coefficient	c_o	10^{-3}	
point mass	m_1	1	slug

Table 2-1 Structural Data.

This coordinate transformation (normal coordinates) will be seen to be very helpful in evaluating equations for sensitivity optimization. Figure 2-7 shows the first three flexible natural mode shapes (excluding the rigid-body mode) of a ten beam element model of the structure shown in Figure 2-1.

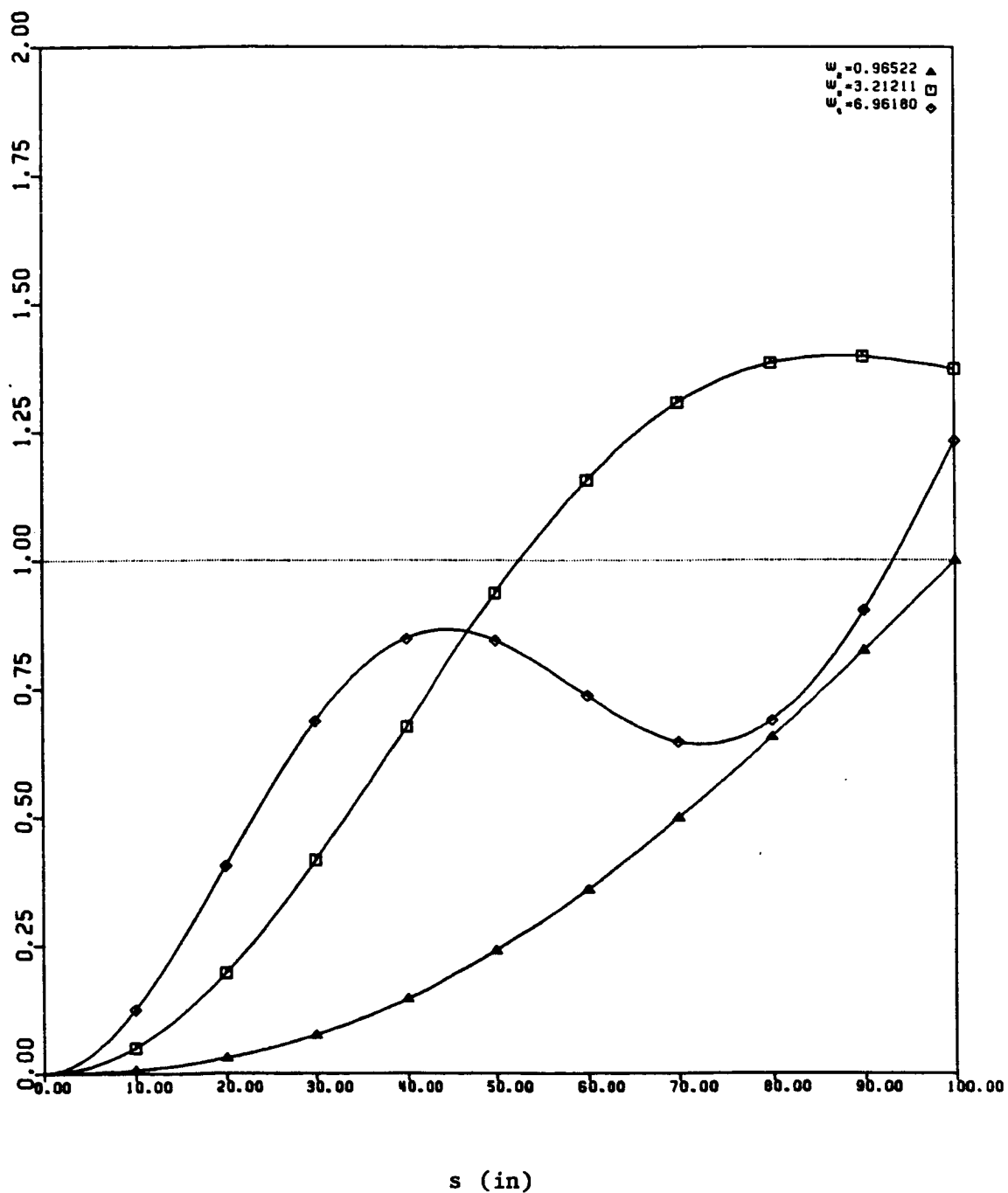


Figure 2-7. First Three Natural Modes of the Ten Beam Element Model.
 (Δ) 2nd mode, (\square) 3rd mode, (\diamond) 4th mode.

Chapter III

CONTROL DESIGN

3.1 Time-Invariant Optimal Linear-Quadratic Regulator Problem

In this section we summarize some of the results of the time-invariant optimal linear-quadratic regulator problem. We assume that the complete state $x(t)$ of the plant can be accurately measured at all times and it is available for feedback. For more details on this topic, see [K1].

Consider the linear time-invariant state equation

$$\dot{x}(t) = Ax(t) + Bu(t), \quad (3.1)$$

where

$x(t)$ = $2n \times 1$ state vector,

A = $2n \times 2n$ system matrix,

B = $2n \times r$ actuator influence matrix,

$u(t)$ = $r \times 1$ control vector.

The quadratic performance measure is

$$J = \int_0^{\infty} [x^T(t)Q_c x(t) + u^T(t)R_c u(t)]dt, \quad (3.2)$$

where Q_c is a $2n \times 2n$ nonnegative definite real symmetric state weighting matrix, and R_c is an $r \times r$ positive definite real symmetric input weighting matrix. The problem of determining an input $u(t)$ for

(3.1) such that the quadratic performance measure (3.2) is minimal is referred to as the time-invariant deterministic linear-quadratic optimal regulator problem, LQR. Note that the quantity $x^T Q_c x$ in (3.2) is a measure of how fast one desires to bring the initial state to the origin (zero state), and the quantity $u^T R_c u$ is a measure of the control effort. Therefore, the relative importance of the error in state and the control effort is determined by the matrices Q_c and R_c .

The steady-state optimal control vector $u(t)$ for the time-invariant deterministic optimal linear-quadratic regulator problem is generated by the linear control law

$$u(t) = -Fx(t), \quad (3.3)$$

where

$$F = R_c^{-1} B^T P \quad (3.4)$$

is the optimal control gain matrix, and the constant nonnegative definite real symmetric matrix P satisfies the algebraic matrix Riccati equation

$$PA + A^T P - PBR_c^{-1} B^T P + Q_c = 0. \quad (3.5)$$

The solution of (3.5) can be obtained by defining the $4n \times 4n$ matrix

$$\Pi = \begin{bmatrix} A & -BR_c^{-1} B^T \\ -Q_c & -A^T \end{bmatrix}. \quad (3.6)$$

When Π has no eigenvalues with zero real part, then

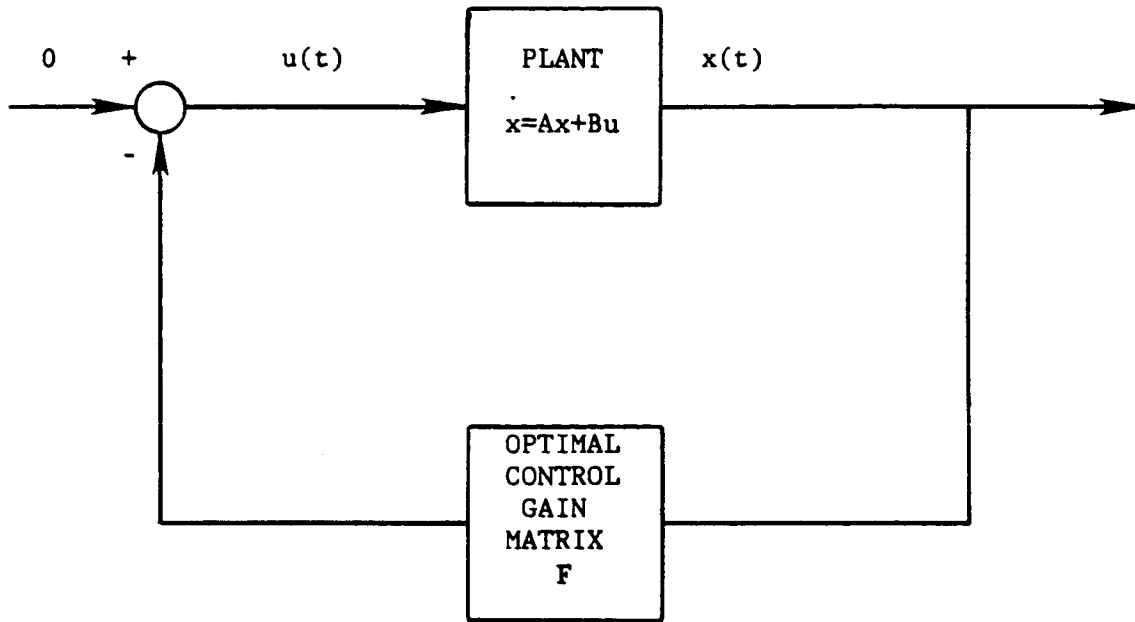


Figure 3-1. Block Diagram of the Optimal Linear-Quadratic Regulator System.

$$P = W_{22}W_{12}^{-1}, \quad (3.7)$$

$$[A-BF]W_{12} = -W_{12}A, \quad (3.8)$$

where

$$\Pi W = W \begin{bmatrix} A & 0 \\ 0 & -A \end{bmatrix}, \quad (3.9)$$

$$W = \begin{bmatrix} W_{11} & W_{12} \\ W_{21} & W_{22} \end{bmatrix}. \quad (3.10)$$

In (3.8)-(3.9), A is a $2n \times 2n$ matrix whose eigenvalues are the eigenvalues of Π with positive real part, and $A-BF$ is the $2n \times 2n$ closed-loop optimal linear-quadratic regulator system matrix. Figure 3-1 shows the block diagram of the optimal linear-quadratic regulator system.

3.2 Time-Invariant Optimal Observer Problem

In this section we summarize some of the results of the time-invariant optimal observer problem. For more details on this topic, see [K1] and [M2].

Consider the linear time-invariant system equations

$$\dot{x}(t) = Ax(t) + w(t), \quad (3.11)$$

$$y(t) = Cx(t) + v(t), \quad (3.12)$$

where

$x(t)$ = $2n \times 1$ state vector,

$w(t)$ = $2n \times 1$ state excitation noise vector,

$y(t)$ = $m \times 1$ observation or measurement vector,

$v(t)$ = $m \times 1$ observation or measurement noise vector,

A = $2n \times 2n$ system matrix,

C = $m \times 2n$ measurement matrix.

The stochastic processes $\{w(t), t \geq t_0\}$ and $\{v(t), t \geq t_0\}$ are uncorrelated zero-mean gaussian white noises with covariance matrices

$$E[w(t)w^T(\tau)] = Q_e \delta(t-\tau) \quad \tau \geq t_0, \quad (3.13)$$

$$E[v(t)v^T(\tau)] = R_e \delta(t-\tau) \quad \tau \geq t_0, \quad (3.14)$$

where E denotes the expected value, and δ denotes the Dirac delta function. In addition, we assume that Q_e is a $2n \times 2n$ positive semidefinite real symmetric matrix, R_e is an $m \times m$ positive definite real symmetric matrix, and the initial state is a zero mean gaussian random $2n$ vector independent of the state excitation noise and

observation noise.

The mean square filtering error is

$$J[\tilde{x}(t|t)] = E[\tilde{x}^T(t|t)\tilde{x}(t|t)], \quad (3.15)$$

where

$$\tilde{x}(t|t) = x(t) - \hat{x}(t|t) \quad (3.16)$$

is the error in the filtered estimate of the state, and $\hat{x}(t|t)$ is the filtered estimate of the state $x(t)$ at time $t \geq t_0$ (initial time) based on measurement over the interval $[t_0, t]$ (conditional expectation). The problem of determining the filtered estimate of the state at some time $t \geq t_0$ (initial time) based on measurements over the interval $[t_0, t]$ such that the mean square error is minimized is referred to as the optimal observer problem or Kalman-Bucy filtering problem, KBF.

The steady-state optimal linear filtered estimate for the system of equations (3.11) and (3.12) is generated by the relation

$$\dot{\hat{x}} = A\hat{x} + G[y(t) - C\hat{x}], \quad (3.17)$$

where $\hat{x} = \hat{x}(t|t)$, $\hat{x}(t_0|t_0) = 0$ and

$$G = \bar{P}C^T R_e^{-1} \quad (3.18)$$

is the optimal observer gain matrix. The constant nonnegative definite real symmetric matrix \bar{P} , covariance matrix of the filtering error, satisfies the algebraic matrix Riccati equation

$$A\bar{P} + \bar{P}A^T - \bar{P}C^T R_e^{-1} C\bar{P} + Q_e = 0. \quad (3.19)$$

3.3 Time-Invariant Stochastic Optimal Linear-Quadratic Regulator Problem

In this section we summarize some of the results of the time-invariant stochastic optimal linear-quadratic regulator problem. For more details on this topic, see [K1] and [M2].

Consider the linear time-invariant system equations

$$\dot{x}(t) = Ax(t) + Bu(t) + w(t), \quad (3.20)$$

$$y(t) = Cx(t) + v(t), \quad (3.21)$$

where

$x(t)$ = $2n \times 1$ state vector,

$w(t)$ = $2n \times 1$ state excitation noise vector,

$y(t)$ = $m \times 1$ observation or measurement vector,

$v(t)$ = $m \times 1$ observation or measurement noise vector,

$u(t)$ = $r \times 1$ control vector,

A = $2n \times 2n$ system matrix,

B = $2n \times r$ actuator influence matrix,

C = $m \times 2n$ measurement matrix.

The stochastic processes $\{w(t), t \geq 0\}$ and $\{v(t), t \geq 0\}$ are uncorrelated zero-mean gaussian white noises with covariance matrices

$$E[w(t)w^T(\tau)] = Q_e \delta(t-\tau) \quad \tau \geq 0, \quad (3.22)$$

$$E[v(t)v^T(\tau)] = R_e \delta(t-\tau) \quad \tau \geq 0, \quad (3.23)$$

where E denotes the expected value, and δ denotes the Dirac delta function. In addition, we assume that Q_e is a $2n \times 2n$ positive

semidefinite real symmetric matrix, R_e is an $m \times m$ positive definite real symmetric matrix, and the initial state is a zero mean gaussian random $2n$ vector independent of the state excitation noise and observation noise.

The quadratic performance measure is

$$J = E\left\{\lim_{\tau \rightarrow \infty} \frac{1}{\tau} \int_0^{\tau} [x^T(t)Q_c x(t) + u^T(t)R_c u(t)]dt\right\}, \quad (3.24)$$

where Q_c is a $2n \times 2n$ nonnegative definite real symmetric state weighting matrix, and R_c is an $r \times r$ positive definite real symmetric input weighting matrix. The problem of determining an input $u(t)$ for (3.20) and (3.21) such that the quadratic performance measure (3.24) is minimal is referred to as the time-invariant stochastic optimal linear-quadratic regulator problem, LQG.

The steady-state optimal control vector $u(t)$ for the time-invariant stochastic optimal linear-quadratic regulator problem is generated by the linear control law

$$u(t) = -F\hat{x}(t), \quad (3.25)$$

where

$$F = R_c^{-1} B^T P \quad (3.26)$$

is the optimal control gain matrix, and the constant nonnegative definite real symmetric matrix P satisfies the algebraic matrix Riccati equation

$$PA + A^T P - PBR_c^{-1} B^T P + Q_c = 0. \quad (3.27)$$

The steady-state optimal linear filtered estimate for the system of equations (3.20) and (3.21) is generated by the relation

$$\dot{\hat{x}} = A\hat{x} + G[y(t) - C\hat{x}] + Bu(t), \quad (3.28)$$

where $\hat{x} = \hat{x}(t|t)$, $\hat{x}(0|0) = 0$, and

$$G = \bar{P}C^T R_e^{-1} \quad (3.29)$$

is the optimal observer gain matrix. The constant nonnegative definite real symmetric matrix \bar{P} , covariance matrix of the filtering error, satisfies the algebraic matrix Riccati equation

$$\bar{A}\bar{P} + \bar{P}\bar{A}^T - \bar{P}C^T R_e^{-1} C\bar{P} + Q_e = 0. \quad (3.30)$$

In view of (3.26) and (3.29), the optimal control gain matrix is independent of all the statistical parameters in the problem, and the optimal observer is independent of the matrices in the performance measure, (separation principle). Figure 3-2 shows the block diagram of the stochastic optimal linear-quadratic regulator system.

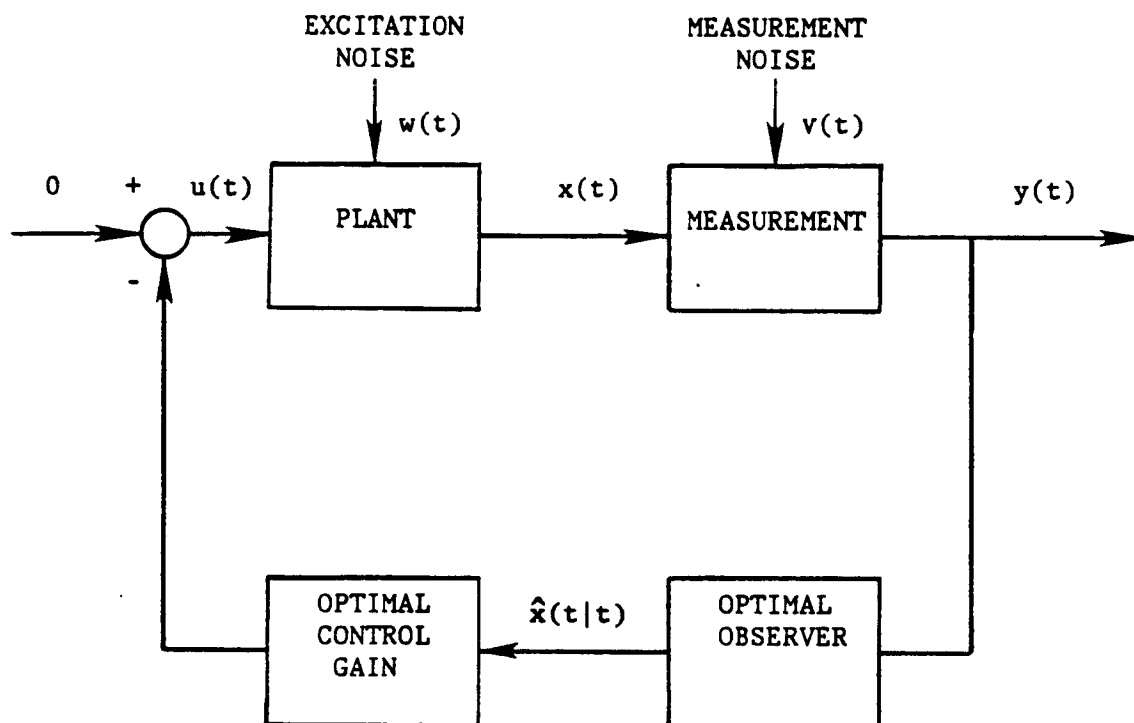


Figure 3-2. Block Diagram of the Stochastic Optimal Linear-Quadratic Regulator System.

3.4 Eigenvalues and Eigenvectors of the Closed-Loop System

In this section we derive equations for an efficient solution of the closed-loop eigenvalue problem for any gains. We want to evaluate the eigenvalues and the right and the left eigenvectors of the closed-loop system by doing the numerical analysis in \mathbb{C}^{2n} (the space of complex $2n$ -vectors) instead of \mathbb{C}^{4n} , where $4n$ is the dimension of the closed-loop eigenvalue problem.

Consider the closed-loop system equations

$$\dot{x} = Ax + Bu, \quad (3.31)$$

$$y = Cx, \quad (3.32)$$

$$\dot{\hat{x}} = A\hat{x} + G(y - C\hat{x}) + Bu, \quad (3.33)$$

$$u = -F\hat{x}, \quad (3.34)$$

where

$x = 2n \times 1$ state vector,

$\hat{x} = 2n \times 1$ filtered estimate of the state vector,

$y = m \times 1$ observation or measurement vector,

$A = 2n \times 2n$ system matrix,

$B = 2n \times r$ actuator influence matrix,

$C = m \times 2n$ measurement matrix,

$F = r \times 2n$ control gain matrix,

$G = 2n \times m$ observer gain matrix,

$u = r \times 1$ control vector.

Combining (3.31)-(3.34), we obtain the closed-loop state equation

$$\dot{z} = A_{cl}z, \quad (3.35)$$

where

$$z = \begin{bmatrix} x \\ \hat{x} \end{bmatrix}, \quad (3.36)$$

$$A_{cl} = \begin{bmatrix} A & -BF \\ GC & A-BF-GC \end{bmatrix}. \quad (3.37)$$

Next, consider the coordinate transformation

$$z = T\bar{z}, \quad (3.38)$$

where

$$\bar{z} = \begin{bmatrix} x \\ \varepsilon \end{bmatrix}, \quad (3.39)$$

$$\varepsilon = x - \hat{x}, \quad (3.40)$$

$$T = T^{-1} = \begin{bmatrix} I & 0 \\ I & -I \end{bmatrix}. \quad (3.41)$$

In view of (3.38), (3.35) yields

$$\dot{\bar{z}} = \bar{A}_{cl}\bar{z}, \quad (3.42)$$

where

$$\bar{A}_{cl} = \begin{bmatrix} A-BF & BF \\ 0 & A-GC \end{bmatrix}. \quad (3.43)$$

This transformation shows that, as is well known, the spectrum of A_{cl} is the union of the spectrum of $[A-BF]$ and the spectrum of $[A-GC]$. We refer to the eigenvalues of $[A-BF]$ as the controller eigenvalues and

to the eigenvalues of $[A-GC]$ as the estimator eigenvalues. Also, from here on, we assume that the eigenvalues of A_{cl} are distinct.

Here, we denote by X_e the $2n \times 2n$ matrix whose columns are the eigenvectors of $[A-GC]$, by X_c the $2n \times 2n$ matrix whose columns are the eigenvectors of $[A-BF]$, and by Z the $4n \times 4n$ matrix whose columns are the eigenvectors of A_{cl} . Also, Λ_e is the $2n \times 2n$ diagonal matrix containing the eigenvalues of $[A-GC]$, Λ_c is the $2n \times 2n$ diagonal matrix containing the eigenvalues of $[A-BF]$, and Λ_{cl} is the $4n \times 4n$ matrix

$$\Lambda_{cl} = \begin{bmatrix} \Lambda_c & 0 \\ 0 & \Lambda_e \end{bmatrix}. \quad (3.44)$$

Hence,

$$[A-BF]X_c = X_c \Lambda_c, \quad (3.45)$$

$$[A-GC]X_e = X_e \Lambda_e, \quad (3.46)$$

$$\bar{A}_{cl} \bar{Z} = \bar{Z} \Lambda_{cl}, \quad (3.47)$$

$$A_{cl} Z = Z \Lambda_{cl}. \quad (3.48)$$

From (3.43)-(3.47), we see that

$$\bar{Z} = \begin{bmatrix} X_c & X_c \tilde{X} \\ 0 & X_e \end{bmatrix}, \quad (3.49)$$

where the $2n \times 2n$ matrix \tilde{X} satisfies

$$\Lambda_c \tilde{X} - \tilde{X} \Lambda_e = -X_c^{-1} B F X_e. \quad (3.50)$$

Note that there exists a unique solution to (3.50) because, by hypothesis, Λ_e and Λ_c have no eigenvalues in common. From (3.38) and (3.49), it follows that

$$Z = T\bar{Z} = \begin{bmatrix} X_c & X_c \tilde{X} \\ X_c & [X_c \tilde{X} - X_e] \end{bmatrix}, \quad (3.51)$$

$$Z^{-1} = \begin{bmatrix} [X_c^{-1} - \tilde{X} X_e^{-1}] & \tilde{X} X_e^{-1} \\ X_e^{-1} & -X_e^{-1} \end{bmatrix}. \quad (3.52)$$

3.5 Determining Right and Left Eigenvectors of the Closed-Loop System with Real Arithmetic

Consider the closed-loop state equation

$$A_{cl}z = \lambda_{cl}z. \quad (3.53)$$

Note that if λ_{cl} is a complex eigenvalue of the closed-loop system matrix, then $\bar{\lambda}_{cl}$ is also an eigenvalue. Which implies

$$A_{cl}\bar{z} = \bar{\lambda}_{cl}\bar{z}. \quad (3.54)$$

From (3.53) and (3.54), we see that

$$A_{cl}\gamma = \sigma\gamma - \omega\xi, \quad (3.55)$$

$$A_{cl}\xi = \sigma\xi + \omega\gamma, \quad (3.56)$$

where

$$\lambda_{cl} = \sigma + j\omega, \quad (3.57)$$

$$z = \gamma + j\xi. \quad (3.58)$$

In matrix form

$$A_{cl} \begin{bmatrix} \gamma & \xi \end{bmatrix} = \begin{bmatrix} \gamma & \xi \end{bmatrix} \begin{bmatrix} \sigma & \omega \\ -\omega & \sigma \end{bmatrix} \quad (3.59)$$

In view of (3.53) and (3.59), (3.48) yields

$$A_{cl}Z_r = Z_r\Lambda_{cl}, \quad (3.60)$$

where

$$Z_r = ZT_r, \quad (3.61)$$

$$\Lambda_{cl} = T_r^{-1}A_{cl}T_r, \quad (3.62)$$

and T_r is a block diagonal transformation matrix that stacks the real and the imaginary parts of the right eigenvectors in columns of the real matrix Z_r . The diagonal elements of T_r corresponding to the real closed-loop eigenvalues are identity (scalar), and the 2x2 diagonal blocks of T_r corresponding to the complex pairs are

$$\frac{1}{2} \begin{bmatrix} 1 & -j \\ 1 & j \end{bmatrix} \quad (3.63)$$

if the eigenvectors corresponding to the complex pairs are in adjacent columns of matrix Z . Similar transformations can be applied to X_c and X_e matrices so that

$$X_{cr} = X_c T_{cr}, \quad (3.64)$$

$$X_{er} = X_e T_{er}. \quad (3.65)$$

From (3.44), (3.60)-(3.62), (3.64) and (3.65), we see that

$$T_r = \begin{bmatrix} T_{cr} & 0 \\ 0 & T_{er} \end{bmatrix}. \quad (3.66)$$

In view of (3.51), (3.52), (3.64) and (3.65), (3.61) yields

$$Z_r = \begin{bmatrix} X_{cr} & X_{cr} \tilde{X}_r \\ X_{cr} & [X_{cr} \tilde{X}_r - X_{er}] \end{bmatrix}, \quad (3.67)$$

$$Z_r^{-1} = \begin{bmatrix} [X_{cr}^{-1} - \tilde{X}_r X_{er}^{-1}] & \tilde{X}_r X_{er}^{-1} \\ X_{er}^{-1} & -X_{er}^{-1} \end{bmatrix}, \quad (3.68)$$

where

$$\Lambda_{cr} \tilde{X}_r - \tilde{X}_r \Lambda_{er} = -X_{cr}^{-1} B F X_{er}, \quad (3.69)$$

$$\Lambda_{cr} = T_{cr}^{-1} \Lambda_c T_{cr}, \quad (3.70)$$

$$\Lambda_{er} = T_{er}^{-1} \Lambda_e T_{er}. \quad (3.71)$$

Then the right and the left eigenvectors of the closed-loop system are

$$Z = Z_r T_r^{-1}, \quad (3.72)$$

$$Z^{-1} = T_r Z_r^{-1}. \quad (3.73)$$

Chapter IV

FUNCTIONAL GAINS

4.1 Functional Control Gains

In this chapter we compare convergence of three approximation schemes using functional gains (Refs. G3 and G4). Consider the structure shown in Figure 2-1. A uniform Euler-Bernoulli beam is cantilevered to a rigid hub at one end and a point mass m_1 is attached to the other end of the beam. The hub can rotate about its fixed center, point 0, and the control is a torque $u(t)$ applied to the hub. Here, we assume that the entire state vector is measured, so that no estimation is required in the closed-loop system (full-state feedback). The generalized displacement vector is

$$x(t) = [\theta, w(t,s), w(t,\ell)]. \quad (4.1)$$

In [G3] and [G4] we worked an optimal LQR problem for the distributed model of this structure. The performance index is

$$J = \int_0^{\infty} [\theta^2 + (\text{Total Energy}) + Ru^2] dt, \quad (4.2)$$

where total energy means kinetic energy plus elastic strain energy in the structure, and R is the control weight. The optimal control has the form

$$u(t) = -\langle f, x(t) \rangle_V - \langle g, \dot{x}(t) \rangle_H, \quad (4.3)$$

where

$\langle \cdot, \cdot \rangle_V$ = strain-energy inner product,

$\langle \cdot, \cdot \rangle_H$ = kinetic-energy inner product.

In (4.3) f and g are functional control gains, which have the form

$$f = (\alpha_f, \phi_f, \beta_f), \quad (4.4)$$

$$g = (\alpha_g, \phi_g, \beta_g), \quad (4.5)$$

where $\alpha_f, \beta_f, \alpha_g, \beta_g$ are scalars and ϕ_f, ϕ_g are functions.

The functional control gains are obtained from the solution to an infinite dimensional Riccati operator equation. Since such an equation can not be solved in closed form, we approximate it with a sequence of finite dimensional Riccati matrix equations. From the solution to the n^{th} Riccati matrix equations, we obtain the approximate functional gains

$$f_n = (\alpha_{f_n}, \phi_{f_n}, \beta_{f_n}), \quad (4.6)$$

$$g_n = (\alpha_{g_n}, \phi_{g_n}, \beta_{g_n}), \quad (4.7)$$

where n is the order of approximation. These functional gains are linear combinations of the basis vectors in the approximation scheme.

4.2 Numerical Results

The above example was modeled using three approximation schemes discussed in Chapter 2. Namely, the Hermite spline, the B-spline and the normal mode approximations, here the normal modes were obtained by using 24 beam elements and Hermite spline approximation. Table 4-1 shows the structural data and the control weight $R=0.05$ in (4.2). The order of approximation for these schemes are

Hermite splines $n = 2n_e + 1,$

B-splines $n = n_e + 1,$

normal modes $n = \text{number of modes},$

where n_e is the number of beam elements.

Here, we compare the convergence of the functional control gain components ϕ_{fn}'' and ϕ_{gn} since the scalars α_{fn} and α_{gn} converge at a faster rate, and the scalars

$$\beta_{fn} = \phi_{fn}''(l), \quad (4.8)$$

$$\beta_{gn} = \phi_{gn}(l). \quad (4.9)$$

Figures 4-1 through 4-3 show the functional control gains based on the three approximation schemes. In each figure, the solid line represents the converged functional gain component ϕ_{fn}'' or ϕ_{gn} , and a dashed line represents a functional control gain component corresponding to a lower order of approximation. Note that s is the

PARAMETER		VALUE	UNIT
hub radius	r	10	in
hub moment of inertia	I_o	10^2	slug.in ²
beam length	l	10^2	in
beam mass per unit length	m_b	10^{-2}	slug/in
2nd moment of cross sectional area	I	$4/3$	in ⁴
modulus of elasticity	E	10^4	slug/in.sec ²
damping coefficient	c_o	10^{-4}	
point mass	m_1	1	slug
fundamental frequency of undamped structure		0.967	rad/sec

Table 4-1 Structural Data .

spacial variable along the bending axis of the beam (Fig. 2-1), and the nodes of the structure are marked with a different symbol for each approximation order. ((.)" indicates second derivative with respect to s.)

For the Hermite spline approximation scheme, Figures 4-1a and 4-1b show the functional control gain component ϕ_{fn}'' and ϕ_{gn} evaluated by using 4,6,8 and 10 beam element model. These figures indicate that the functional control gains converge for 8 beam element model; i.e., $n=17$. For the B-spline approximation scheme, Figures 4-2a and 4-2b show the functional control gain component ϕ_{fn}'' and ϕ_{gn} evaluated by using 4,6,8 and 10 beam element model. These figures indicate that the functional control gains converge for 8 beam element model; i.e.,

n=9. Because cubic B-splines have continuous first and second derivatives, the ϕ_{fn}'' is continuous at the nodes of the structure. For the normal mode approximation scheme, Figures 4-3a and 4-3b show the functional control gain component ϕ_{fn}'' and ϕ_{gn} evaluated by using 5,7,9,11 and 13 modes (including one rigid body mode). These figures indicate that the functional control gains converge for 9 normal mode model; i.e., n=9.

Figures 4-1 through 4-3 indicate that the convergence of the B-spline approximation is much faster compared to the convergence of the Hermite splines. This will be our justification of using B-splines for integrated structural and control optimization. Note that similar functions (functional estimator gains) exist for observer gains (see G3 and G4) which can be used with the functional control gains to determine the convergence of the optimal compensators for distributed models.

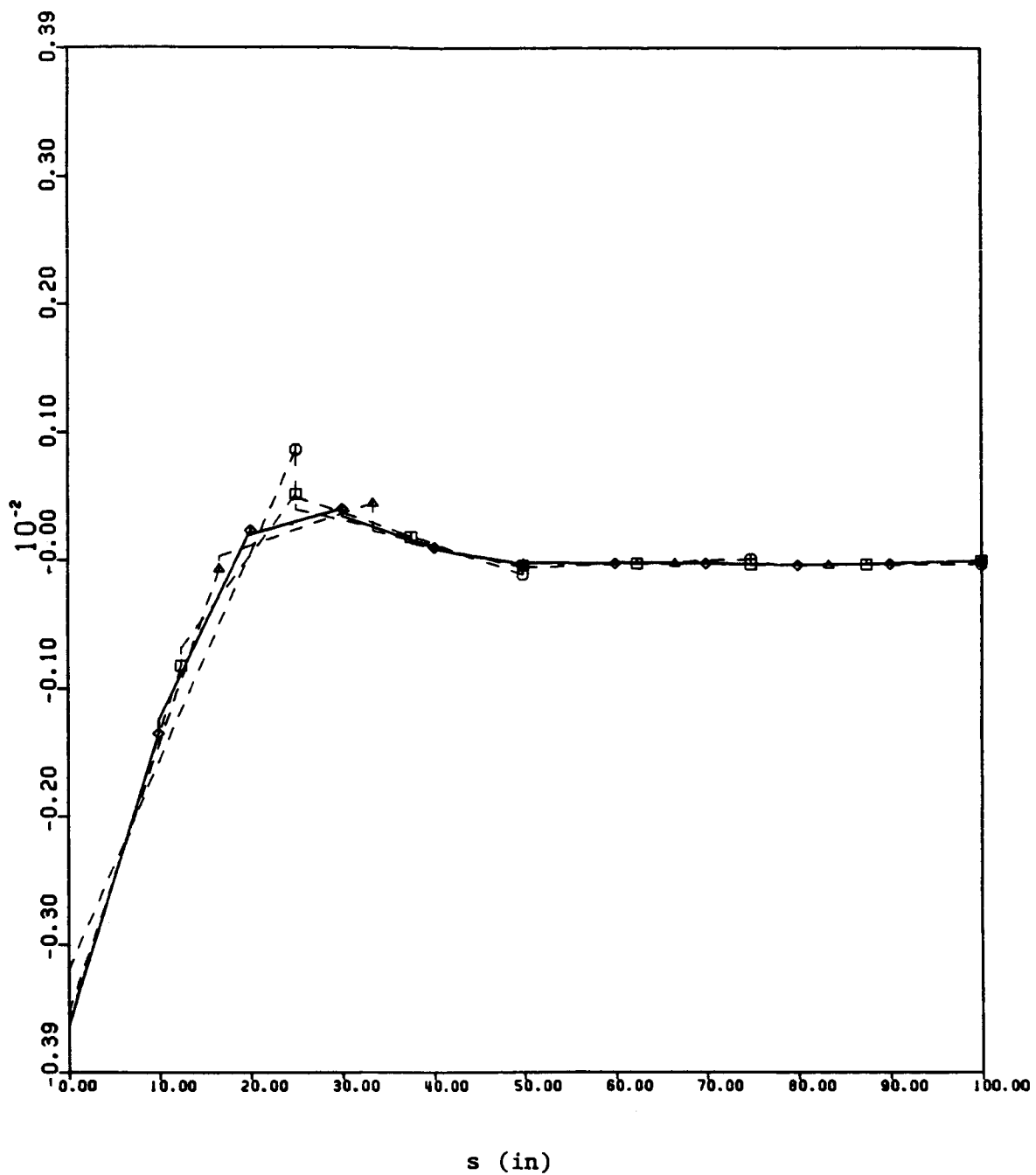


Figure 4-1a. Functional Control Gain Component ϕ_{fn}'' Based on the Hermite Splines. (\circ) $n_e=4$, (\triangle) $n_e=6$, (\square) $n_e=8$, (\diamond) $n_e=10$.

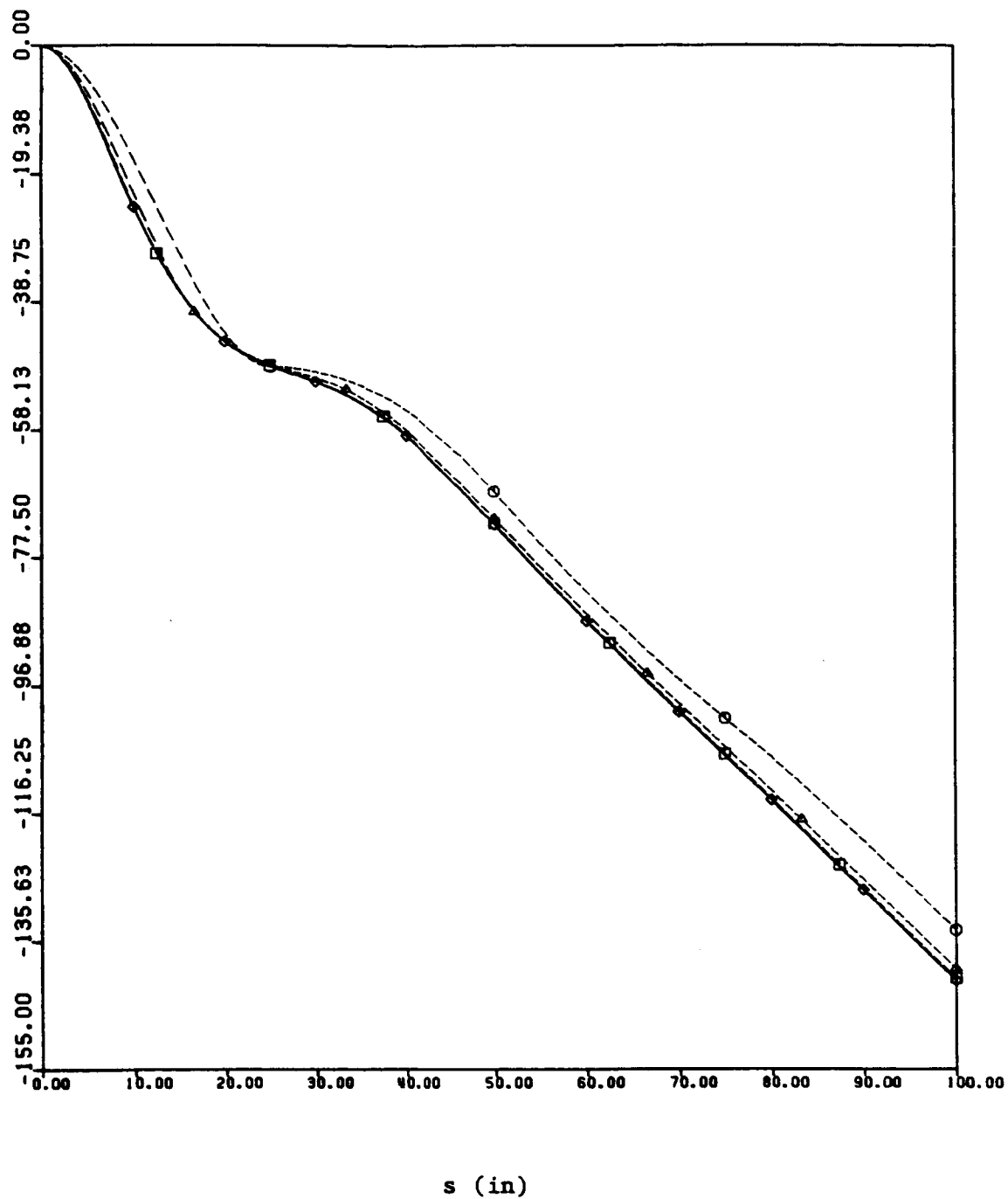


Figure 4-1b. Functional Control Gain Component ϕ_{gn} Based on the Hermite Splines. (\circ) $n_e=4$, (\triangle) $n_e=6$, (\square) $n_e=8$, (\diamond) $n_e=10$.

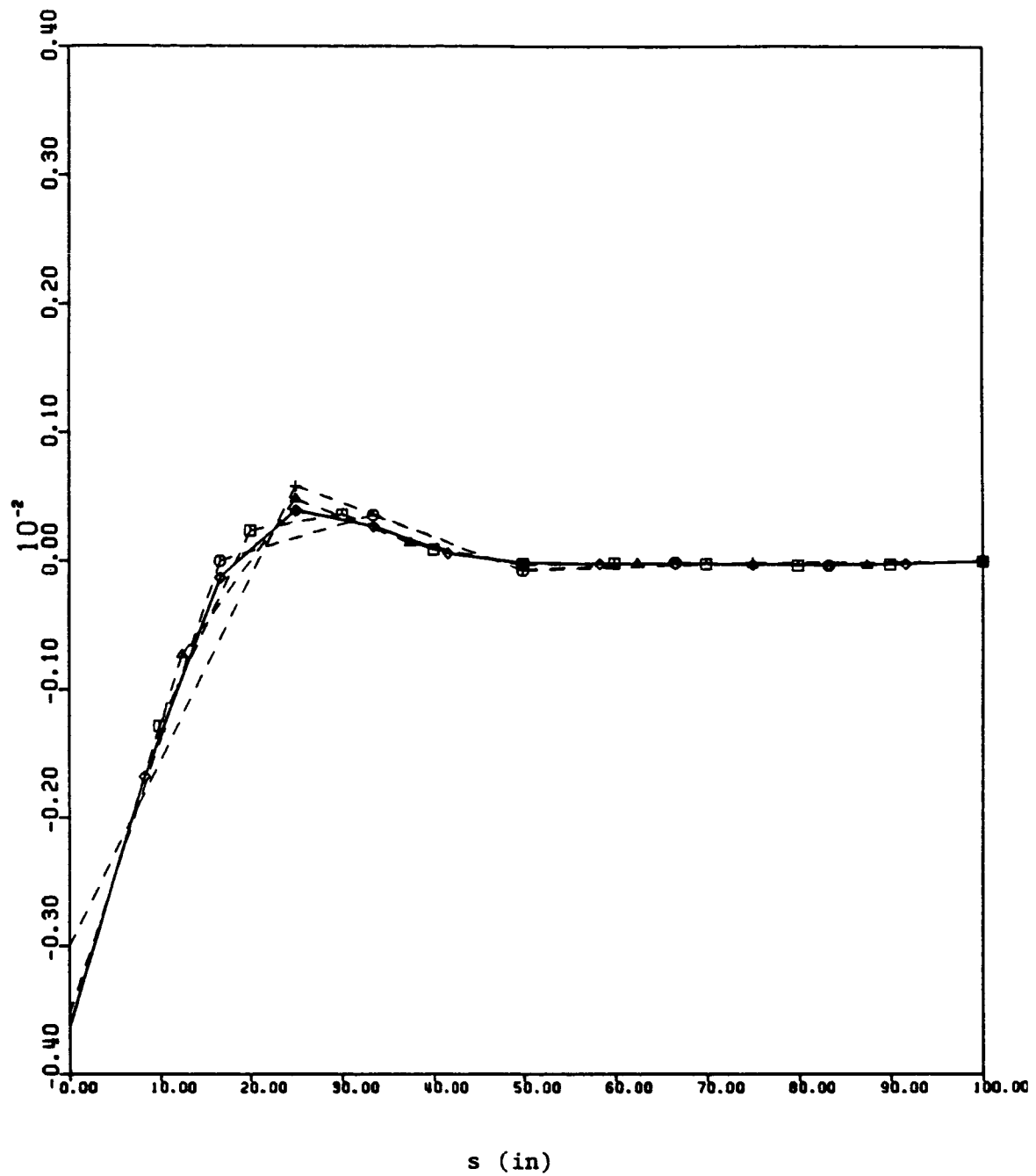


Figure 4-2a. Functional Control Gain Component ϕ''_{fn} Based on the B-splines. (+) $n_e=4$, (o) $n_e=6$, (Δ) $n_e=8$, (\boxplus) $n_e=10$.

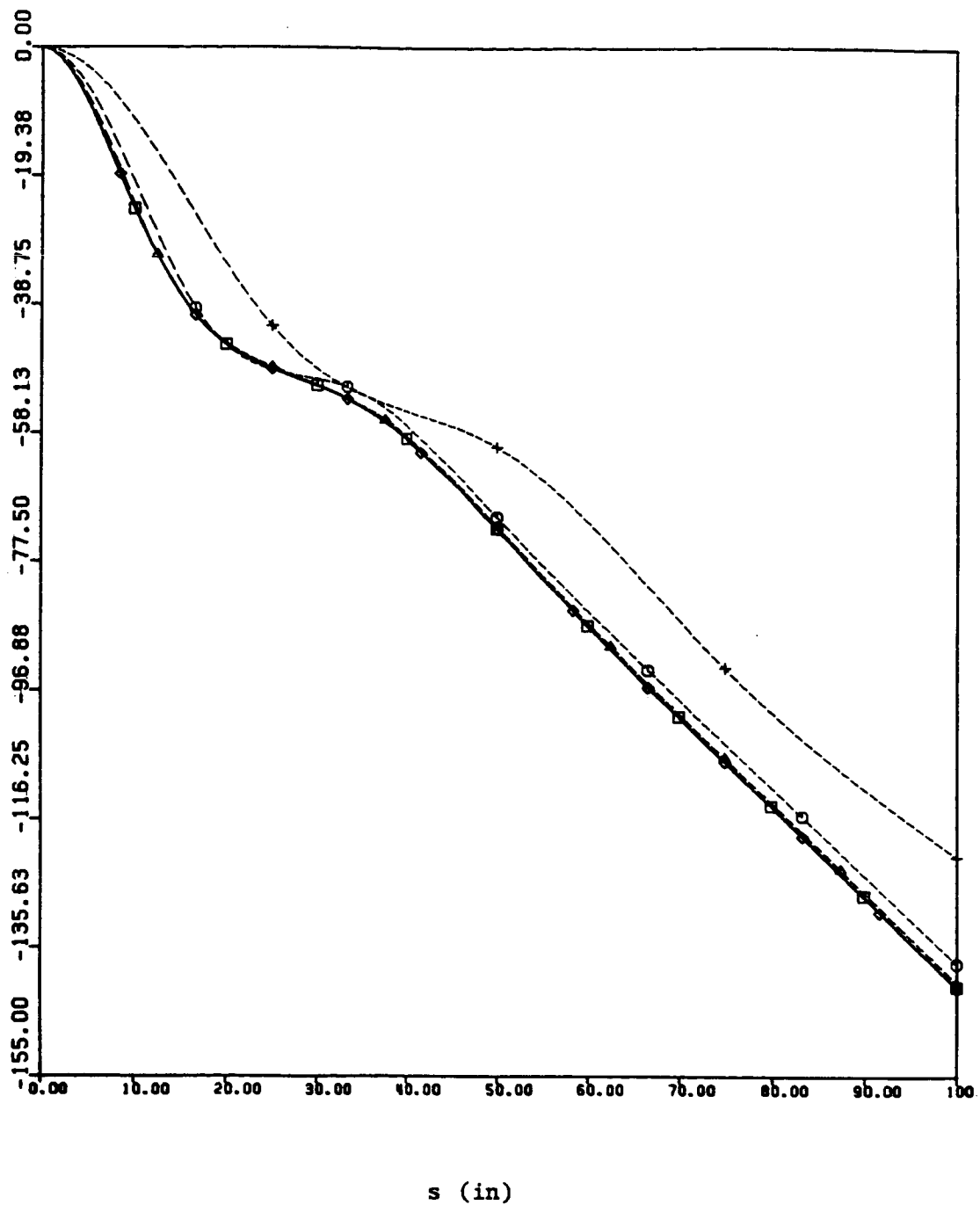


Figure 4-2b. Functional Control Gain Component ϕ_{gn} Based on the B-splines. (+) $n_e=4$, (o) $n_e=6$, (Δ) $n_e=8$, (\square) $n_e=10$.

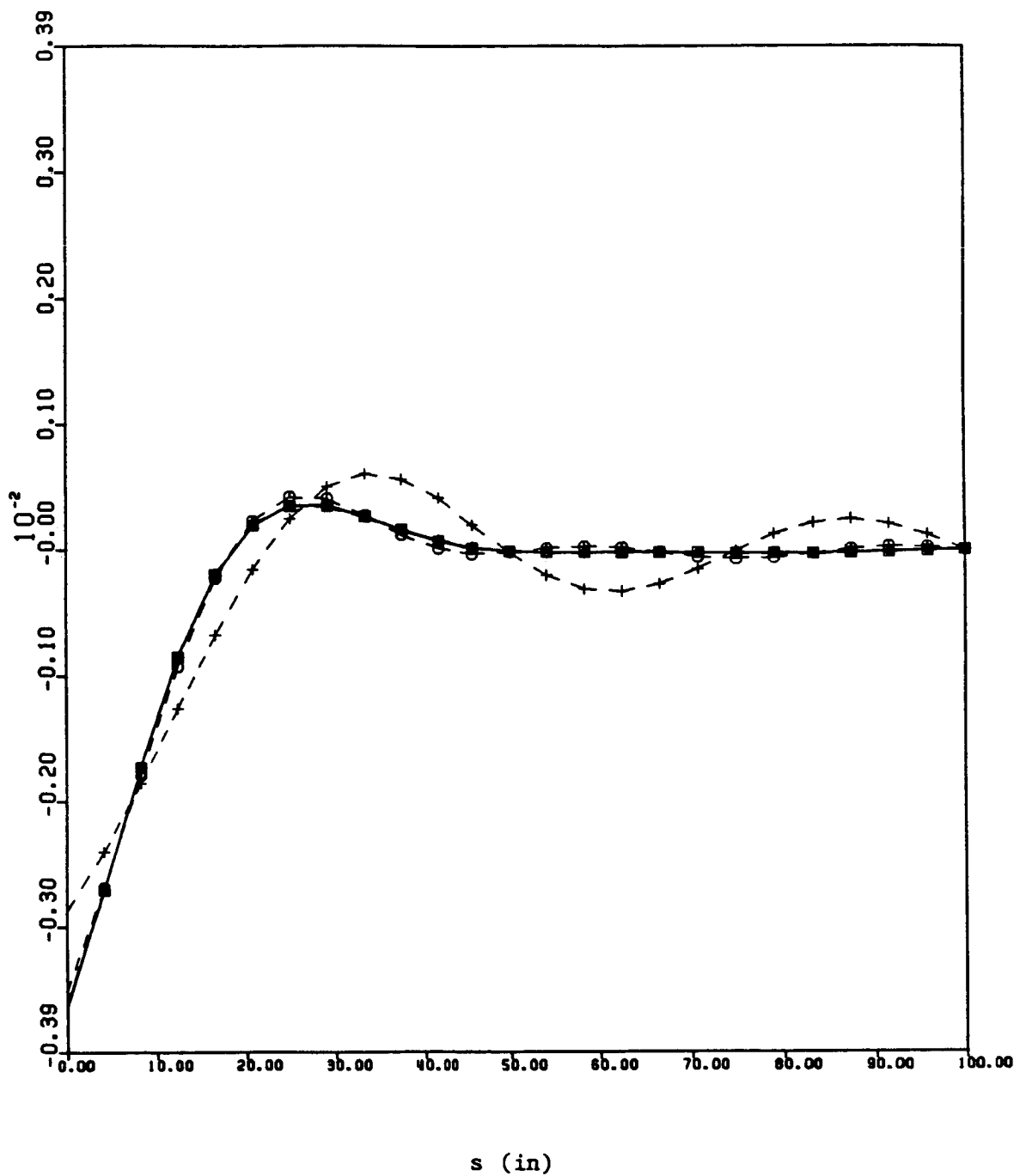


Figure 4-3a. Functional Control Gain Component ϕ_{fn}'' Based on the Normal Modes. (+) $n=5$, (o) $n=7$, (Δ) $n=9$, (\boxminus) $n=11$, (\diamond) $n=13$.

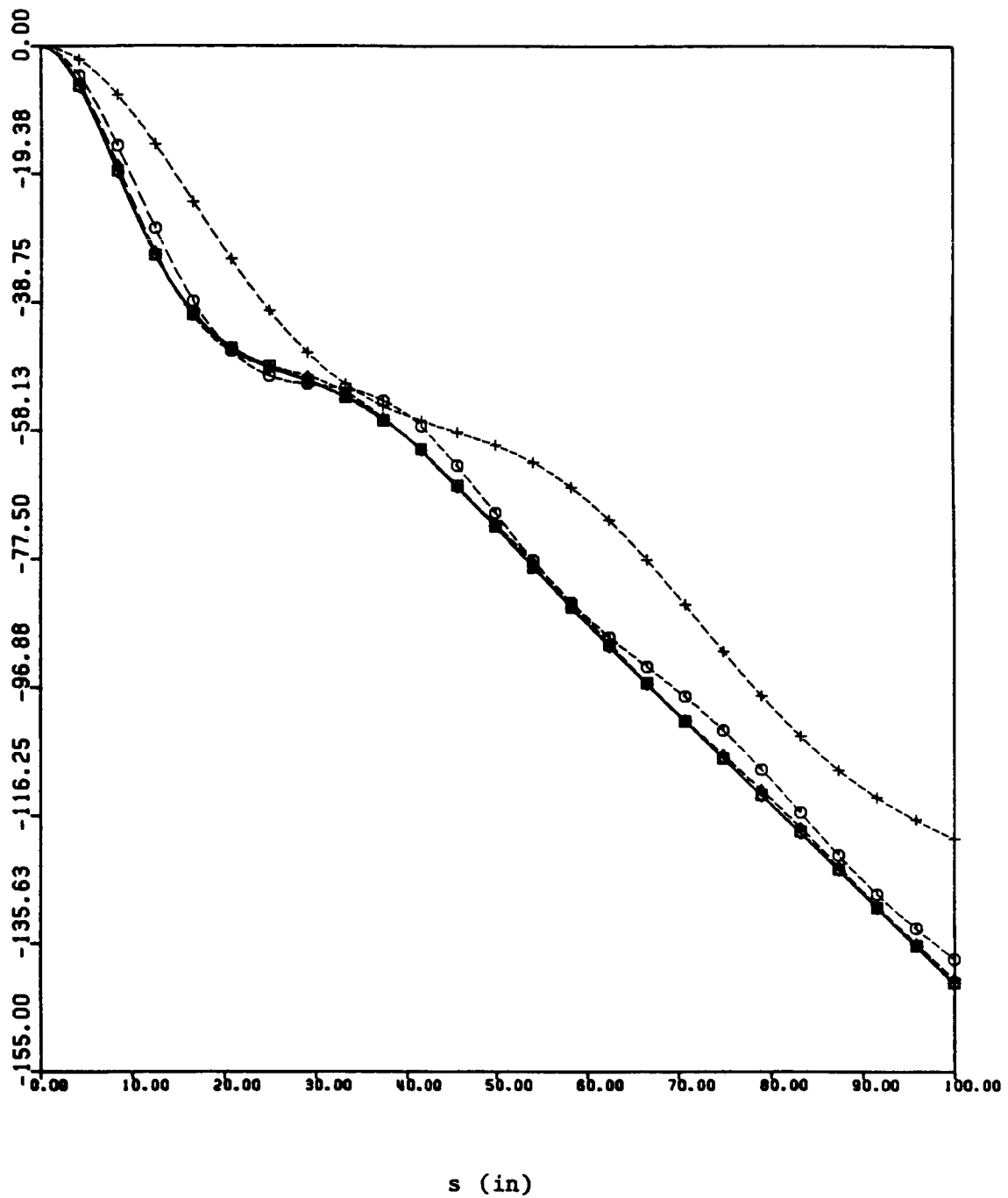


Figure 4-3b. Functional Control Gain Component ϕ_{gn} Based on the Normal Modes. (+) $n=5$, (o) $n=7$, (Δ) $n=9$, (\square) $n=11$, (\diamond) $n=13$.

Chapter V

SENSITIVITY OF CLOSED-LOOP EIGENVALUES AND ROBUSTNESS

5.1 First-Order Sensitivity of the Closed-Loop Eigenvalues

In Section 3.4 we assume that the plant is known exactly, so that the matrices A , B and C in the compensator are the same as those in the plant. Now we assume that the plant is a function of a parameter β , so that

$$A = A(\beta), \quad (5.1)$$

$$B = B(\beta), \quad (5.2)$$

$$C = C(\beta). \quad (5.3)$$

The compensator is designed for a nominal parameter value β_0 , and the closed-loop system is

$$\dot{z} = A_{cl}(\beta)z, \quad (5.4)$$

where the state $z(t)$ is a $4n$ -vector, and

$$A_{cl}(\beta) = \begin{bmatrix} A(\beta) & -B(\beta)F \\ GC(\beta) & [A(\beta_0) - B(\beta_0)F - GC(\beta_0)] \end{bmatrix}. \quad (5.5)$$

The gain matrices F and G are determined by some compensator design philosophy.

When $\beta = \beta_0$, we have the situation in Section 3.4. Here, we study the first-order sensitivity of the eigenvalues of $A_{cl}(\beta)$ with

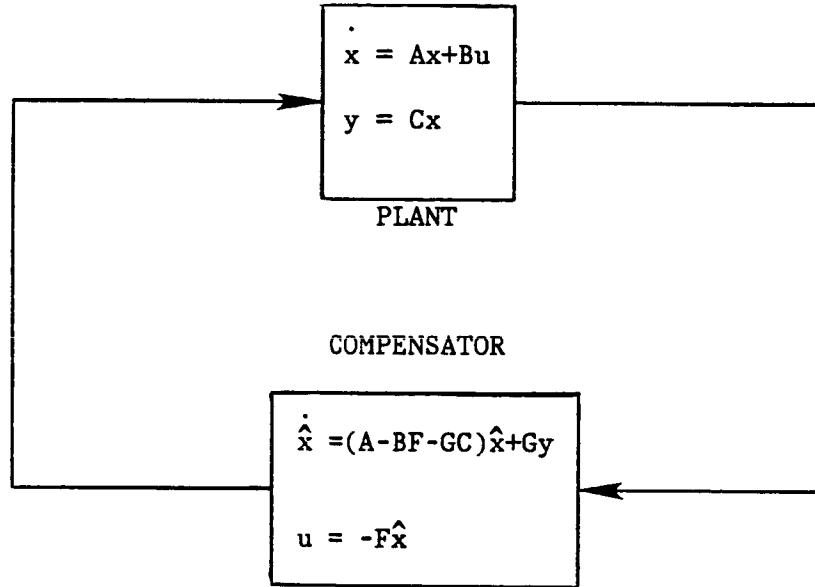


Figure 5-1. Closed-Loop System.

respect to an error between the true plant parameter β and the nominal value β_0 assumed for compensator design. By standard results [L1,P1,N1], we have

$$\Lambda_{cl\beta} = \text{diag}[Z^{-1}A_{cl\beta}Z], \quad (5.6)$$

where $\text{diag}[\cdot]$ means the diagonal matrix with the same diagonal elements, Λ_{cl} is the $4n \times 4n$ diagonal matrix containing the eigenvalues of A_{cl} , Z is the $4n \times 4n$ matrix whose columns are the eigenvectors of A_{cl} , and

$$A_{cl\beta} = \frac{\partial}{\partial \beta} A_{cl} = \begin{bmatrix} A_{\beta} & -B_{\beta}F \\ GC_{\beta} & 0 \end{bmatrix}. \quad (5.7)$$

The subscript β always indicates the partial derivative with respect to β . Using (3.51) and (3.52) for the nominal parameter value β_0 , we obtain

$$Z(\beta_0) = \begin{bmatrix} X_c & X_c \tilde{X} \\ X_c & [X_c \tilde{X} - X_e] \end{bmatrix}, \quad (5.8)$$

and

$$Z^{-1}(\beta_0) = \begin{bmatrix} [X_c^{-1} - \tilde{X} X_e^{-1}] & \tilde{X} X_e^{-1} \\ X_e^{-1} & -X_e^{-1} \end{bmatrix}, \quad (5.9)$$

where X_e is the $2n \times 2n$ matrix whose columns are the eigenvectors of $[A(\beta_0) - GC(\beta_0)]$, X_c is the $2n \times 2n$ matrix whose columns are the eigenvectors of $[A(\beta_0) - B(\beta_0)F]$, and the $2n \times 2n$ matrix \tilde{X} satisfies

$$\Lambda_c \tilde{X} - \tilde{X} \Lambda_e = -X_c^{-1} B(\beta_0) F X_e, \quad (5.10)$$

where Λ_e is the $2n \times 2n$ diagonal matrix containing the eigenvalues of $[A(\beta_0) - GC(\beta_0)]$ (estimator eigenvalues) and Λ_c is the $2n \times 2n$ diagonal matrix containing the eigenvalues of $[A(\beta_0) - B(\beta_0)F]$ (controller eigenvalues). We assume that the eigenvalues of $\Lambda_{cl}(\beta_0)$ are distinct, so that there exists a unique solution to (5.10). Note that the spectrum of $\Lambda_{cl}(\beta_0)$ is the union of the spectrum of $[A(\beta_0) - B(\beta_0)F]$ and the spectrum of $[A(\beta_0) - GC(\beta_0)]$. Carrying out the multiplication in

(5.6) yields

$$\begin{aligned} \Lambda_{cl\beta}(\beta_0) &= \frac{\partial}{\partial \beta} \Lambda_{cl}(\beta_0) \\ &= \text{diag} \begin{bmatrix} \Gamma_1 & 0 \\ 0 & \Gamma_2 \end{bmatrix} \end{aligned} \quad (5.11)$$

where

$$\begin{aligned} \Gamma_1 &= X_c^{-1} [A_\beta(\beta_0) - B_\beta(\beta_0)F] X_c \\ &\quad - \tilde{X} X_e^{-1} [A_\beta(\beta_0) - B_\beta(\beta_0)F - G C_\beta(\beta_0)] X_c \end{aligned} \quad (5.12)$$

and

$$\Gamma_2 = X_e^{-1} B_\beta(\beta_0) F X_e + X_e^{-1} [A_\beta(\beta_0) - B_\beta(\beta_0)F - G C_\beta(\beta_0)] X_c \tilde{X}. \quad (5.13)$$

5.2 Sensitive and Insensitive Control Designs

Consider the following Taylor series expansion of a closed-loop eigenvalue with respect to a parameter β

$$\lambda_{cl} = \lambda_{cl}(\beta_0) + \lambda_{cl\beta}(\beta_0)\delta\beta + \frac{1}{2}\lambda_{cl\beta\beta}(\beta_0)\delta\beta^2 + \dots \quad (5.14)$$

or

$$\begin{aligned} \delta\lambda_{cl} &= \lambda_{cl} - \lambda_{cl}(\beta_0) \\ &= \lambda_{cl\beta}(\beta_0)\delta\beta + \frac{1}{2}\lambda_{cl\beta\beta}(\beta_0)\delta\beta^2 + \dots \end{aligned} \quad (5.15)$$

where

$$\delta\beta = \beta - \beta_0, \quad (5.16)$$

and β_0 is the nominal value of β . For insensitive control designs, we want

$$\operatorname{Re}[\delta\lambda_{cl_j}(\beta_0)] = 0 \quad j = 1, \dots, 4n, \quad (5.17)$$

where $4n$ is the dimension of the A_{cl} matrix. Equation (5.11) represents the first partial derivatives of the closed-loop eigenvalues, and the second partial derivatives of the closed-loop eigenvalues follows from (A.17)

$$\lambda_{cl_j\beta\beta} = \frac{2 \sum_{\substack{i=1 \\ i \neq j}}^{4n} [y_j^T A_{cl\beta} z_i][y_i^T A_{cl\beta} z_j]}{[\lambda_{cl_i} - \lambda_{cl_j}]}, \quad j = 1, \dots, 4n, \quad (5.18)$$

where y_j is the left eigenvector corresponding to λ_{cl_j} and z_i is the right eigenvector corresponding to λ_{cl_i} . The objective of (5.17) can be obtained to a certain extent by following certain guidelines in the control design. In the following discussion, we drop the argument β_0 for convenience. Consider the following cases:

1. $\lambda_{c_i} \rightarrow \lambda_{ol_i}$ for $i = 1, \dots, 2n$.
2. $\lambda_{e_i} \rightarrow \lambda_{ol_i}$ for $i = 1, \dots, 2n$.
3. $|\lambda_{c_i} - \lambda_{e_j}| \rightarrow 0$ for some i and j where $i, j = 1, \dots, 2n$.
4. $|\lambda_{cl_i} - \lambda_{cl_j}| \rightarrow 0$ for some i and j , $i \neq j$ and $i, j = 1, \dots, 4n$.
5. $|\operatorname{Re}(\lambda_{cl_i})| \gg |\operatorname{Im}(\lambda_{cl_i})| \neq 0$ for some i , $i = 1, \dots, 4n$.

Where λ_{ol_i} is an eigenvalue of matrix A , λ_{c_i} is a controller eigenvalue, λ_{e_i} is an estimator eigenvalue, $\operatorname{Re}(\cdot)$ implies to the real part of a complex number and $\operatorname{Im}(\cdot)$ implies to the imaginary part of a complex number.

Case-1

$$\lambda_{c_i} \rightarrow \lambda_{ol_i} \quad \text{for } i = 1, \dots, 2n.$$

As the eigenvalues of $[A-BF]$ matrix (controller eigenvalues) converge to the eigenvalues of the open-loop system matrix A , the matrix product BF converges to the null matrix. Consider equation (5.10)

$$\tilde{\Lambda}_c \tilde{X} - \tilde{X} \tilde{\Lambda}_e = -\tilde{X}_c^{-1} B F \tilde{X}_e = 0. \quad (5.19)$$

For distinct closed-loop eigenvalues, (5.19) indicates that

$$\tilde{X} = 0. \quad (5.20)$$

In view of (5.20), (5.11) yields

$$\Lambda_{cl\beta} = \begin{bmatrix} \Lambda_c = \Lambda_{ol\beta} & 0 \\ 0 & 0 \end{bmatrix}, \quad (5.21)$$

where Λ_{ol} is the $2n \times 2n$ diagonal matrix containing the eigenvalues of matrix A .

Case-2

$$\lambda_{e_i} \rightarrow \lambda_{ol_i} \quad \text{for } i = 1, \dots, 2n.$$

As the eigenvalues of $[A-GC]$ matrix (estimator eigenvalues) converge to the eigenvalues of the open-loop system matrix A , the matrix product GC converges to the null matrix. Consider equation (5.10)

$$\tilde{\Lambda}_c \tilde{X} - \tilde{X} \tilde{\Lambda}_e = -\tilde{X}_c^{-1} B F \tilde{X}_e. \quad (5.22)$$

Adding identity to the right hand side, we obtain

$$\tilde{\Lambda}_c \tilde{X} - \tilde{X} \tilde{\Lambda}_e = -X_c^{-1} B F X_e + [X_c^{-1} A X_e - X_c^{-1} A X_e] \quad (5.23)$$

or

$$\tilde{\Lambda}_c \tilde{X} - \tilde{X} \tilde{\Lambda}_e = X_c^{-1} [A - B F] X_c [X_c^{-1} X_e] - [X_c^{-1} X_e] X_e^{-1} A X_e. \quad (5.24)$$

In view of (3.45) and (3.46), we see that

$$X_c^{-1} [A - B F] X_c = \Lambda_c, \quad (5.25)$$

$$X_e^{-1} A X_e = \Lambda_e = \Lambda_{ol}. \quad (5.26)$$

From (5.24) - (5.26), it follows that

$$\tilde{\Lambda}_c [\tilde{X} - X_c^{-1} X_e] - [\tilde{X} - X_c^{-1} X_e] \Lambda_e = 0. \quad (5.27)$$

For distinct closed-loop eigenvalues, (5.27) indicates that

$$\tilde{X} - X_c^{-1} X_e = 0 \quad (5.28)$$

or

$$\tilde{X} = X_c^{-1} X_e. \quad (5.29)$$

In view of (5.29), (5.11) yields

$$\Lambda_{cl\beta} = \begin{bmatrix} 0 & 0 \\ 0 & \Lambda_{e\beta} = \Lambda_{ol\beta} \end{bmatrix}. \quad (5.30)$$

Case-3

$$|\lambda_{c_i} - \lambda_{e_j}| \rightarrow 0 \quad \text{for some } i \text{ and } j \text{ where } i, j = 1, \dots, 2n.$$

Consider equation (5.10)

$$\Lambda_c \tilde{X} - \tilde{X} \Lambda_e = -X_c^{-1} B F X_e^\Delta = Q. \quad (5.31)$$

From (5.31), it follows that

$$\tilde{x}_{ij} = \frac{q_{ij}}{\lambda_{c_i} - \lambda_{e_j}} \quad \text{for } i, j = 1, \dots, 2n. \quad (5.32)$$

Equation (5.32) indicates that the i - j element of the matrix \tilde{X} approaches infinity like the reciprocal of the difference between the i^{th} controller eigenvalue and the j^{th} estimator eigenvalue, except in rare special circumstances. This element of \tilde{X} in general enters the derivative of each closed-loop eigenvalue, according to (5.11), and produces the large sensitivity when estimator eigenvalues are close to controller eigenvalues.

Case-4

$$|\lambda_{cl_i} - \lambda_{cl_j}| \rightarrow 0 \text{ for some } i \text{ and } j, i \neq j \text{ and } i, j = 1, \dots, 4n.$$

Equation (5.18) indicates that the second partial derivatives of the closed-loop eigenvalues approach infinity like the reciprocal of the difference between any two closed-loop eigenvalues, except in rare special circumstances. Therefore, as $|\lambda_{cl_i} - \lambda_{cl_j}| \rightarrow 0$ for some i and $j, i \neq j$, and $i, j = 1, \dots, 4n$, then

$$|\lambda_{cl_{k\beta\beta}}| \rightarrow \infty \quad \text{for } k = 1, \dots, 4n. \quad (5.33)$$

Note: If an eigenvalue is complex with a small imaginary part then

$$\frac{1}{|(\lambda_{cl} - \bar{\lambda}_{cl})|} = \frac{1}{2|\text{Im}(\lambda_{cl})|} = \text{large}. \quad (5.34)$$

Case-5

$$|\text{Re}(\lambda_{cl_i})| \gg |\text{Im}(\lambda_{cl_i})| \neq 0 \quad \text{for some } i, i = 1, \dots, 4n.$$

Consider the closed-loop state equation

$$A_{cl}z = \lambda_{cl}z. \quad (5.35)$$

Note that if λ_{cl} is a complex eigenvalue of the closed-loop system matrix, then $\bar{\lambda}_{cl}$ is also an eigenvalue. Which implies

$$A_{cl}\bar{z} = \bar{\lambda}_{cl}\bar{z}, \quad (5.36)$$

where $(\bar{\cdot})$ indicates complex conjugate. From (5.35) and (5.36), we see that

$$A_{cl} \bar{\gamma} = \sigma \bar{\gamma} - \omega \bar{\xi}, \quad (5.37)$$

$$A_{cl} \xi = \sigma \xi + \omega \gamma, \quad (5.38)$$

where

$$\lambda_{cl} = \sigma + j\omega, \quad (5.39)$$

$$z = \gamma + j\xi. \quad (5.40)$$

Note that (5.37) and (5.38) indicate that if

$$|\sigma| \gg |\omega|, \quad (5.41)$$

then γ and ξ become nearly linearly dependent. Which implies that

$$z^{-1} \rightarrow \infty. \quad (5.42)$$

In general, elements of matrix Z^{-1} enter the derivative of each closed-loop eigenvalue, according to (5.6), and produces the large sensitivity when closed-loop eigenvectors become nearly linearly dependent. Similarly, elements of X_c^{-1} and X_e^{-1} enter the derivative of each closed-loop eigenvalue, according to (5.11), and produces the large sensitivity when controller eigenvectors and/or estimator eigenvectors become nearly linearly dependent.

Guidelines

In summary, we present the following guidelines for less sensitive control designs:

1. For smaller first partial derivatives of the closed-loop eigenvalues, have

$$|\lambda_{c_i} - \lambda_{e_j}| \gg 0 \quad i, j = 1, \dots, 2n. \quad (5.43)$$

2. For smaller second partial derivatives of the closed-loop eigenvalues, have

$$|\lambda_{cl_i} - \lambda_{cl_j}| \gg 0 \quad i \neq j \text{ and } i, j = 1, \dots, 4n. \quad (5.44)$$

3. For less sensitive controller eigenvalues (eigenvalues of $[A(\beta_0) - B(\beta_0)F]$ matrix), have

$$|\lambda_{c_i}| > |\lambda_{e_i}| \quad i = 1, \dots, 2n. \quad (5.45)$$

4. For less sensitive observer eigenvalues (eigenvalues of $[A(\beta_0) - GC(\beta_0)]$ matrix), have

$$|\lambda_{e_i}| > |\lambda_{c_i}| \quad i = 1, \dots, 2n. \quad (5.46)$$

5. Keep the closed-loop, the controller and the estimator eigenvectors from becoming nearly linearly dependent.
6. Increase number of actuators and/or sensors.

The following section illustrates the effect of large eigenvalue-sensitivity and some of the above guidelines on robustness. Robustness means insensitivity of the closed-loop performance with respect to plant uncertainties.

5.3 Example

The structure in Figure 2-1 consists of a uniform Euler-Bernoulli beam cantilevered to a rigid hub at one end, with a point mass m_1 attached to the other end of the beam. The hub can rotate about its fixed center, point 0, and the control is a torque $u(t)$ applied to the hub. There are two sensors, which measure the rigid-body angle θ and the displacement of the point mass m_1 , $w(t, \ell)$.

In illustrating the effect of eigenvalue-sensitivity on robustness, we use a finite element model of the structure, constructed with three uniform beam elements and cubic B-splines as interpolation functions (see Sec. 2.3 and Chapter 4). Because cubic B-splines have continuous first and second derivatives, the three-element model of the structure in Figure 2-1 has four degrees of freedom, including the rigid-body mode.

We model Voigt-Kelvin viscoelastic damping in the beam, which means that the damping matrix is a constant times the stiffness matrix. We take the state vector $x(t)$ to represent the modal displacements and velocities of the three-element/four-mode model, so that the matrix A is

$$A(\beta) = \begin{bmatrix} 0 & I \\ -\beta\Omega^2 & -c_0\Omega^2 \end{bmatrix}, \quad (5.47)$$

where Ω is a 4×4 diagonal matrix containing the natural frequencies of the model, c_0 is the damping coefficient and β is an uncertain parameter with nominal value $\beta_0 = 1$. The first element of Ω is zero,

corresponding to the rigid-body mode. When we refer to the natural frequencies of the structure, we will mean the three nonzero elements of Ω only. We assume that the matrices B and C do not depend on β .

Of course, this model may not be sufficiently accurate for designing a compensator for the real structure. In [G3, G4, G5], we have studied the question of how accurate a finite element model is necessary for compensator design and how many modes must be represented in the estimator. While robustness with respect to truncation errors is as important as robustness with respect to parameter errors, we assume here that the three-element model is the structure, to illustrate best the effect on robustness of the eigenvalue-sensitivity discussed in the previous sections.

For our four-mode model of the structure, based on β_0 , we designed a family of linear-quadratic-gaussian (LQG) compensators (Sec. 3.3). The control gain for all compensators is computed with

$$\alpha_c = 0.2, \quad (5.48)$$

$$R_c = 0.01, \quad (5.49)$$

and Q_c such that

$$x^T Q_c x = 500\theta^2 + 2(\text{Total Energy}). \quad (5.50)$$

Total energy means kinetic energy plus elastic strain energy in the structure. The positive scalar α_c (added to the diagonal element of $A(\beta_0)$ in the algebraic matrix Riccati equation 3.27) guarantees that the eigenvalues of $[A(\beta_0) - BF]$ (the controller eigenvalues) have real

PARAMETER		VALUE	UNIT
hub radius	r	10	in
hub moment of inertia	I_o	10^2	slug.in ²
beam length	l	10^2	in
beam mass per unit length	m_b	10^{-2}	slug/in
2nd moment of cross sectional area	I	4/3	in ⁴
modulus of elasticity	E	10^4	slug/in.sec ²
damping coefficient	c_o	10^{-3}	
point mass	m_1	1	slug
fundamental frequency of undamped structure		0.967	rad/sec

Table 5-1. Structural Data.

parts to the left of $-\alpha_c$.

The compensators differ in the estimator gains, which are computed with

$$\alpha_e = \text{variable} = 0.0, 0.2, 0.4, \dots, 3.8, \quad (5.51)$$

$$R_e = \begin{bmatrix} 10 & 0 \\ 0 & 10 \end{bmatrix}, \quad (5.52)$$

$$Q_e = \begin{bmatrix} 0 & 0 \\ 0 & I \end{bmatrix}, \quad (5.53)$$

where each block in Q_e is a 4×4 matrix. The positive scalar α_e (added to the diagonal element of $A(\beta_0)$ in the algebraic matrix Riccati equation 3.30) guarantees that the eigenvalues of $[A(\beta_0) - GC]$ (the estimator eigenvalues) have real parts to the left of $-\alpha_e$. Note that each estimator is a Kalman-Bucy filter for the control system with A replaced by $[A(\beta_0) + I\alpha_e]$.

We designed twenty estimators for the values of α_e indicated in (5.51), and with each of these estimators, we formed the closed-loop matrix $A_{cl}(\beta)$ in (5.5) for a range of β 's. Our measure of robustness for a compensator is how much β can vary, from the nominal value of 1, before the closed-loop system becomes unstable; i.e., before some eigenvalue of $A_{cl}(\beta)$ has nonnegative real part. Figure 5-2 summarizes the results of the robustness test. The solid line connects the eigenvalues of $[A(\beta_0) - BF]$, which are the same for each compensator. (Only eigenvalues with positive imaginary parts are plotted.) For each compensator, a dashed line connects the eigenvalues of $[A(\beta_0) - GC]$, and the number above each of these estimator eigenvalue plots indicates the percent change in $\sqrt{\beta}$ (from the nominal value of 1) at which the closed-loop system with that compensator becomes unstable. We prefer to look at $\sqrt{\beta}$ because it represents the change in open-loop plant frequencies.

The compensators that place the estimator eigenvalues close to the controller eigenvalues produce a nonrobust closed-loop system, allowing no more than -11% modeling error in the natural frequencies. As the distance between estimator eigenvalues and controller eigenvalues increases, the robustness increases until the compensator will tolerate up to $\pm 22\%$ frequency error and maintain a stable closed-loop system. We have found that the most robust compensator represented in Figure 5-2 also will tolerate up to $\pm 22\%$ error in any one of the three plant frequencies when the others remain at their nominal values. It is important to note that the robustness increases as the estimator eigenvalues move away from the controller eigenvalues, even though the performance also increases in the sense that estimator errors decay at faster exponential rates. (Guideline number 1.)

Eventually, for $\alpha_e > 2.6$, the robustness starts to decrease again. Close examination of our numerical results indicates that the estimator eigenvectors approach linear dependence for the largest values of α_e , so that large terms enter the right sides of (5.12) and (5.13) in the matrix X_e^{-1} . This is another demonstration of the relationship between robustness and sensitivity of closed-loop eigenvalues with respect to parameter errors. (Guideline number 5.)

In general, as the real part of a conjugate pair of complex eigenvalues becomes large negatively, the corresponding conjugate pair of eigenvectors become nearly linearly dependent. In our

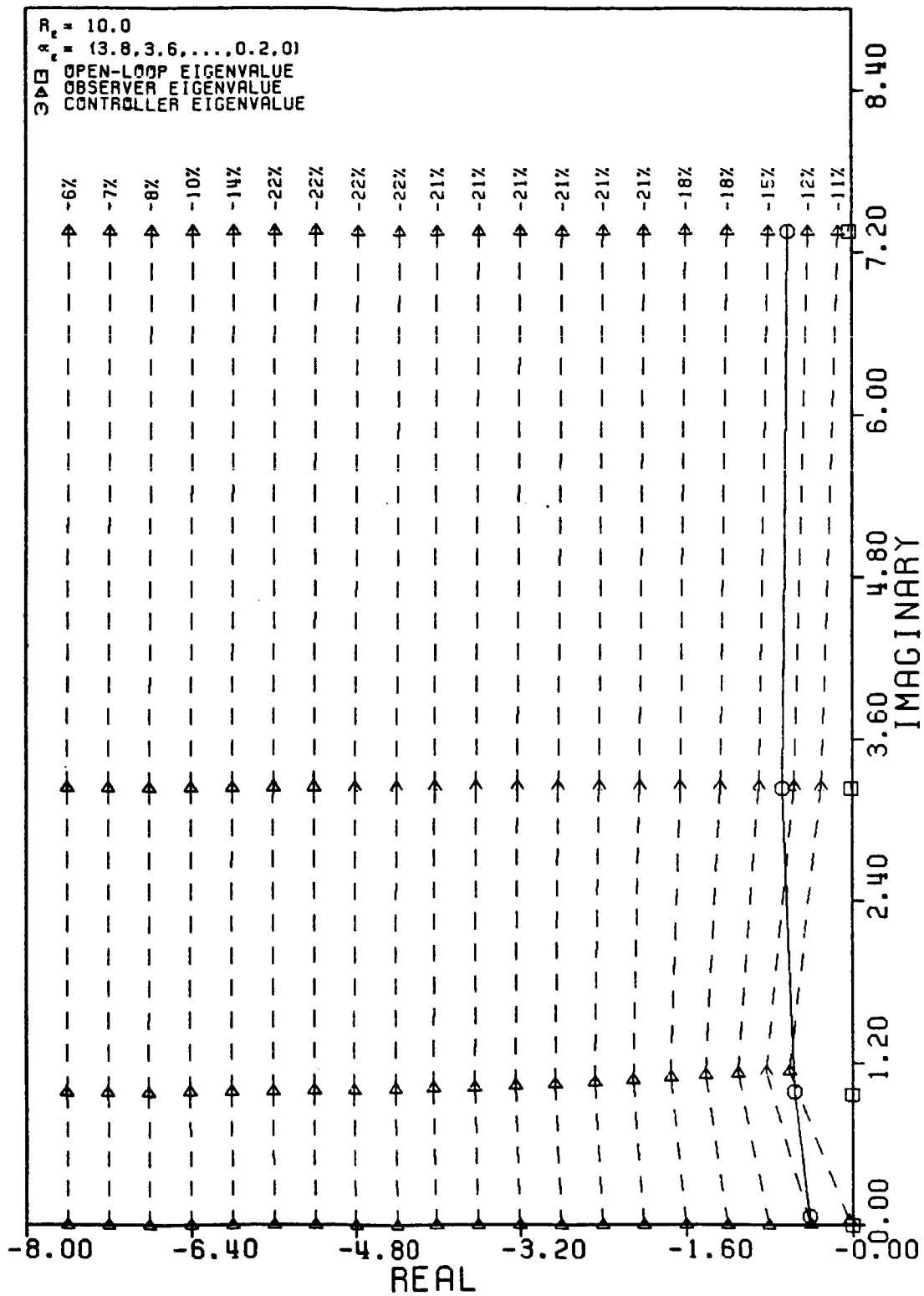


Figure 5-2. Robustness Test Results.

example, this happens first for the eigenvalues nearest the real axis, whose frequency is between 0.035 and 10^{-6} rather than zero, as the graph might suggest. And it happens to a lesser extent for the pair of eigenvalues with frequency approximately 1.

Another reason that the robustness cannot be improved more just by moving all of the estimator eigenvalues farther to the left is that the pairs of controller and estimator eigenvalues near the real axis cause large second-order sensitivity in the closed-loop eigenvalues. (Guideline number 2.) Note that second-order eigenvalue sensitivities with respect to the uncertain parameter involve the reciprocal of the difference of any two closed-loop eigenvalues.

To reduce both the first-order sensitivity produced by almost linearly dependent estimator eigenvectors and the second-order sensitivity produced by closed-loop eigenvalues near the real axis, we designed a new compensator with

$$\alpha_c = 0.02, \quad (5.54)$$

$$R_c = 1.0, \quad (5.55)$$

$$Q_c = \begin{bmatrix} 12 & 1.25 & 6.2 & 35 & 0 \\ \hline 0 & 0 & 0 & 0 & 0 \end{bmatrix} \times 1000, \quad (5.56)$$

$$\alpha_e = 0.25, \quad (5.57)$$

$$R_e = \begin{bmatrix} 1 & 0 \\ 0 & 1 \end{bmatrix}, \quad (5.58)$$

$$Q_e = \left[\begin{array}{cc|ccc} & & & & & \\ & 0 & & 0 & & \\ \hline & & & & & \\ & 0 & & 1 & 10 & 10 & 20 \end{array} \right] \times 100. \quad (5.59)$$

The resulting closed-loop eigenvalues are shown in Table 5-2. With this compensator, the closed-loop system first becomes unstable at $\sqrt{\beta} \approx -50\%$, as opposed to -22% for the most robust compensator represented in Figure 5-2.

Eigenvalues of $[A(\beta_0)-BF]$	Eigenvalues of $[A(\beta_0)-GC]$
$-0.4221 \pm i0.5805$	$-0.5347 \pm i0.1362$
$-0.5915 \pm i1.0571$	$-1.2888 \pm i2.2618$
$-0.6861 \pm i3.3011$	$-2.2686 \pm i5.7000$
$-0.6773 \pm i7.3835$	$-12.914 \pm i13.902$

Table 5-2. Closed-Loop Eigenvalues with Robust Compensator.

The above numerical results illustrate the significant effect that the closed-loop eigenvalue sensitivity derived in Section 1 has on robustness with respect to modeling errors. The results in Section 2 suggest and the example confirms that controller and estimator eigenvalues should be separated for a robust design. Almost linearly dependent estimator eigenvectors or controller eigenvectors and large second-order eigenvalue-sensitivity diminish robustness also.

In the example, we chose to move the estimator eigenvalues to the left of the controller eigenvalues. While such relative placement of controller and estimator eigenvalues is used frequently in compensator design so that the faster decaying estimator error will make the compensator approximate full-state feedback, we have seen no mention in the literature of the relationship demonstrated here between controller/estimator eigenvalue location and robustness. We have found that, to improve robustness by reducing closed-loop eigenvalue sensitivity, the eigenvalue separation may be achieved as well by placing some or all of the controller eigenvalues sufficiently to the left of nearby estimator eigenvalues or, not surprisingly, by separating imaginary parts of eigenvalues. This is important in controlling complex flexible structures, which often have lightly damped modes along with heavily damped modes, making it impractical to place all estimator eigenvalues to the left of all controller eigenvalues.

Although the analysis in the previous sections and the example deal with a single uncertain parameter, it should be clear that the results apply to any number of parameters. The formulas in Section 1 give the sensitivities of the closed-loop eigenvalues with respect to each parameter.

Chapter VI

SENSITIVITY OPTIMIZATION FOR FIXED STRUCTURE

Consider the following Taylor series expansion of an eigenvalue with respect to a parameter β

$$\lambda(\beta) = \lambda(\beta_0) + \lambda_{\beta}(\beta_0)\delta\beta + \frac{1}{2}\lambda_{\beta\beta}(\beta_0)\delta\beta^2 + \dots \quad (6.1)$$

or

$$\delta\lambda(\beta) \stackrel{\Delta}{=} \lambda(\beta) - \lambda(\beta_0) = \lambda_{\beta}(\beta_0)\delta\beta + \frac{1}{2}\lambda_{\beta\beta}(\beta_0)\delta\beta^2 + \dots, \quad (6.2)$$

where

$$\beta = \omega^2, \quad (6.3)$$

$$\delta\beta = \beta - \beta_0, \quad (6.4)$$

β_0 is the nominal value of β , and ω is a natural frequency. Using the chain-rule, equation (6.2) can be expanded in terms of ω as

$$\delta\lambda(\omega) = 2\omega_0^2\lambda_{\beta}(\beta_0)\varepsilon + [2\omega_0^4\lambda_{\beta\beta}(\beta_0) + \omega_0^2\lambda_{\beta}(\beta_0)]\varepsilon^2 + \dots, \quad (6.5)$$

where

$$\varepsilon = (\omega/\omega_0) - 1. \quad (6.6)$$

A closed-loop system is robust with respect to ω if

$$\operatorname{Re}[(\delta\lambda_{cl_j}(\omega))] \approx 0 \quad j = 1, \dots, 4n, \quad (6.7)$$

where $4n$ is the dimension of the closed-loop eigenvalue problem.

6.1 First-Order Sensitivity Optimization

Problem Statement

Find elements of the gain matrices F and G (design variables) that minimize the first-order sensitivities of the closed-loop eigenvalues with respect to plant uncertainties (natural frequencies), subject to eigenvalue constraints but no side constraints on design variables; i.e., choose F and G to minimize

$$J(F,G) = \left(\sum_{i=1}^{4n} [\gamma_i^2 |\operatorname{Re}(\nabla \lambda_{c_i})| \omega]^2 \right)^{\frac{1}{2}}, \quad (6.8)$$

subject to

$$\operatorname{Re}(\lambda_{c_i})^l \leq \max_i \operatorname{Re}(\lambda_{c_i}) \leq \operatorname{Re}(\lambda_{c_i})^u \quad i = 1, \dots, 2n, \quad (6.9)$$

$$\operatorname{Re}(\lambda_{e_i})^l \leq \max_i \operatorname{Re}(\lambda_{e_i}) \leq \operatorname{Re}(\lambda_{e_i})^u \quad i = 1, \dots, 2n, \quad (6.10)$$

$$\min_i |\operatorname{Im}(\lambda_{c_i})| \geq \operatorname{Im}(\lambda_{c_i})^l \quad i = 1, \dots, 2n, \quad (6.11)$$

$$\min_i |\operatorname{Im}(\lambda_{e_i})| \geq \operatorname{Im}(\lambda_{e_i})^l \quad i = 1, \dots, 2n. \quad (6.12)$$

In (6.8)-(6.12),

$$\nabla = \left[\frac{\partial}{\partial \beta_1} \dots \frac{\partial}{\partial \beta_n} \right], \quad (6.13)$$

$$\omega^T = [\omega_1^2 \dots \omega_n^2], \quad (6.14)$$

$$\beta_i = \omega_i^2, \quad (6.15)$$

and

F = $r \times 2n$ control gain matrix,

r = number of actuators,

n = number of structural modes used in compensator design,

$G = 2n \times m$ estimator gain matrix,

m = number of sensors (measurement),

$\lambda_{c_i} = i^{\text{th}}$ controller eigenvalue,

$\lambda_{e_i} = i^{\text{th}}$ estimator eigenvalue,

$\lambda_{cl_i} = i^{\text{th}}$ closed-loop eigenvalue,

$\omega_i = i^{\text{th}}$ uncertain plant parameter (natural frequencies),

$\gamma_i = i^{\text{th}}$ scalar weighting factor,

$\text{Re}(\cdot)$ = real part of a complex number,

$\text{Im}(\cdot)$ = imaginary part of a complex number,

$\max(\cdot)$ = maximum value,

$\min(\cdot)$ = minimum value,

$|\cdot|$ = absolute value,

$(\cdot)^l$ = lower bound,

$(\cdot)^u$ = upper bound,

$(\cdot)_0$ = nominal value.

In problems with a rigid-body mode, ω_1 is zero and we use only the sensitivities with respect to the nonzero frequencies in (6.8), so that $\frac{\partial}{\partial \beta_1}$ and ω_1^2 are not included in (6.13) and (6.14).

6.2 Second-Order Sensitivity Optimization

Problem Statement

Find elements of the gain matrices F and G (design variables) that minimize the second-order sensitivities of the closed-loop eigenvalues with respect to plant uncertainties (natural frequencies), subject to eigenvalue constraints but no side constraints on design variables; i.e., choose F and G to minimize

$$J(F,G) = \left\{ \sum_{i=1}^n [\gamma_i^2 |\operatorname{Re}(\nabla \lambda_{cl_i})| \omega + \Gamma_i [2\omega^T |\operatorname{Re}(H_i)| \omega + |\operatorname{Re}(\nabla \lambda_{cl_i})| \omega]^2] \right\}^{\frac{1}{2}}, \quad (6.16)$$

subject to

$$\operatorname{Re}(\lambda_{c_i})^l \leq \max_i \operatorname{Re}(\lambda_{c_i}) \leq \operatorname{Re}(\lambda_{c_i})^u \quad i = 1, \dots, 2n, \quad (6.17)$$

$$\operatorname{Re}(\lambda_{e_i})^l \leq \max_i \operatorname{Re}(\lambda_{e_i}) \leq \operatorname{Re}(\lambda_{e_i})^u \quad i = 1, \dots, 2n, \quad (6.18)$$

$$\min_i |\operatorname{Im}(\lambda_{c_i})| \geq \operatorname{Im}(\lambda_{c_i})^l \quad i = 1, \dots, 2n, \quad (6.19)$$

$$\min_i |\operatorname{Im}(\lambda_{e_i})| \geq \operatorname{Im}(\lambda_{e_i})^l \quad i = 1, \dots, 2n. \quad (6.20)$$

In (6.16),

H = hessian matrix,

Γ_i = scalar weighting factor.

Although we have some experience in this area, we have not been able to achieve significant improvement using the second-order sensitivity optimization compared to the first-order sensitivity optimization. The most robust designs are obtained by using small values of scalar weighting factors ($\Gamma_i < 0.1$, $i=1, \dots, 4n$) in the objective function (6.16). Close examination of our results indicates that there are considerable numerical errors involved in the second-order sensitivities of the closed-loop eigenvalues (5.18), which are due to the truncation errors in the closed-loop eigenvectors. It has been our experience that in minimizing the first-order sensitivities of the closed-loop eigenvalues with respect to natural frequencies, one also significantly reduces the second-order sensitivities of the closed-loop eigenvalues.

Because the second-order sensitivity optimization does not offer significant improvement in robustness compared to the first-order sensitivity optimization, and more efficient first-order sensitivity numerical optimization, only the first-order sensitivity optimization results are presented in the next section.

6.3 Example

Consider the structure shown in Figure 2-1. A uniform Euler-Bernoulli beam is cantilevered to a rigid hub at one end and a point mass m_1 is attached to the other end of the beam. The hub can rotate about its fixed center, point O, and the control is a torque $u(t)$ applied to the hub. There are two sensors, which measure the rigid body angle θ and the displacement of the point mass m_1 , $w(t, \ell)$.

In illustrating the effectiveness of first-order closed-loop eigenvalue-sensitivity optimization on robustness, we use a finite element model of the structure, constructed with ten identical beam elements and cubic B-splines as interpolation functions (see Sec. 2.3). Because cubic B-splines have continuous first and second derivatives, the ten-element model of the structure in Figure 2-1 has eleven degrees of freedom, including the rigid-body mode.

We model Voigt-Kelvin viscoelastic damping in the beam, which means that the damping matrix is a constant times the stiffness matrix. Table 6-1 shows the structural data used for the calculations. We take the state vector $x(t)$ to represent the first five modal displacements and velocities of the ten-element model, so that the matrix A is

$$A(\Omega) = \begin{bmatrix} 0 & I \\ -\Omega^2 & -c_0 \Omega^2 \end{bmatrix} \quad (6.21)$$

where Ω is a 5×5 diagonal matrix containing the natural frequencies (uncertain parameters) of the model, c_0 is the damping coefficient and

PARAMETER		VALUE	UNIT
hub radius	r	10	in
hub moment of inertia	I_o	10^2	slug.in ²
beam length	l	10^2	in
beam mass per unit length	m_b	10^{-2}	slug/in
2nd moment of cross sectional area	I	$4/3$	in ⁴
modulus of elasticity	E	5×10^4	slug/in.sec ²
damping coefficient	c_o	10^{-3}	
point mass	m_1	1	slug
fundamental frequency of undamped structure		2.159	rad/sec

Table 6-1 Structural Data.

Ω_o is a 5x5 diagonal matrix containing the nominal natural frequencies of the model. The first element of Ω is zero, corresponding to the rigid-body mode. When we refer to the natural frequencies of the structure, we will mean the four nonzero elements of Ω only. We assume that the matrices B and C do not depend on uncertain parameters. (See Eqn. 5.5).

For our five-mode model of the structure, based on the nominal values of the natural frequencies, we designed an initial linear-

quadratic-gaussian (LQG) compensators (see Sections 3.3 and 5.3) with

$$\alpha_c = 0.0, \quad (6.22)$$

$$R_c = 1.0, \quad (6.23)$$

$$Q_c = \begin{bmatrix} 8 & 5 & 10 & 100 & 1000 & 0 \\ \hline 0 & 0 & 0 & 0 & 0 & 0 \end{bmatrix} \times 1000, \quad (6.24)$$

$$\alpha_e = 0.3, \quad (6.25)$$

$$R_e = \begin{bmatrix} 1 & 0 \\ 0 & 1 \end{bmatrix}, \quad (6.26)$$

$$Q_e = \begin{bmatrix} 0 & 0 \\ 0 & 10 & 1 & 1 & 1 & 20 \end{bmatrix} \times 1000. \quad (6.27)$$

We take the gain matrices F and G of the initial compensator and use them as the initial guess in the first-order sensitivity optimization problem of Sec. 6.1. For this example, we have the 1×10 control gain matrix F and the 10×2 estimator gain matrix G , so that there are 30 (control) design variables. The scalar weighting factors and lower bounds and upper bounds in (6.8)-(6.12) are

$$\operatorname{Re}(\lambda_{c_i})^u = 0.95 \chi \operatorname{Re}[\lambda_{c_i}(F_0)] \quad i = 1, \dots, 2n, \quad (6.28)$$

$$\operatorname{Re}(\lambda_{e_i}^u) = -0.40 \quad i = 1, \dots, 2n, \quad (6.29)$$

$$\text{Im}(\lambda_{c_i})^L = 0.20 \quad i = 1, \dots, 2n, \quad (6.30)$$

$$\text{Im}(\lambda_{e_i})^L = 0.20 \quad i = 1, \dots, 2n, \quad (6.30)$$

$$\gamma_i = \max \left[\frac{1}{|\text{Re}(\lambda_{cl_i})|}, \frac{1}{|\text{Im}(\lambda_{cl_i})|} \right] \quad i = 1, \dots, 4n. \quad (6.31)$$

Note that (6.28) indicates that the magnitude of the real part of the controller eigenvalues can decrease by 5% only.

The optimum design was obtained by using the ADS optimizer (Ref. V2), where the sequential unconstrained minimization technique (SUMT) using the exterior penalty function method, and Broydon-Fletcher-Goldfarb-Shanno (BFGS) variable metric method for unconstrained minimization of pseudo-objective function (created by the exterior penalty function method) were selected, see [V1]. Also, the 30 design variables were scaled by the ADS program, and finite difference gradients were used in the optimization problem. Since there are considerably more truncation errors involved in evaluation of the closed-loop eigenvectors compared to the closed-loop eigenvalues, and the gradient of the objective function (6.8) involves the first-order sensitivity of the closed-loop eigenvectors with respect to the natural frequencies, the finite difference gradients result in better numerical optimization compared to the analytic gradients (see Appendix B). The optimization converges in 1 SUMT iteration which includes 22 unconstrained minimization (BFGS) iterations. Figure (6-1) shows the iteration history of the unconstrained minimization

(BFGS) where the objective function $J(F,G)$ (normalized with respect to its initial value 10.5998) is reduced by 82%. For the optimized design, only the constraint on the real part of the controller eigenvalues (6.9) is active. Table 6-2 lists the design variables of the initial and the optimized compensators. Table 6-3 and Figure 6-2 show the open-loop and the closed-loop eigenvalues of the initial and the optimized designs. In Figure 6-2, the dashed lines connect the eigenvalues of the initial design and the solid lines connect the eigenvalues of the optimized design.

Our measure of robustness for a compensator is how much the natural frequencies can vary, from their nominal values, before the closed-loop system becomes unstable; i.e., before some eigenvalue of A_{cl} has nonnegative real part. The robustness of the closed-loop eigenvalues was tested by varying the natural frequencies of the plant by a constant percentage times a variation factor (1,0 or -1 for each natural frequency), while maintaining the original damping of the plant and the original natural frequencies in the compensator. Tables 6-4 through 6-7 present the robustness test results of the full-state feedback and the closed-loop initial and optimized designs. (Full-state feedback means that the entire state vector is measured, so that no estimation is required in the closed-loop system.) Unless the term full-state feedback is emphasized, by closed-loop design or compensator we will mean a closed-loop design or a compensator which uses estimation. In each one of the robustness tables, each row represents nine full-state feedback or closed-loop designs where the

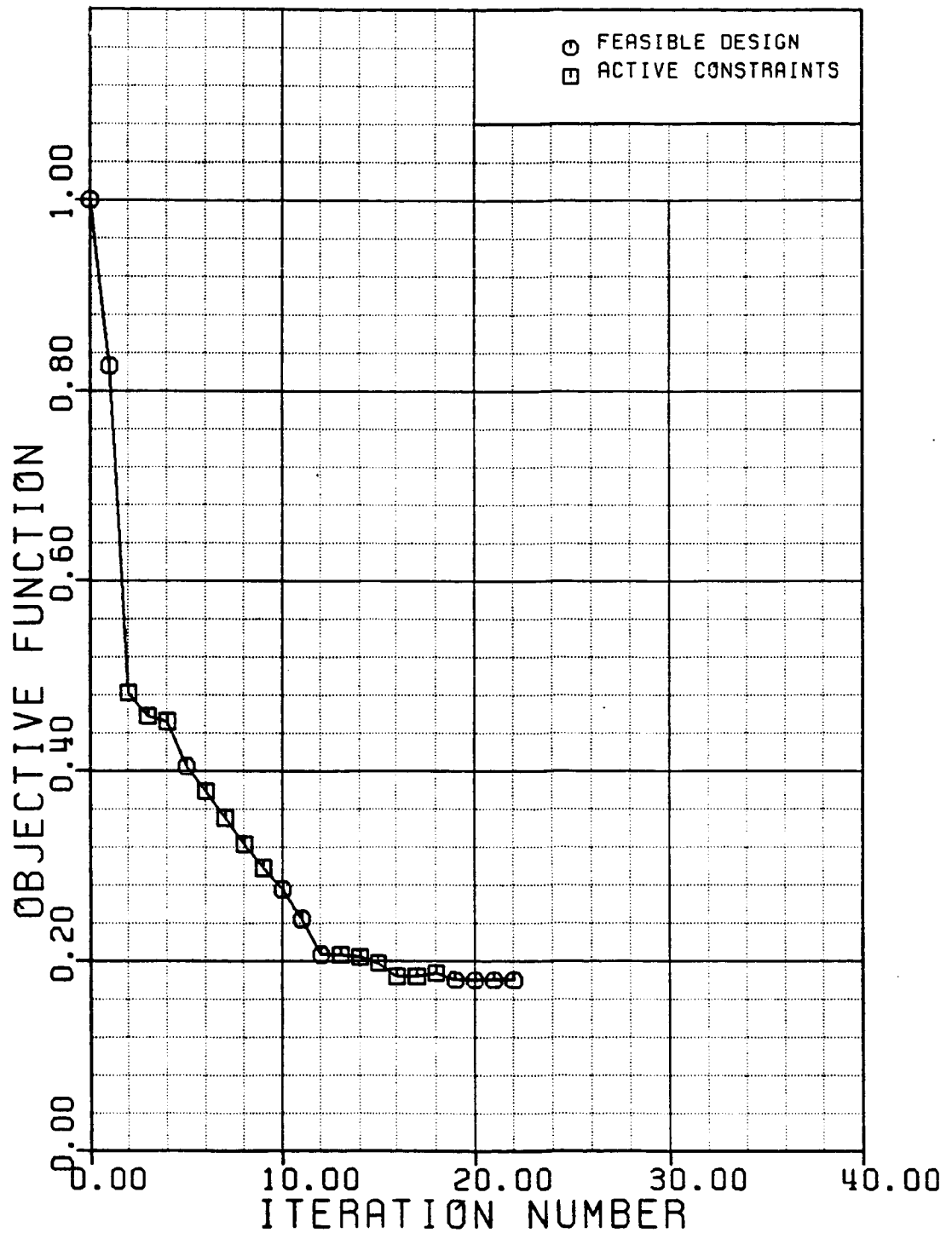


Figure 6-1 Iteration History of the unconstrained minimization (BFGS)

	INITIAL DESIGN			OPTIMIZED DESIGN		
j	F_{1j}	G_{j1}	G_{j2}	F_{1j}	G_{j1}	G_{j2}
1	89.443	247.57	0.7453	76.004	245.98	0.8780
2	-47.212	-0.0360	9.9207	-43.206	-0.0869	9.5176
3	-32.144	-0.0251	-0.3027	-122.42	-0.0811	0.1453
4	-56.023	-0.0028	0.0944	30.085	-0.0515	0.0741
5	-90.007	-0.0131	0.7929	-812.43	-0.0391	-0.8872
6	181.06	163.33	0.5014	185.84	165.15	0.6273
7	-24.205	-0.0593	27.796	-28.734	-0.0051	27.913
8	-12.242	-0.3045	35.710	-12.401	-0.2879	35.801
9	-15.444	-0.3024	34.285	-15.720	-0.2831	34.216
10	-17.147	-1.2148	136.14	-43.750	-1.2100	136.09

Table 6-2. Design Variables of the Initial and the Optimized Compensators.

natural frequencies of the plant were perturbed by a percentage (indicated by a percentage sign %) times a variation factor for each natural frequency (listed in the left portion of the tables). In these tables, "." indicates a stable design and "x" indicates an unstable design.

For the initial compensator, Table 6-4 indicates that the closed-loop system with full-state feedback becomes unstable for 50% variations in plant frequencies, and Table 6-6 shows that the closed-

loop system with the compensator becomes unstable for 20% variations in plant frequencies. For the optimized compensator, Table 6-5 shows that the closed-loop system with full-state feedback becomes unstable for 50% variations in plant frequencies, and Table 6-7 shows that the closed-loop system with the compensator becomes unstable for 60% variations in plant frequencies. This indicates a considerable improvement (factor of 3) compared to the robustness of the initial design. Note that the optimized compensator results in an unstable closed-loop system only when the variations in natural frequencies are such that the first and the second natural frequencies cross over. In addition, note that the robustness of the optimized design is better than the robustness of the full-state feedback initial and optimized designs. For each of the above robustness tests, there are 720 variations. That is

$$N = [n_1^{n_2} - 1]n_3, \quad (6.32)$$

where

$N = 720$ is the total number of variations,

$n_1 = 3$ is the number of variation factors (1, 0 or -1),

$n_2 = 4$ is the number of uncertain parameters,

$n_3 = 9$ is the number of variation percentages (10%, ..., 90%).

Table 6-8 summarizes the number of variations out of 720 which result in unstable designs.

In investigating robustness with respect to unmodeled modes, we connected the initial and the optimized five-mode compensators (one at

OPEN-LOOP EIGENVALUES	CLOSED-LOOP EIGENVALUES	
	CONTROLLER	ESTIMATOR
0.0	-0.5415±i0.5580	-0.9598±i0.5876
0.0		
-0.0023±i2.1583	-0.5721±i2.2293	-2.5932±i5.0472
-0.0258±i7.1826	-0.3937±i7.1932	-8.0933±i12.011
-0.1212±i15.567	-0.5001±i15.575	-3.9348±i15.290
-0.4208±i29.007	-0.7097±i29.012	-8.5054±i29.711

a) Initial Design.

OPEN-LOOP EIGENVALUES	CLOSED-LOOP EIGENVALUES	
	CONTROLLER	ESTIMATOR
0.0	-0.5437±i0.4447	-0.9536±i0.6092
0.0		
-0.0023±i2.1583	-0.5528±i2.1675	-2.2813±i5.0528
-0.0258±i7.1826	-0.4901±i7.5214	-8.4082±i10.656
-0.1212±i15.567	-0.4790±i15.448	-3.0969±i15.487
-0.4208±i29.007	-1.2052±i29.340	-6.7944±i33.110

b) Optimized Design.

Table 6-3. Open-Loop and Closed-Loop Eigenvalues of the Initial and the Optimized Designs of the 5-Mode Compensators.

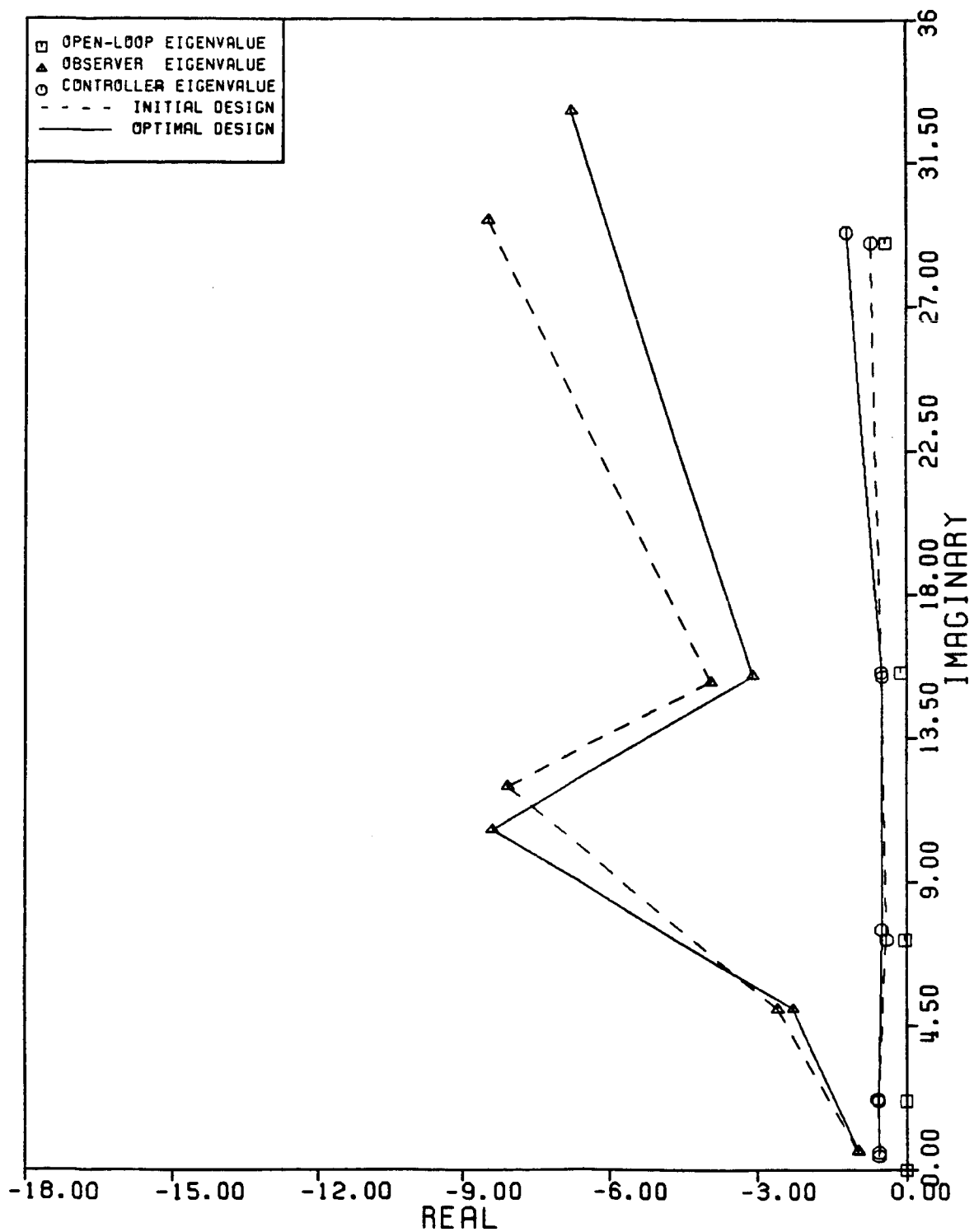


Figure 6-2. Open-Loop and Closed-Loop Eigenvalues of the Initial and the Optimized Designs of the 5-Mode Compensators.

NATURAL FREQUENCY VARIATION FACTORS				VARIATION PERCENTAGE								
ω_2	ω_3	ω_4	ω_5	10%	20%	30%	40%	50%	60%	70%	80%	90%
1	1	1	1
-1	1	1	1	x	x	x	x	x
1	-1	1	1	x
1	1	-1	1	x
1	1	1	-1
1	1	-1	-1	x
1	-1	1	-1	x
1	-1	-1	1	x
-1	-1	1	1	x	x	x	x	x
-1	1	-1	1	x	x	x	x	x
-1	1	1	-1	x	x	x	x	x
-1	-1	-1	-1	x	x	x	x	x
1	-1	-1	-1	x
-1	1	-1	-1	x	x	x	x	x
-1	-1	1	-1	x	x	x	x	x
-1	-1	-1	1	x	x	x	x	x
0	1	1	1
0	-1	1	1	x
0	1	-1	1	x
0	1	1	-1
0	-1	-1	-1	x
0	1	-1	-1	x
0	-1	1	-1	x
0	-1	-1	1	x
1	0	1	1
-1	0	1	1	x	x	x	x	x
1	0	-1	1	x
1	0	1	-1
-1	0	-1	-1	x	x	x	x	x
1	0	-1	-1	x
-1	0	1	-1	x	x	x	x	x
-1	0	-1	1	x	x	x	x	x
1	1	0	1
-1	1	0	1	x	x	x	x	x
1	-1	0	1	x
1	1	0	-1
-1	-1	0	-1	x	x	x	x	x
1	-1	0	-1	x
-1	1	0	-1	x	x	x	x	x
-1	-1	0	1	x	x	x	x	x

Table 6-4. Robustness Test Results of the Full-State Feedback Initial Design.

NATURAL FREQUENCY VARIATION FACTORS				VARIATION PERCENTAGE									
ω_2	ω_3	ω_4	ω_5	10%	20%	30%	40%	50%	60%	70%	80%	90%	
1	1	1	0	
-1	1	1	0	x	x	x	x	x	
1	-1	1	0	x	
1	1	-1	0	x	
-1	-1	-1	0	x	x	x	x	x	
1	-1	-1	0	x	
-1	1	-1	0	x	x	x	x	x	
-1	-1	1	0	x	x	x	x	x	
0	0	1	1	
0	0	1	-1	
0	0	-1	-1	x	
0	0	-1	1	x	
0	1	0	1	
0	1	0	-1	
0	-1	0	-1	x	
0	-1	0	1	x	
0	1	1	0	
0	1	-1	0	x	
0	-1	-1	0	x	
0	-1	1	0	x	
1	0	1	0	
1	0	-1	0	x	
-1	0	-1	0	x	x	x	x	x	
-1	0	1	0	x	x	x	x	x	
1	0	0	1	
1	0	0	-1	
-1	0	0	-1	x	x	x	x	x	
-1	0	0	1	x	x	x	x	x	
1	1	0	0	
1	-1	0	0	x	
-1	-1	0	0	x	x	x	x	x	
-1	1	0	0	x	x	x	x	x	
1	0	0	0	
0	1	0	0	
0	0	1	0	
0	0	0	1	
-1	0	0	0	x	x	x	x	x	
0	-1	0	0	x	
0	0	-1	0	x	
0	0	0	-1	

Table 6-4. (Cont.) Robustness Test Results of the Full-State Feedback Initial Design.

NATURAL FREQUENCY VARIATION FACTORS				VARIATION PERCENTAGE								
ω_2	ω_3	ω_4	ω_5	10%	20%	30%	40%	50%	60%	70%	80%	90%
1	1	1	1
-1	1	1	1	x	x	x	x	x
1	-1	1	1	x	.	x	x	x
1	1	-1	1
1	1	1	-1	x	x
1	1	-1	-1	x	x
1	-1	1	-1	x	.	x	x	x
1	-1	-1	1	x	.	x	x	x
-1	-1	1	1	x	x	x	x	x
-1	1	-1	1	x	x	x	x	x
-1	1	1	-1	x	x	x	x	x
-1	-1	-1	-1	x	x	x	x	x
1	-1	-1	-1	x	.	x	x	x
-1	1	-1	-1	x	x	x	x	x
-1	-1	1	-1	x	x	x	x	x
-1	-1	-1	1	x	x	x	x	x
0	1	1	1
0	-1	1	1	x	x	x	x
0	1	-1	1
0	1	1	-1	x
0	-1	-1	-1	x	x	x	x
0	1	-1	-1	x
0	-1	1	-1	x	x	x	x
0	-1	-1	1	x	x	x	x
1	0	1	1
-1	0	1	1	x	x	x	x	x
1	0	-1	1
1	0	1	-1	x	x
-1	0	-1	-1	x	x	x	x	x
1	0	-1	-1	x	x
-1	0	1	-1	x	x	x	x	x
-1	0	-1	1	x	x	x	x	x
1	1	0	1
-1	1	0	1	x	x	x	x	x
1	-1	0	1	x	.	x	x	x
1	1	0	-1	x	x
-1	-1	0	-1	x	x	x	x	x
1	-1	0	-1	x	.	x	x	x
-1	1	0	-1	x	x	x	x	x
-1	-1	0	1	x	x	x	x	x

Table 6-5. Robustness Test Results of the Full-State Feedback Optimized Design.

NATURAL FREQUENCY VARIATION FACTORS				VARIATION PERCENTAGE								
ω_2	ω_3	ω_4	ω_5	10%	20%	30%	40%	50%	60%	70%	80%	90%
1	1	1	0
-1	1	1	0	x	x	x	x	x
1	-1	1	0	x	.	x	x	x
1	1	-1	0
-1	-1	-1	0	x	x	x	x	x
1	-1	-1	0	x	.	x	x	x
-1	1	-1	0	x	x	x	x	x
-1	-1	1	0	x	x	x	x	x
0	0	1	1
0	0	1	-1	x
0	0	-1	-1	x
0	0	-1	1
0	1	0	1
0	1	0	-1	x
0	-1	0	-1	x	x	.	x
0	-1	0	1	x	x	.	x
0	1	1	0
0	1	-1	0
0	-1	-1	0	x	x	x	x
0	-1	1	0	x	x	x	x
1	0	1	0
1	0	-1	0
-1	0	-1	0	x	x	x	x	x
-1	0	1	0	x	x	x	x	x
1	0	0	1
1	0	0	-1	x	x
-1	0	0	-1	x	x	x	x	x
-1	0	0	1	x	x	x	x	x
1	1	0	0
1	-1	0	0	x	.	x	x	x
-1	-1	0	0	x	x	x	x	x
-1	1	0	0	x	x	x	x	x
1	0	0	0
0	1	0	0
0	0	1	0
0	0	0	1
-1	0	0	0	x	x	x	x	x
0	-1	0	0	x	x	x	x
0	0	-1	0
0	0	0	-1	x

Table 6-5. (Cont.) Robustness Test Results of the Full-State Feedback Optimized Design.

NATURAL FREQUENCY VARIATION FACTORS				VARIATION PERCENTAGE								
ω_2	ω_3	ω_4	ω_5	10%	20%	30%	40%	50%	60%	70%	80%	90%
1	1	1	1	x	.	.
-1	1	1	1	x	x	x
1	-1	1	1	.	x	x	x	x	x	x	.	.
1	1	-1	1	x	.	.
1	1	1	-1	x	.	.
1	1	-1	-1	x	.	.
1	-1	1	-1	.	x	x	x	x	x	x	.	.
1	-1	-1	1	.	x	x	x	x	x	x	x	x
-1	-1	1	1	.	x	x	x	x	.	.	.	x
-1	1	-1	1	x	x	x
-1	1	1	-1	x	x	x
-1	-1	-1	-1	.	x	x	x	x	.	x	.	x
1	-1	-1	-1	.	x	x	x	x	x	x	.	x
-1	1	-1	-1	x	x	x
-1	-1	1	-1	.	x	x	x	x	.	.	.	x
-1	-1	-1	1	.	x	x	x	x	.	x	.	x
0	1	1	1	x	.	.
0	-1	1	1	.	x	x	x	x	.	.	x	x
0	1	-1	1	x	.	.
0	1	1	-1	x	.	.
0	-1	-1	-1	.	x	x	x	x	.	x	x	x
0	1	-1	-1	x	.	.
0	-1	1	-1	.	x	x	x	x	.	.	x	x
0	-1	-1	1	.	x	x	x	x	.	x	x	x
1	0	1	1
-1	0	1	1	x	x
1	0	-1	1
1	0	1	-1
-1	0	-1	-1	x	x
1	0	-1	-1
-1	0	1	-1	x	x
-1	0	-1	1	x	x
1	1	0	1	x	.	.
-1	1	0	1	x	.	.
1	-1	0	1	.	x	x	x	x	x	x	x	x
1	1	0	-1	x	.	.
-1	-1	0	-1	.	x	x	x	x	.	.	.	x
1	-1	0	-1	.	x	x	x	x	x	x	.	.
-1	1	0	-1	x	x	x
-1	-1	0	1	.	x	x	x	x	.	.	.	x

Table 6-6. Robustness Test Results of the Initial 5-Mode Compensator.

NATURAL FREQUENCY VARIATION FACTORS				VARIATION PERCENTAGE								
ω_2	ω_3	ω_4	ω_5	10%	20%	30%	40%	50%	60%	70%	80%	90%
1	1	1	0	x	.	.
-1	1	1	0	x	x	x
1	-1	1	0	.	x	x	x	x	x	x	.	.
1	1	-1	0	x	.	.
-1	-1	-1	0	.	x	x	x	x	.	x	.	x
1	-1	-1	0	.	x	x	x	x	x	x	x	.
-1	1	-1	0	x	x	x
-1	-1	1	0	.	x	x	x	x	.	.	.	x
0	0	1	1
0	0	1	-1
0	0	-1	-1
0	0	-1	1
0	1	0	1	x	.	.
0	1	0	-1	x	.	.
0	-1	0	-1	.	x	x	x	x	.	.	x	x
0	-1	0	1	.	x	x	x	x	.	.	x	x
0	1	1	0	x	.	.
0	1	-1	0	x	.	.
0	-1	-1	0	.	x	x	x	x	.	x	x	x
0	-1	1	0	.	x	x	x	x	.	.	x	x
1	0	1	0
1	0	-1	0
-1	0	-1	0	x	x
-1	0	1	0	x	x
1	0	0	1
1	0	0	-1
-1	0	0	-1	x	x
-1	0	0	1	x	x
1	1	0	0	x	.	.
1	-1	0	0	.	x	x	x	x	x	x	.	.
-1	-1	0	0	.	x	x	x	x	.	.	.	x
-1	1	0	0	x	x	x
1	0	0	0
0	1	0	0	x	.	.
0	0	1	0
0	0	0	1
-1	0	0	0	x	x
0	-1	0	0	.	x	x	x	x	.	.	x	x
0	0	-1	0
0	0	0	-1

Table 6-6. (Cont.) Robustness Test Results of the Initial 5-Mode Compensator.

NATURAL FREQUENCY VARIATION FACTORS				VARIATION PERCENTAGE								
ω_2	ω_3	ω_4	ω_5	10%	20%	30%	40%	50%	60%	70%	80%	90%
1	1	1	1
-1	1	1	1
1	-1	1	1	x	.	.	.
1	1	-1	1
1	1	1	-1
1	1	-1	-1
1	-1	1	-1	x	.	.	.
1	-1	-1	1	x	.	.	.
-1	-1	1	1
-1	1	-1	1
-1	1	1	-1
-1	-1	-1	-1
1	-1	-1	-1	x	.	.	.
-1	1	-1	-1
-1	-1	1	-1
-1	-1	-1	1
0	1	1	1
0	-1	1	1	x	x
0	1	-1	1
0	1	1	-1
0	-1	-1	-1	x	x
0	1	-1	-1
0	-1	1	-1	x	x
0	-1	-1	1	x	x
1	0	1	1
-1	0	1	1
1	0	-1	1
1	0	1	-1
-1	0	-1	-1
1	0	-1	-1
-1	0	1	-1
-1	0	-1	1
1	1	0	1
-1	1	0	1
1	-1	0	1	x	.	.	.
1	1	0	-1
-1	-1	0	-1
1	-1	0	-1	x	.	.	.
-1	1	0	-1
-1	-1	0	1

Table 6-7. Robustness Test Results of the Optimized 5-Mode Compensator.

NATURAL FREQUENCY VARIATION FACTORS				VARIATION PERCENTAGE								
ω_2	ω_3	ω_4	ω_5	10%	20%	30%	40%	50%	60%	70%	80%	90%
1	1	1	0
-1	1	1	0
1	-1	1	0	x	.	.	.
1	1	-1	0
-1	-1	-1	0
1	-1	-1	0	x	.	.	.
-1	1	-1	0
-1	-1	1	0
0	0	1	1
0	0	1	-1
0	0	-1	-1
0	0	-1	1
0	1	0	1
0	1	0	-1
0	-1	0	-1	x	x
0	-1	0	1	x	x
0	1	1	0
0	1	-1	0
0	-1	-1	0	x	x
0	-1	1	0	x	x
1	0	1	0
1	0	-1	0
-1	0	-1	0
-1	0	1	0
1	0	0	1
1	0	0	-1
-1	0	0	-1
-1	0	0	1
1	1	0	0
1	-1	0	0
-1	-1	0	0	x	.	.	.
-1	1	0	0
1	0	0	0
0	1	0	0
0	0	1	0
0	0	0	1
-1	0	0	0
0	-1	0	0
0	0	-1	0	x	x
0	0	0	-1
0	0	0	-1

Table 6-7. (Cont.) Robustness Test Results of the Optimized 5-Mode Compensator.

DESIGN	NUMBER OF UNSTABLE VARIATIONS FROM 720
initial full-state feedback	165
optimized full-state feedback	223
initial closed-loop (compensator)	226
optimized closed-loop (compensator)	27

Table 6-8. Number of Variations which Result in Unstable Designs.

a time) to the eleven-mode plant, and performed the robustness test by varying first four natural frequencies of the plant by a constant percentage times a variation factor (1,0 or -1 for each natural frequency), while maintaining the original damping of the plant and the original natural frequencies in the compensator. For the initial compensator, the results of the robustness test are identical to those of Table 6-6. For the optimized compensator, the results of the robustness test are identical to the results in Table 6-7. These robustness tests indicate that for this example the robustness of the initial and the optimized compensators are insensitive to the unmodeled modes, which is partially due to well separated natural frequencies of the eleven-mode plant.

In comparing the performance of the initial and the optimized compensators, we use the performance index discribed in Section 3.1, repeated here for convenience

$$J_p = \int_0^{\infty} [x^T(t)Q_c x(t) + u^T(t)R_c u(t)] dt. \quad (6.33)$$

From (6.33), we see that

$$J_p = J_x + J_u, \quad (6.34)$$

where

$$J_x = \int_0^{\infty} [x^T(t) Q_c x(t)] dt, \quad (6.35)$$

$$J_u = \int_0^{\infty} [u^T(t) R_c u(t)] dt. \quad (6.36)$$

J_x is the quantity we wish to control and J_u is the control effort.

In general, smaller values of J_x for a given initial condition indicate that the initial state converges faster to the origin (zero state). However, as indicated by Tables 6-10 and 6-12 and Figure 6-3, this is not always the case. Tables 6-9 through 6-12 show the performances of the initial and the optimized compensators for various initial conditions. For the initial compensator, Table 6-9 shows the performance of the initial five-mode compensator connected to the five-mode plant, and Table 6-10 shows the performance of the initial five-mode compensator connected to the eleven-mode plant. (In evaluating the performance of a five mode compensator connected to an eleven-mode plant, the terms in matrix Q_c corresponding to the additional plant modes are zero.) Note that Tables 6-9 and 6-10 indicate that the performance of the initial compensator is insensitive to the unmodeled modes.

For the optimized compensator, Table 6-11 shows the performance of the optimized five-mode compensator connected to the five-mode plant, and Table 6-12 shows the performance of the optimized five-mode

compensator connected to the eleven-mode plant. These tables indicate that the performance of the optimized compensator is insensitive to the unmodeled modes.

Figures (6-3) - (6-8) show the response of the rigid-body angle $\theta(t)$ and the control $u(t)$ for various initial conditions. (All plots have been scaled such that $\theta(0)=1$.) In each Figure, the dashed lines represent the time histories corresponding to the initial compensator connected to the eleven-mode plant, and the solid lines represent the time histories corresponding to the optimized compensator connected to the eleven-mode plant. (For the initial and the optimized designs, the time histories of the 5-mode plants connected to the 5-mode compensators coincide with those shown in Figures 6-3 through 6-9.) For the initial design, Figure 6-3 shows that the settling time of the rigid-body angle is 10.05 seconds, which is 3.45 times the period of the first flexible open-loop mode ($T_2=2.91$ seconds). For the optimized design, Figure 6-3 shows that the settling time of the rigid-body angle is 6.80 seconds, which is 2.34 times the period of the first flexible open-loop mode ($T_2=2.91$ seconds). (The settling time is the time required for the response curve to reach and stay within $\pm 5\%$ of its initial value.) Note that the overshoot present in the rigid-body angle response is partially due to the tip mass m_1 which is as heavy as the initial beam; i.e. $m_1 = 1$ slug. Although we have improved the robustness of the initial design by factor of three, Tables 6-10 and 6-12 indicate and Figures 6-3 through 6-8 confirm that

there is no significant difference in the performances (value of J_x)
of the optimized and the initial compensators.

INITIAL CONDITION OF THE STRUCTURE	INITIAL CONDITION OF THE ESTIMATOR	COST $\times 10^{-8}$		
		J_p	J_x	J_u
1st mode	1st mode	2.6937	2.3111	0.3826
1st mode	0	4.8392	3.5551	1.2841
2nd mode	0	0.0702	0.0302	0.0400
3rd mode	0	0.0702	0.0275	0.0427
4th mode	0	0.4195	0.2848	0.1347
5th mode	0	4.2116	3.5246	0.6870

Table 6-9. Performance of the 5-Mode Initial Compensator Connected to the 5-Mode Plant for Various Initial Conditions.

INITIAL CONDITION OF THE STRUCTURE	INITIAL CONDITION OF THE ESTIMATOR	COST $\times 10^{-8}$			RESPONSE OF THE RIGID-BODY ANGLE
		J_p	J_x	J_u	
1st mode	1st mode	2.6937	2.3113	0.3824	Fig. 6-3
1st mode	0	4.8392	3.5555	1.2837	Fig. 6-4
2nd mode	0	0.0699	0.0302	0.0397	Fig. 6-5
3rd mode	0	0.0700	0.0275	0.0425	Fig. 6-6
4th mode	0	0.4193	0.2849	0.1344	Fig. 6-7
5th mode	0	4.2121	3.5275	0.6846	Fig. 6-8

Table 6-10. Performance of the 5-Mode Initial Compensator Connected to the 11-Mode Plant for Various Initial Conditions.

INITIAL CONDITION OF THE STRUCTURE	INITIAL CONDITION OF THE ESTIMATOR	COST $\times 10^{-8}$		
		J_p	J_x	J_u
1st mode	1st mode	2.7757	2.5227	0.2530
1st mode	0	4.4691	3.4190	1.0501
2nd mode	0	0.2242	0.0310	0.1932
3rd mode	0	0.2055	0.0219	0.1836
4th mode	0	0.6307	0.2005	0.4302
5th mode	0	6.2618	2.3757	3.8861

Table 6-11. Performance of the 5-Mode Optimized Compensator Connected to the 5-Mode Plant for Various Initial Conditions.

INITIAL CONDITION OF THE STRUCTURE	INITIAL CONDITION OF THE ESTIMATOR	COST $\times 10^{-8}$			RESPONSE OF THE RIGID-BODY ANGLE
		J_p	J_x	J_u	
1st mode	1st mode	2.7758	2.5229	0.2529	Fig. 6-3
1st mode	0	4.4690	3.4193	1.0497	Fig. 6-4
2nd mode	0	0.2180	0.0309	0.1871	Fig. 6-5
3rd mode	0	0.2002	0.0218	0.1784	Fig. 6-6
4th mode	0	0.6221	0.2002	0.4219	Fig. 6-7
5th mode	0	6.2174	2.4009	3.8165	Fig. 6-8

Table 6-12. Performance of the 5-Mode Optimized Compensator Connected to the 11-Mode Plant for Various Initial Conditions.

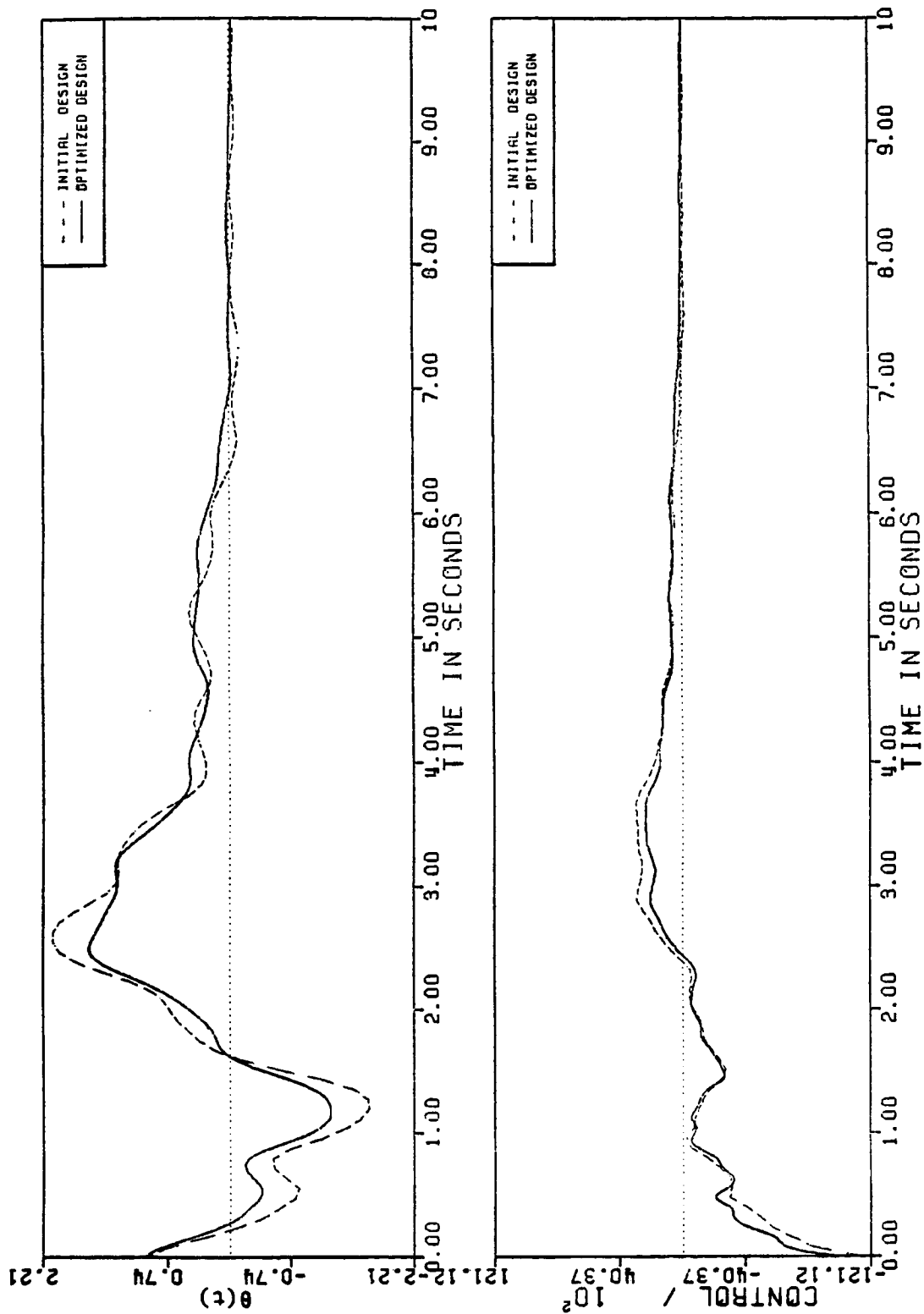


Figure 6-3. Time Histories of the Rigid-Body Angle and the Hub Torque. 11-mode plant, 5-mode compensator, I.C. of the structure = 1st mode, I.C. of the estimator = 1st mode.

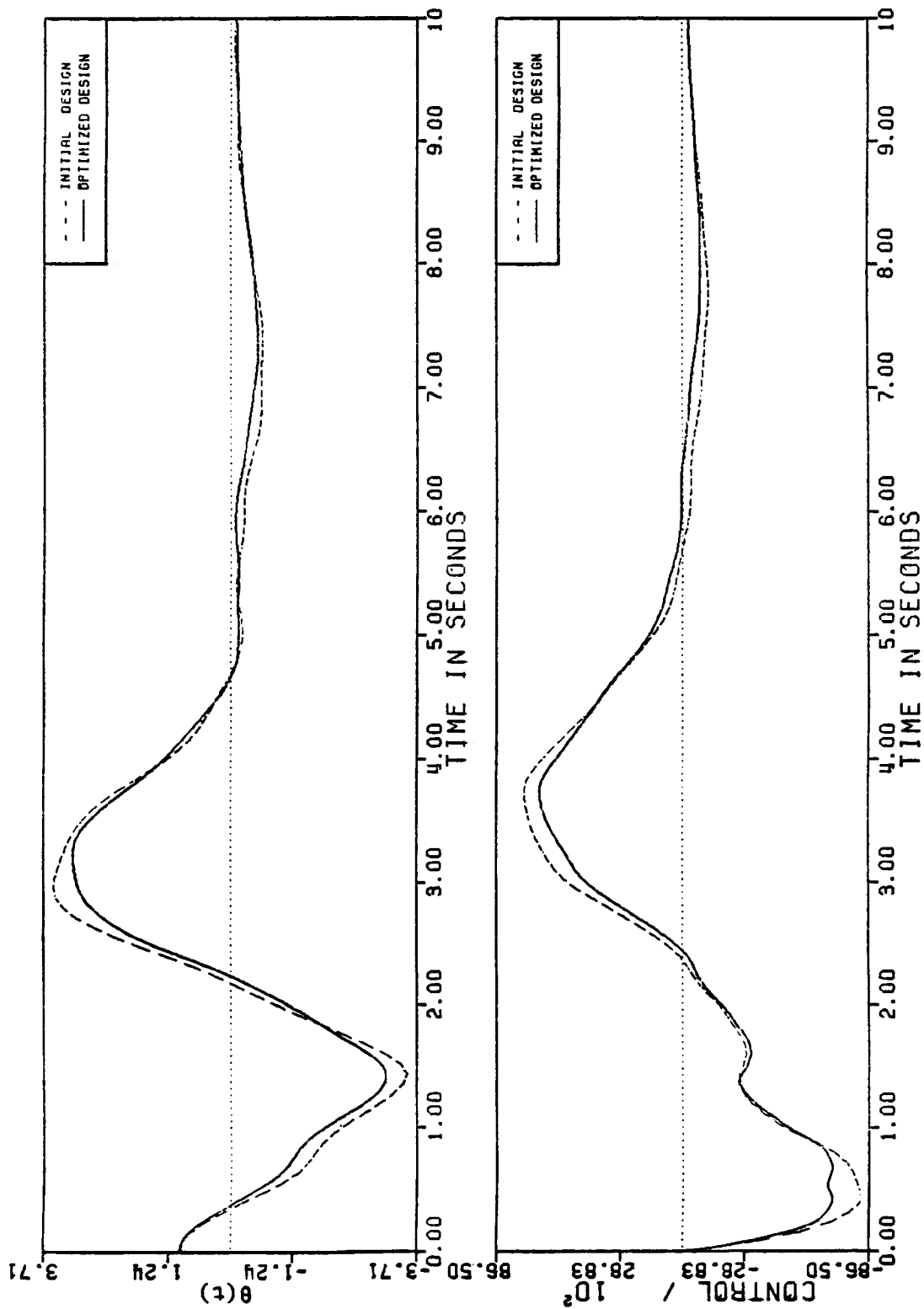


Figure 6-4. Time Histories of the Rigid-Body Angle and the Hub Torque. 11-mode plant, 5-mode compensator, I.C. of the structure = 1st mode, I.C. of the estimator = 0.

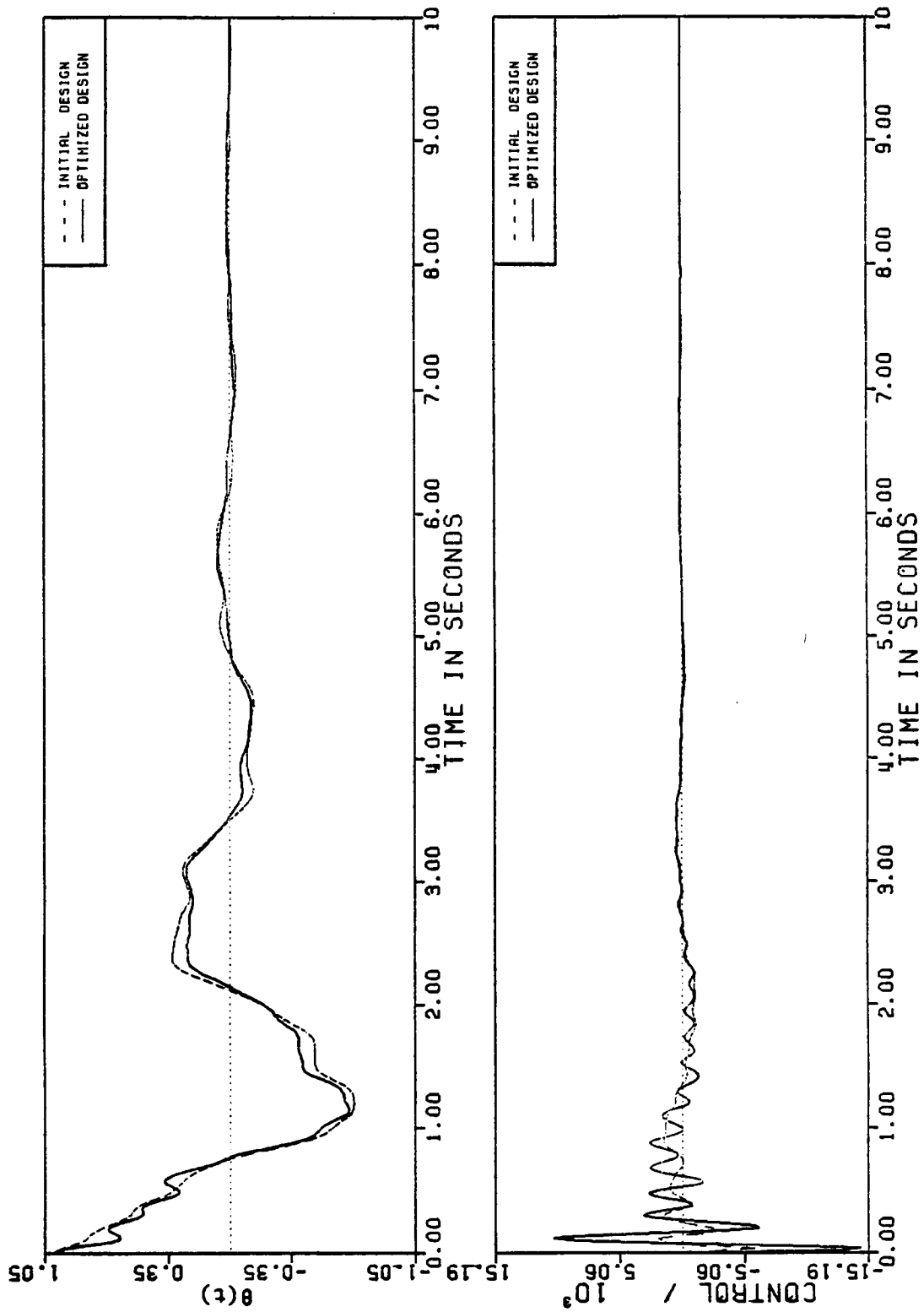


Figure 6-5. Time Histories of the Rigid-Body Angle and the Hub Torque. 11-mode plant, 5-mode compensator, I.C. of the structure = 2nd mode, I.C. of the estimator = 0.

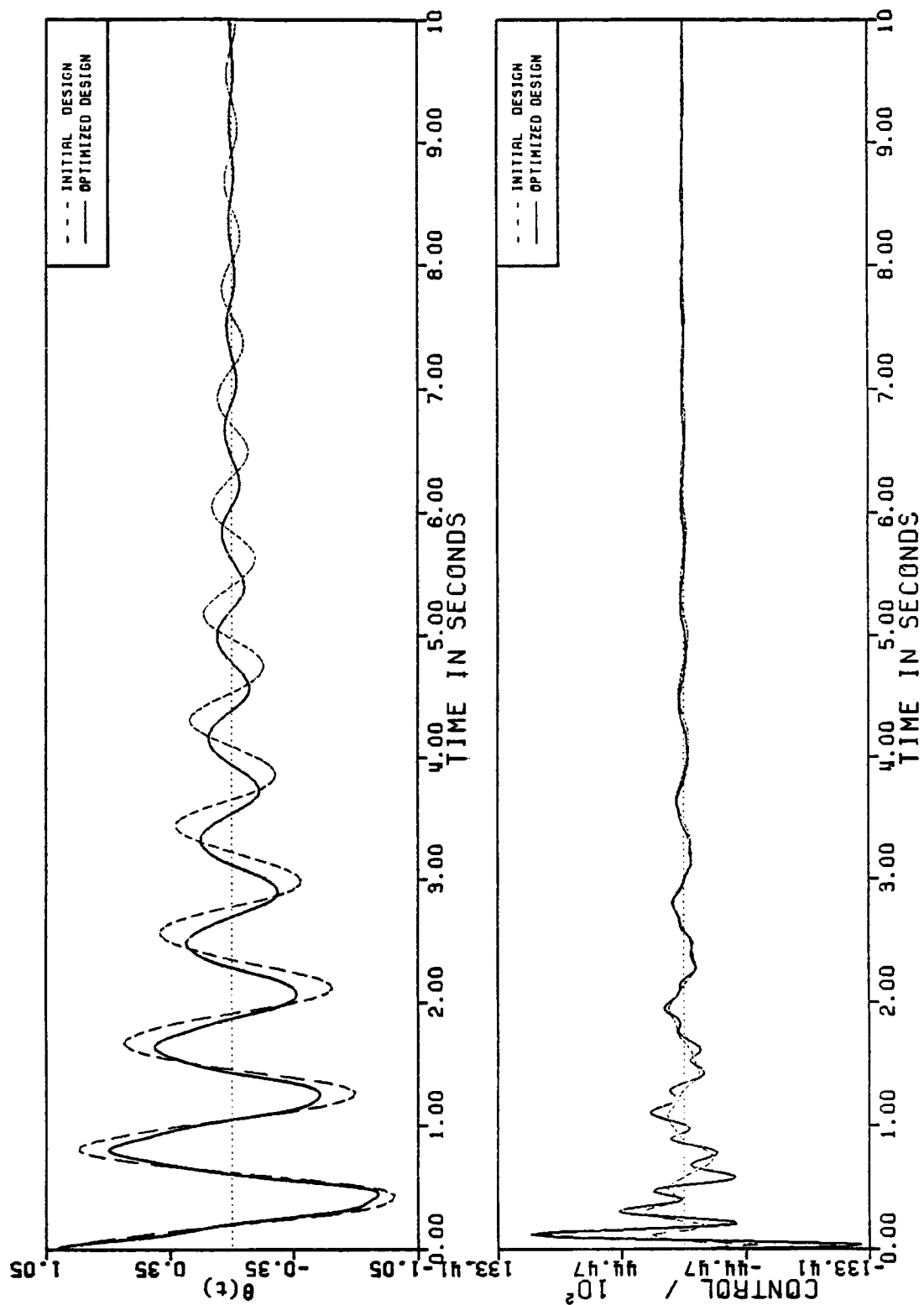


Figure 6-6. Time Histories of the Rigid-Body Angle and the Hub Torque. 11-mode plant, 5-mode compensator, I.C. of the structure = 3rd mode, I.C. of the estimator = 0.

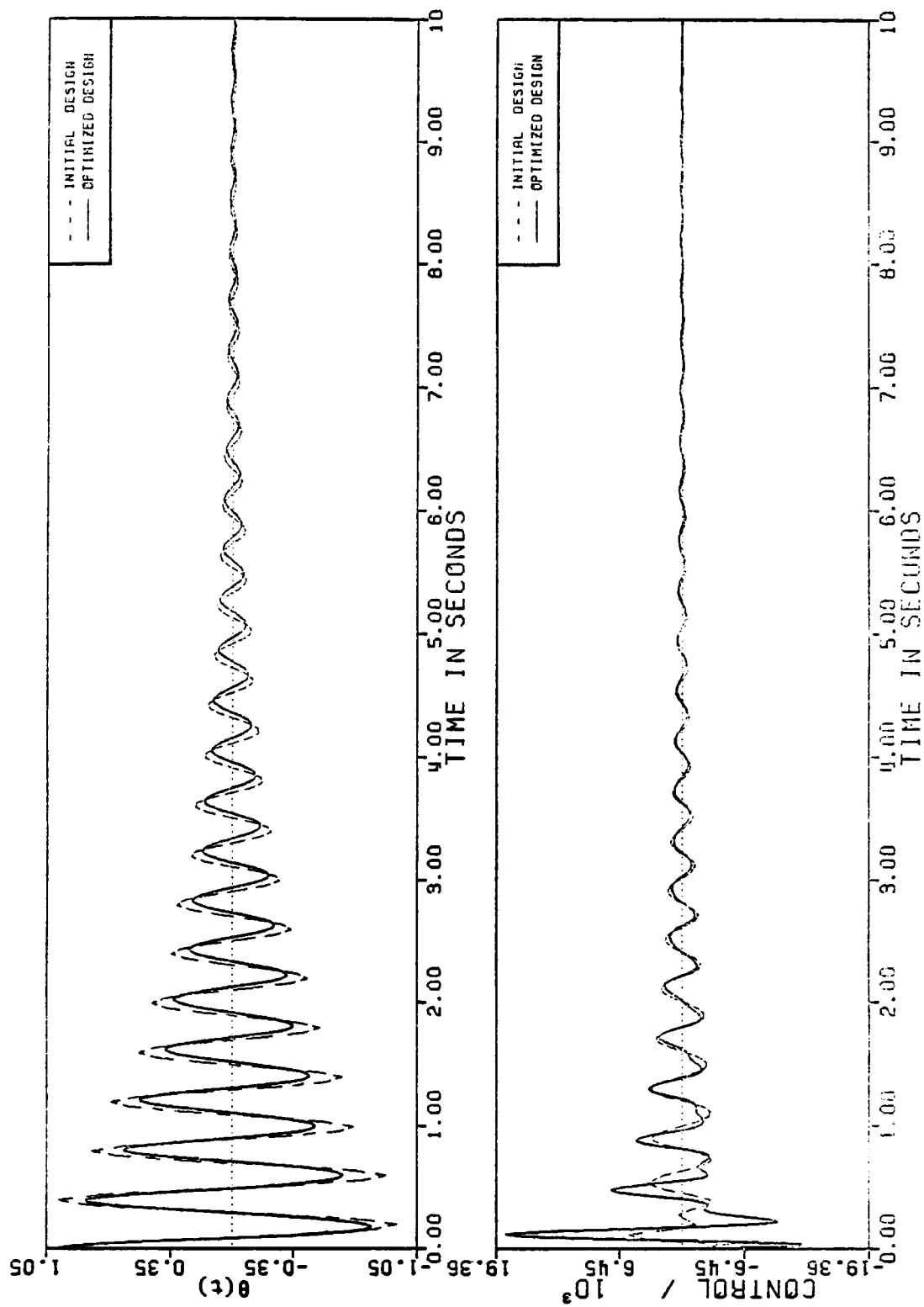


Figure 6-7. Time Histories of the Rigid-Body Angle and the Hub Torque. 11-mode plant, 5-mode compensator, I.C. of the structure = 4th mode, I.C. of the estimator = 0.

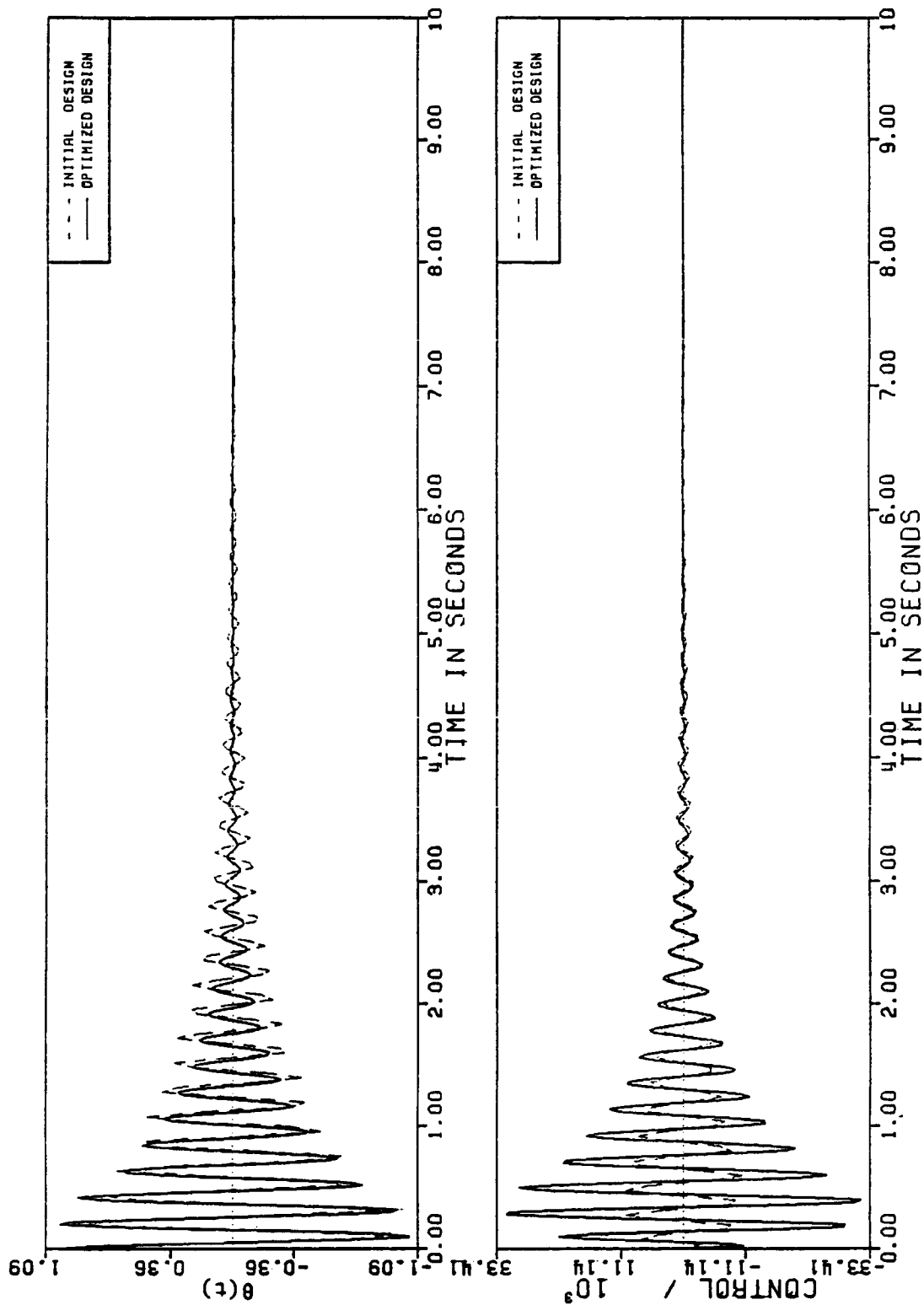


Figure 6-8. Time Histories of the Rigid-Body Angle and the Hub Torque. 11-mode plant, 5-mode compensator, I.C. of the structure = 5th mode, I.C. of the estimator = 0.

Chapter VII

SENSITIVITY AND STRUCTURAL WEIGHT OPTIMIZATION

7.1 First-Order Sensitivity and Structural Weight Optimization

Problem Statement

Find the elements of h (structural design variables), and the gain matrices F and G (control design variables) that minimize (7.1), which includes the structural weight and the first-order sensitivities of the closed-loop eigenvalues with respect to plant uncertainties (natural frequencies), subject to eigenvalue constraints and partial side constraints on design variables; i.e., choose F , G and h to minimize

$$J(F, G, h) = [J_c(F, G, h) / J_c(F_0, G_0, h_0)] + \alpha [W(h) / W(h_0)], \quad (7.1)$$

subject to

$$\operatorname{Re}(\lambda_{c_i})^l \leq \max_i \operatorname{Re}(\lambda_{c_i}) \leq \operatorname{Re}(\lambda_{c_i})^u \quad i = 1, \dots, 2n, \quad (7.2)$$

$$\operatorname{Re}(\lambda_{e_i})^l \leq \max_i \operatorname{Re}(\lambda_{e_i}) \leq \operatorname{Re}(\lambda_{e_i})^u \quad i = 1, \dots, 2n, \quad (7.3)$$

$$\min_i |\operatorname{Im}(\lambda_{c_i})| \geq \operatorname{Im}(\lambda_{c_i})^l \quad i = 1, \dots, 2n, \quad (7.4)$$

$$\min_i |\operatorname{Im}(\lambda_{e_i})| \geq \operatorname{Im}(\lambda_{e_i})^l \quad i = 1, \dots, 2n, \quad (7.5)$$

$$h_i^l \leq h_i \leq h_i^u \quad i = 1, \dots, n_s. \quad (7.6)$$

In (7.1)-(7.6),

$$J_c(F, G, h) = \left\{ \sum_{i=1}^{4n} [\gamma_i^2 |\operatorname{Re}(\nabla \lambda_{cl_i})| \omega]^2 \right\}^{\frac{1}{2}}, \quad (7.7)$$

$$h = [h_1, \dots, h_{n_s}], \quad (7.8)$$

$$\nabla = \left[\frac{\partial}{\partial \beta_1} \dots \frac{\partial}{\partial \beta_n} \right], \quad (7.9)$$

$$\omega^T = [\omega_1^2 \dots \omega_n^2], \quad (7.10)$$

$$\beta_i = \omega_i^2, \quad (7.11)$$

and

F = $r \times 2n$ control gain matrix,

r = number of actuators,

n = number of structural modes used in compensator design,

G = $2n \times m$ estimator gain matrix,

m = number of sensors (measurement),

$J_c(F, G, h)$ = control objective function,

$W(h)$ = structural weight,

$h_i = i^{\text{th}}$ structural design variable (cross-sectional height).

α = structural weight weighting factor,

$\lambda_{c_i} = i^{\text{th}}$ controller eigenvalue,

$\lambda_{e_i} = i^{\text{th}}$ estimator eigenvalue,

$\lambda_{cl_i} = i^{\text{th}}$ closed-loop eigenvalue,

$\omega_i = i^{\text{th}}$ uncertain plant parameter (natural frequencies),

$\gamma_i = i^{\text{th}}$ scalar weighting factor,

n_s = number of structural design variables,

$\text{Re}(\cdot)$ = real part of a complex number,

$\text{Im}(\cdot)$ = imaginary part of a complex number,

$\max(\cdot)$ = maximum value,

$\min(\cdot)$ = minimum value,

$|\cdot|$ = absolute value,

$(\cdot)^l$ = lower bound,

$(\cdot)^u$ = upper bound,

$(\cdot)_0$ = nominal value.

In problems with a rigid-body mode, ω_1 is zero and we use only the sensitivities with respect to the nonzero frequencies in (7.1), so that $\frac{\partial}{\partial \beta_1}$ and ω_1^2 are not included in (7.9) and (7.10).

7.2 Example

In the following sections, we consider the structural model described in Sec. 6.3 with the exception that the heights of the cross sections at the beam nodes are also design variables. Here, the initial structural design variables were selected so that the initial structure was identical to that of Sec. 6.3, (uniform beam).

To illustrate the relationship between structural weight optimization and performance, we design our compensators based on two sets of structural modes. In Section 7.2.1, we control the first 4-modes of the structure with compensators based on four modes, and in Section 7.2.2, we control the first 5-modes of the structure with compensators based on five modes. In each of these sections, we present three optimized designs which demonstrate the trade off between the control objective function and the structural weight minimization, and we present numerical results to compare the robustness of one of the optimized compensator/structure designs with the robustness of the initial design. Also, we compare the performance of the optimal and initial designs by computing quadratic performance indices and time histories for certain initial conditions.

7.2.1 Four-Mode Compensator Example

We take the state vector $x(t)$ to represent the first four modal displacements and velocities of the ten-element model, so that the matrix A is

$$A(\Omega) = \begin{bmatrix} 0 & I \\ -\Omega^2 & -c_0 \Omega_0 \end{bmatrix} \quad (7.12)$$

where Ω is a 4×4 diagonal matrix containing the natural frequencies (uncertain parameters) of the model, c_0 is the damping coefficient and Ω_0 is a 4×4 diagonal matrix containing the nominal natural frequencies of the model. The first element of Ω is zero, corresponding to the rigid-body mode. When we refer to the natural frequencies of the plant, we will mean the three nonzero elements of Ω only. We assume that the matrices B and C do not depend on uncertain parameters. (See Eqn. 5.5).

For our four-mode model of the initial structure, based on the nominal values of the plant natural frequencies, we designed an initial linear-quadratic-gaussian (LQG) compensators (see Sections 3.3 and 5.3) with

$$\alpha_c = 0.0, \quad (7.13)$$

$$R_c = 1.0, \quad (7.14)$$

$$Q_c = \begin{bmatrix} 8 & 5 & 10 & 100 & & 0 \\ & & & & & \\ \text{---} & \text{---} & \text{---} & \text{---} & \text{---} & \text{---} \\ & & 0 & & & 0 \end{bmatrix} \times 1000, \quad (7.15)$$

$$\alpha_e = 0.3, \quad (7.16)$$

$$R_e = \begin{bmatrix} 1 & 0 \\ 0 & 1 \end{bmatrix}, \quad (7.17)$$

$$Q_e = \begin{bmatrix} 0 & & & 0 \\ \text{---} & & & \text{---} \\ & 10 & 1 & 1 & 1 \\ 0 & & & & \end{bmatrix} \times 1000. \quad (7.18)$$

To demonstrate the trade off between the control objective $J_c(F, G, h)$ and the structural weight $W(h)$ minimization, consider three optimization problems where the objective functions are constructed with $\alpha = 2, 3$ and 5 in (7.1). Since we use the ten element model of the structure, we have 11 structural design variables (the heights of the cross sections at the beam nodes). Also, we have the 1×8 control gain matrix F and the 8×2 estimator gain matrix G , so that there are 24 control design variables. Therefore, we have a total of $11 + 24 = 35$ design variables. The scalar weighting factors and lower bounds and upper bounds in (7.1)-(7.6) are

$$\operatorname{Re}(\lambda_{c_i})^u = 0.90 \times \operatorname{Re}[\lambda_{c_i}(F_0, h_0)] \quad i = 1, \dots, 2n, \quad (7.19)$$

$$\operatorname{Re}(\lambda_{e_i})^u = -0.40 \quad i = 1, \dots, 2n, \quad (7.20)$$

$$\operatorname{Im}(\lambda_{c_i})^l = 0.20 \quad i = 1, \dots, 2n, \quad (7.21)$$

$$\operatorname{Im}(\lambda_{e_i})^l = 0.20 \quad i = 1, \dots, 2n, \quad (7.22)$$

$$\gamma_i = \max \left[\frac{1}{|\operatorname{Re}(\lambda_{cl_i})|}, \frac{1}{|\operatorname{Im}(\lambda_{cl_i})|} \right] \quad i = 1, \dots, 4n, \quad (7.23)$$

$$h_i^l = 0.25 \quad i = 1, \dots, n_s, \quad (7.24)$$

$$h_i^u = 3.0 \quad i = 1, \dots, n_s. \quad (7.25)$$

Note that (7.19) indicates that the magnitude of the real part of the controller eigenvalues can decrease by 10% only.

Each of the optimized designs were obtained by using the ADS optimizer (Ref. V2), where the sequential unconstrained minimization technique (SUMT) using the exterior penalty function method, and Broydon-Fletcher-Goldfarb-Shanno (BFGS) variable metric method for unconstrained minimization of pseudo-objective function (created by the exterior penalty function method) were selected, see [V1]. Also, the 35 design variables were scaled by the ADS program, and finite difference gradients were used in the optimization problems. Each of the three optimization problems converges in 1 SUMT iteration which includes fewer than 45 unconstrained minimization (BFGS) iterations. The constraint on the real part of the controller eigenvalues (7.19) and the side constraint corresponding to the height of the cross-section at the last beam node (tip end) are active for all three optimized designs. Table 7-1 shows the numerical values of the control objective functions and the structural weights. In general, larger values of α result in more structural weight and less control objective function reduction. However, there are some exceptions due to the complexity of the numerical optimization and nonlinearity of the objective function, as indicated by Case B of Table 7-1. Figure 7-1 shows the initial and the three optimized substructures (beams).

CASE	α	INITIAL DESIGN			OPTIMIZED DESIGN			ITERATION HISTORY FIGURE
		W	J_c	J	W	J_c	J	
A	2	1.000	12.42	3.000	0.585	1.274	1.273	-
B	3	1.000	12.42	4.000	0.601	1.016	1.884	-
C	5	1.000	12.42	6.000	0.540	1.824	2.845	7-2,7-3

Table 7-1. Control Objective and Structural Weighth of the Initial and Three Optimized Designs with 4-Mode Compensators.

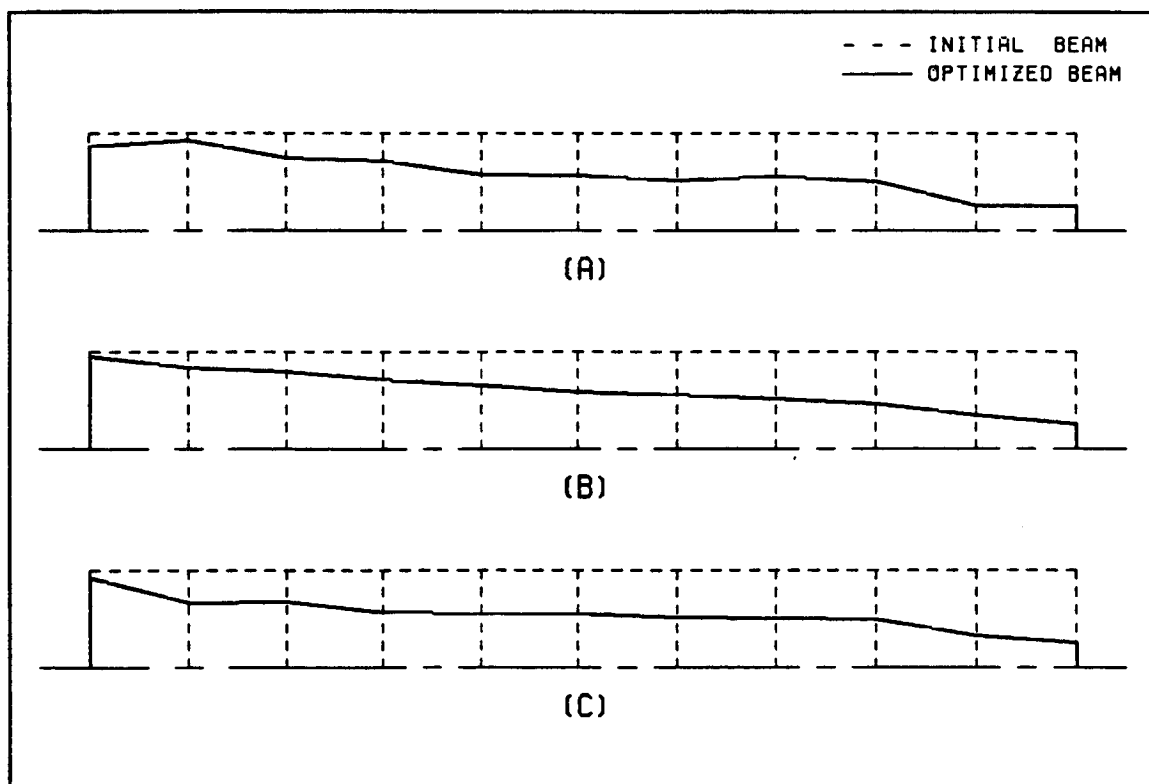


Figure 7-1. The Initial and Three Optimized substructures (Beams). (A) $\alpha = 2$, (B) $\alpha = 3$, (C) $\alpha = 5$. (4-mode compensators.)

The initial substructure is drawn in dashed line and an optimized substructure is drawn in solid line. (Only the portion of a beam over the center-line is shown.)

To see the effect of first-order closed-loop eigenvalue sensitivity and structural weight optimization on robustness, consider for example Case C ($\alpha=5$) of the three optimized designs. For this case, the optimization converges in 1 SUMT iteration which includes 33 unconstrained minimization (BFGS) iterations. Figure (7-2) shows the unconstrained minimization (BFGS) iteration history of the objective function where $J(F,G,h)$ (normalized with respect to its initial value 6.0) is reduced by 53%. Figure (7-3) shows the unconstrained minimization (BFGS) iteration histories of the control objective function and the structural weight, where $J_c(F,G,h)$ (normalized with respect to its initial value 12.42) is reduced by 85% and $W(h)$ (normalized with respect to its initial value 1.0) is reduced by 46%. Table 7-2 lists the natural frequencies and the structural design variables of the initial and the optimized structures, Table 7-3 lists the control design variables of the initial and the optimized compensators. Figure 7-4 shows first three flexible mode-shapes of the initial and the optimized structures. In this figure, nodes of the initial structure are marked with squares and nodes of the optimized structure are marked with circles. Note that Fig. 7-2 also shows the increased flexibility of the optimized design due to its significant weight reduction. Table 7-4 and Figure 7-5 show the open-loop and the closed-loop eigenvalues of the initial and the optimized

designs. In Figure 7-5, the dashed lines connect the eigenvalues of the initial design and the solid lines connect the eigenvalues of the optimized design. (Only eigenvalues with positive imaginary parts are plotted.)

Our measure of robustness for a compensator is how much the plant natural frequencies can vary, from their nominal values, before the closed-loop system becomes unstable; i.e., before some eigenvalue of A_{cl} has nonnegative real part. The robustness of the closed-loop eigenvalues was tested by varying the natural frequencies of the plant by a constant percentage times a variation factor (1,0 or -1 for each natural frequency), while maintaining the original damping of the plant and the original natural frequencies in the compensator. Tables 7-5 and 7-6 present the robustness test results of the initial and the optimized closed-loop designs. In each one of the robustness tables, each row represents nine closed-loop designs where the natural frequencies of the plant were perturbed by a percentage (indicated by a percentage sign %) times a variation factor for each natural frequency (listed in the left portion of the tables). In these tables, "." indicates a stable design and "x" indicates an unstable design. For the initial plant and compensator, Table 7-5 shows that the closed-loop design becomes unstable for 20% variations in plant frequencies. For the optimized plant and compensator, Table 7-6 shows that the closed-loop design becomes unstable for 60% variations in plant frequencies. Note that we have improved the robustness of the closed-loop system by factor of three and at the same time reduced the

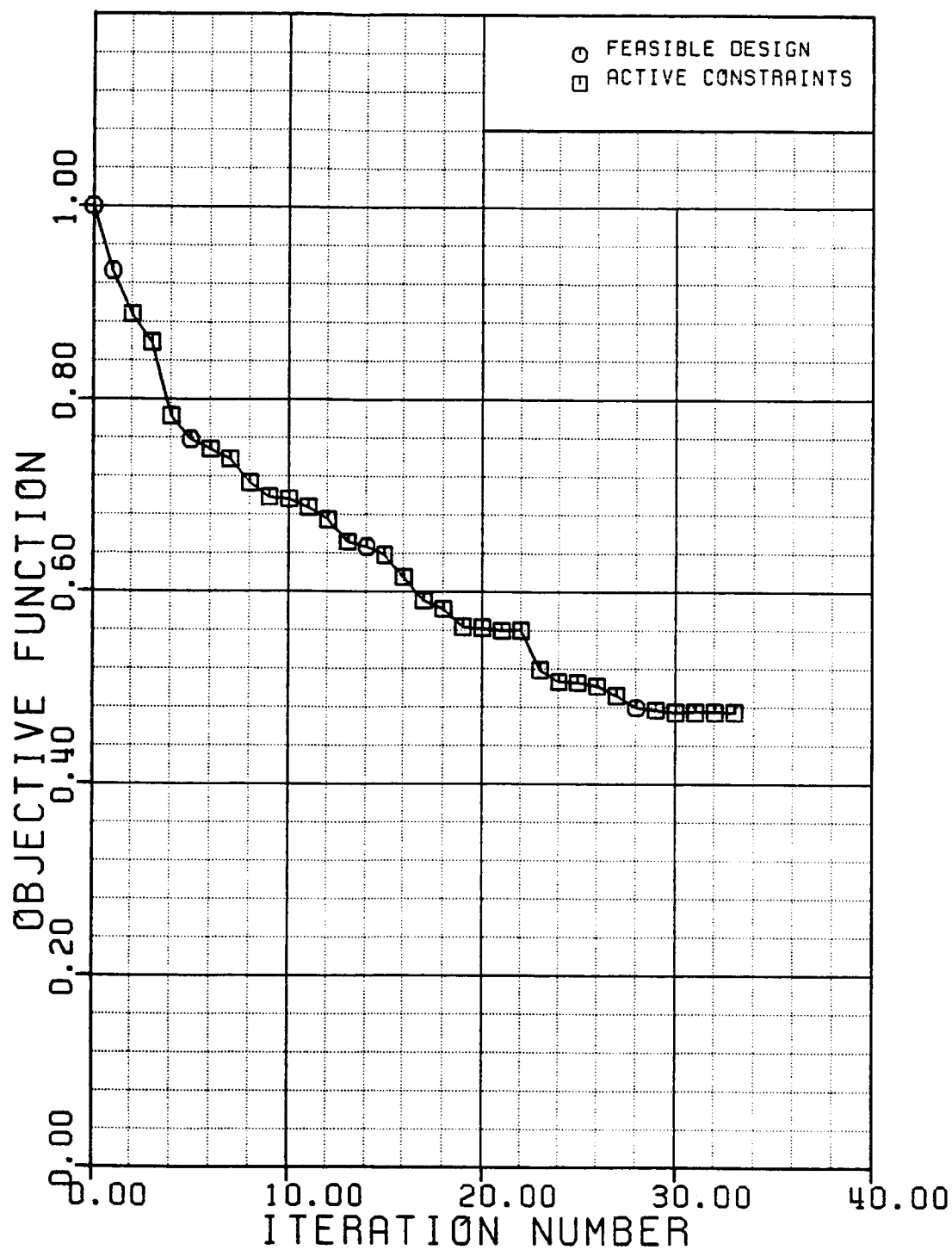


Figure 7-2 Unconstrained Minimization (BFGS) Iteration History of the Objective Function. (4-mode compensator.)

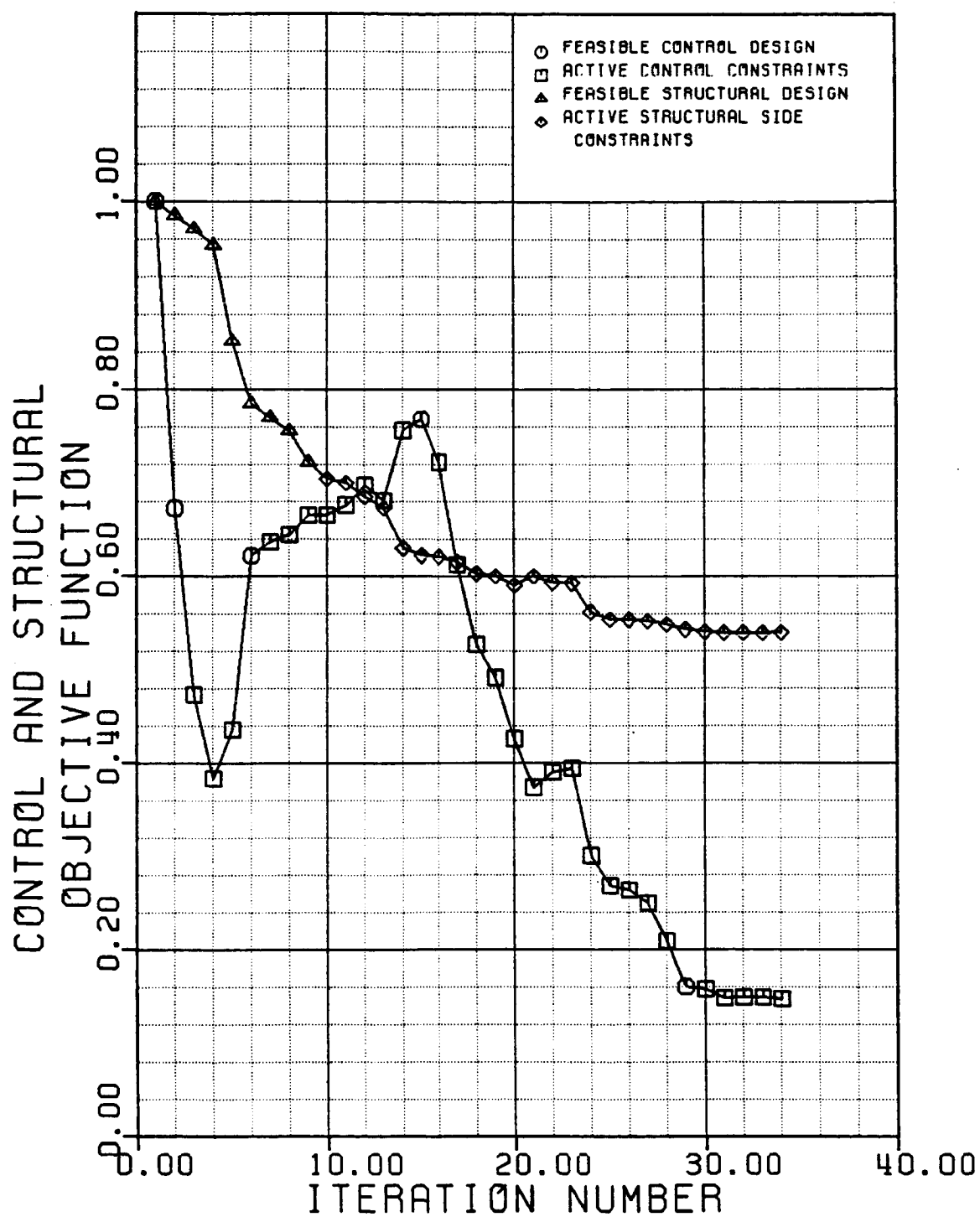


Figure 7-3. Unconstrained Minimization (BFGS) Iteration Histories of the Control and the Structural Objective Functions. (4-mode compensator.)

	INITIAL DESIGN		OPTIMIZED DESIGN	
j	ω_j	h_j	ω_j	h_j
1	0.0	1.0000	0.0	0.9160
2	2.1583	1.0000	1.0938	0.6571
3	7.1826	1.0000	3.8530	0.6746
4	15.568	1.0000	8.3850	0.5577
5	29.010	1.0000	15.295	0.5541
6	47.901	1.0000	25.732	0.5550
7	72.399	1.0000	39.379	0.5076
8	103.14	1.0000	56.958	0.4998
9	141.47	1.0000	78.785	0.4862
10	188.23	1.0000	107.67	0.3219
11	235.33	1.0000	143.92	0.2500

Table 7-2 Natural Frequencies and Structural Design Variables of the Initial and the Optimized Structures. (Connected to 4-mode compensators.)

weight of the structure by 46%. Note also that the optimized compensator results in an unstable closed-loop system only when the variations in plant natural frequencies are such that the first and the second, or the first and the third natural frequencies cross over. For each of the above robustness tests, there are 234 variations. That is

$$N = [n_1^{n_2} \ -1]n_3, \quad (7.26)$$

	INITIAL DESIGN			OPTIMIZED DESIGN		
j	F_{1j}	G_{j1}	G_{j2}	F_{1j}	G_{j1}	G_{j2}
1	89.443	247.57	0.8999	51.652	248.21	1.5785
2	-47.304	-0.0367	9.4221	-30.796	-0.1230	8.5970
3	-32.620	-0.0192	-0.9078	-61.482	0.2556	-1.0041
4	-59.663	-0.0043	-0.6771	-137.45	0.2074	-2.2364
5	180.96	163.33	0.5941	188.67	163.11	1.5511
6	-24.166	-0.0802	28.381	-23.670	-0.1944	28.364
7	-12.218	-0.3183	34.970	-19.625	-0.2851	35.205
8	-15.399	-0.3109	32.302	-15.326	-0.3317	32.482

Table 7-3. Controller and Observer Gains of the Initial and the Optimized 4-Mode Compensators.

where

$N = 234$ is the total number of variations,

$n_1 = 3$ is the number of variation factors (1,0 or -1),

$n_2 = 3$ is the number of uncertain parameters,

$n_3 = 9$ is the number of variation percentages (10%, ..., 90%).

For the initial plant and compensator, 39 variations out of 234 result in unstable designs and for the optimized plant and compensator, 20 variations out of 234 result in unstable designs.

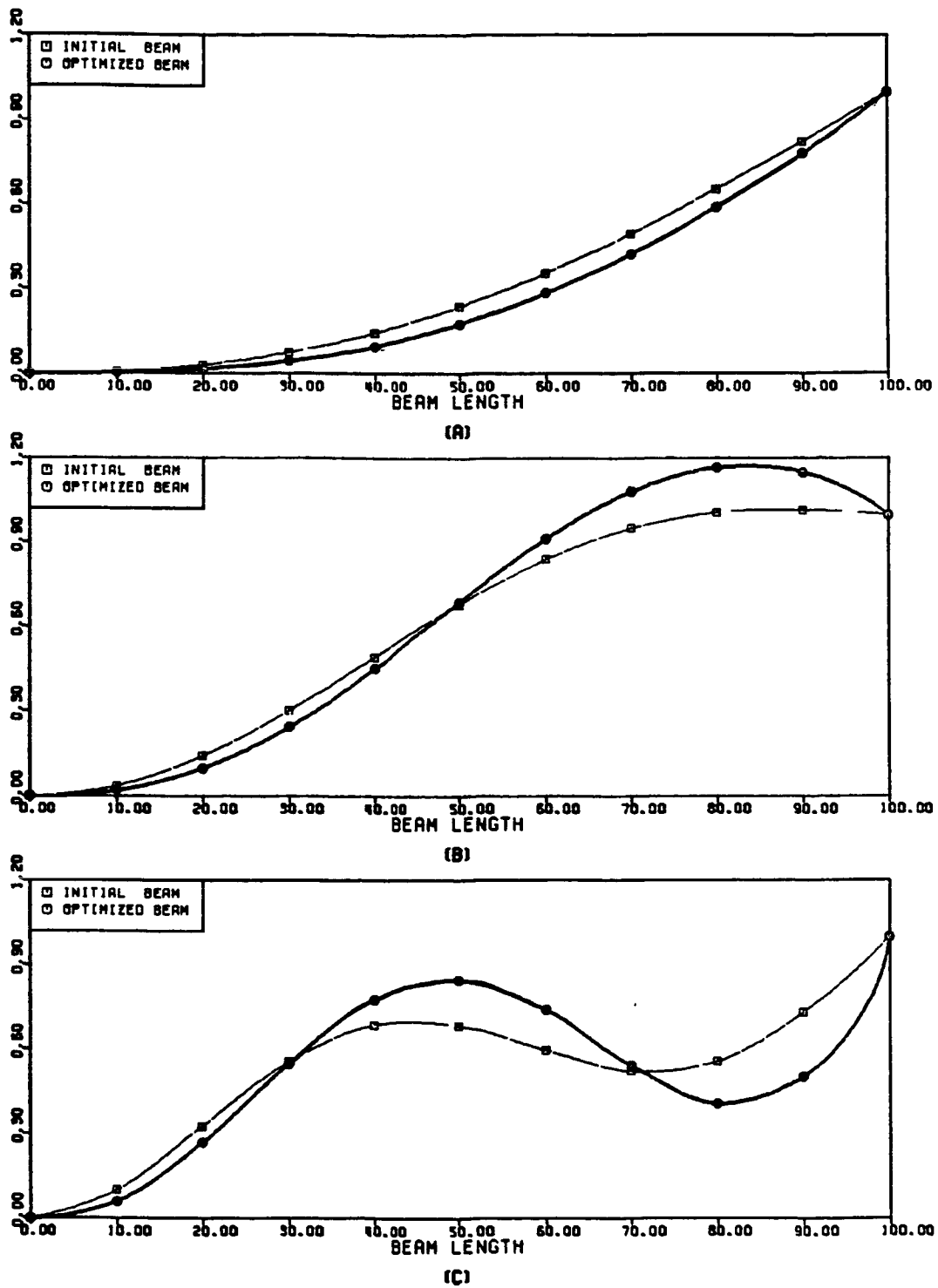


Figure 7-4. First Three Flexible Mode-Shapes of the Initial and The Optimized structures. (A) 1st Mode, (B) 2nd Mode, (C) 3rd Mode. (4-mode compensator.)

OPEN-LOOP EIGENVALUES	CLOSED-LOOP EIGENVALUES	
	CONTROLLER	ESTIMATOR
0.0	$-0.5417 \pm i0.5582$	$-0.9598 \pm i0.5876$
0.0		
$-0.0023 \pm i2.1583$	$-0.5726 \pm i2.2294$	$-2.5781 \pm i5.0525$
$-0.0258 \pm i7.1826$	$-0.3940 \pm i7.1932$	$-9.5443 \pm i12.874$
$-0.1212 \pm i15.567$	$-0.5008 \pm i15.575$	$-4.1680 \pm i14.585$

a) Initial Design.

OPEN-LOOP EIGENVALUES	CLOSED-LOOP EIGENVALUES	
	CONTROLLER	ESTIMATOR
0.0	$-0.4874 \pm i0.3632$	$-1.0429 \pm i0.5320$
0.0		
$-0.0006 \pm i1.0938$	$-0.5932 \pm i0.9629$	$-0.5963 \pm i2.5730$
$-0.0074 \pm i3.8530$	$-0.5933 \pm i3.9054$	$-1.1779 \pm i7.0272$
$-0.0352 \pm i8.3850$	$-0.5082 \pm i8.5587$	$-10.110 \pm i18.828$

b) Optimized Design.

Table 7-4. Open-Loop and Closed-Loop Eigenvalues of the Initial and the Optimized Designs of 4-Mode Compensators.

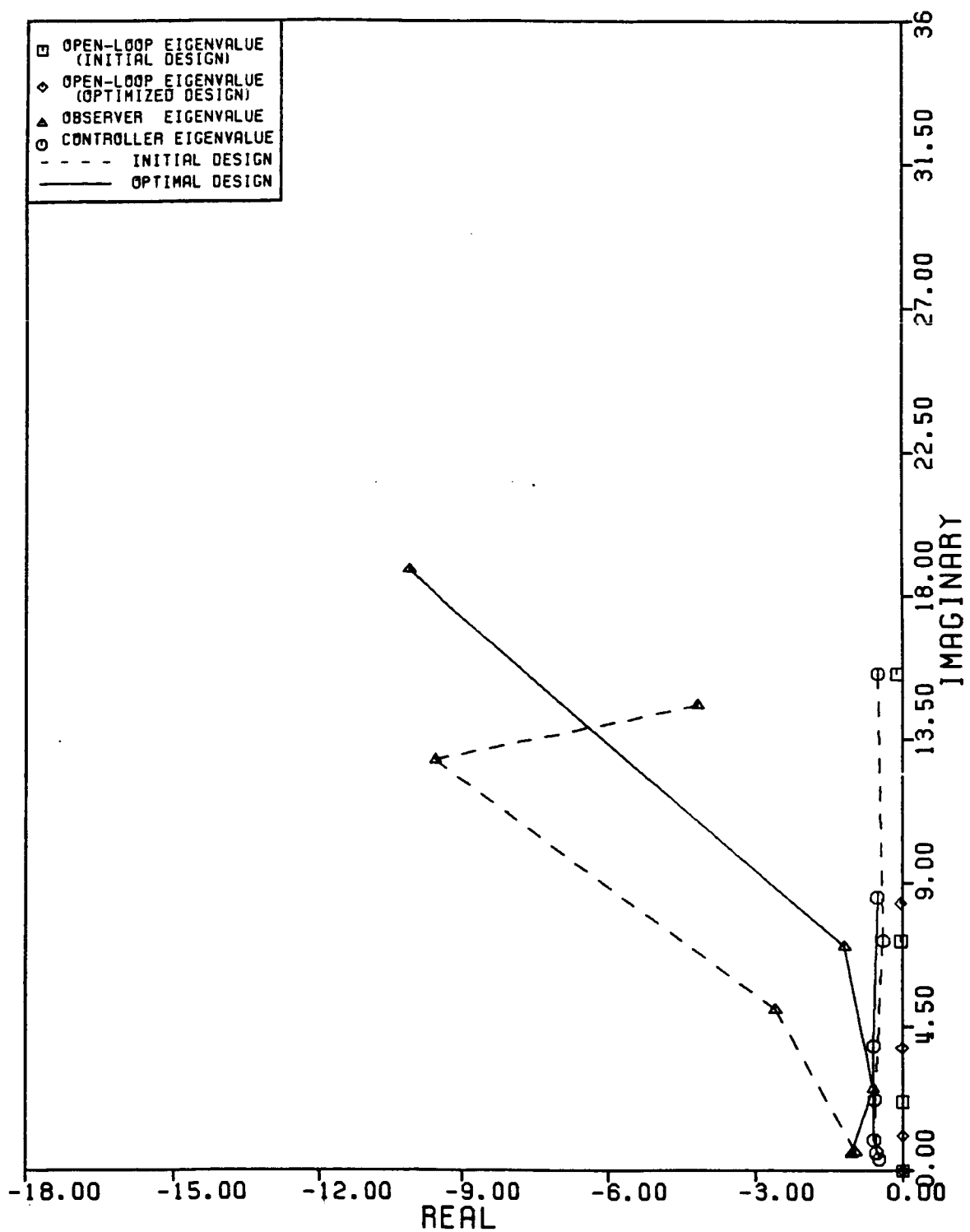


Figure 7-5. Open-Loop and Closed-Loop Eigenvalues of the Initial and the Optimized Designs of 4-Mode Compensators.

NATURAL FREQUENCY VARIATION FACTORS			VARIATION PERCENTAGE								
ω_2	ω_3	ω_4	10%	20%	30%	40%	50%	60%	70%	80%	90%
1	1	1
-1	1	1
1	-1	1	.	x	x	x	.	x	x	.	.
1	1	-1
-1	-1	1	.	x	x	x
-1	1	-1
1	-1	-1	.	x	x	x	.	x	x	.	.
-1	-1	-1	.	x	x	x
0	1	1
0	1	-1
0	-1	-1	.	x	x	x	.	.	.	x	x
0	-1	1	.	x	x	x	.	.	.	x	x
1	0	1
1	0	-1
-1	0	-1
-1	0	1
1	1	0
1	-1	0	.	x	x	x	.	x	x	.	.
-1	-1	0	.	x	x	x
-1	1	0
1	0	0
0	1	0
0	0	1
-1	0	0
0	-1	0	.	x	x	x	.	.	.	x	x
0	0	-1

Table 7-5. Robustness Test Results of the Initial 4-Mode Plant and Compensator.

In investigating robustness with respect to unmodeled modes, we connected the initial four-mode compensator to the initial eleven-mode plant and the optimized four-mode compensator to the optimized eleven-mode plant, and performed the robustness test by varying first three natural frequencies of the plants by a constant percentage times a variation factor (1,0 or -1 for each natural frequency), while

NATURAL FREQUENCY VARIATION FACTORS			VARIATION PERCENTAGE								
ω_2	ω_3	ω_4	10%	20%	30%	40%	50%	60%	70%	80%	90%
1	1	1
-1	1	1
1	-1	1	x	x	x	x
1	1	-1	x	.
-1	-1	1
-1	1	-1
1	-1	-1	x	x	x	x
-1	-1	-1
0	1	1
0	1	-1	x
0	-1	-1	x	x
0	-1	1	x	x
1	0	1
1	0	-1
-1	0	-1
-1	0	1
1	1	0
1	-1	0	x	x	x	x
-1	-1	0
-1	1	0
1	0	0
0	1	0
0	0	1
-1	0	0
0	-1	0	x	x
0	0	-1

Table 7-6. Robustness Test Results of the Optimized 4-Mode Plant and Compensator.

maintaining the original damping of each plant and the original natural frequencies in each compensator. For the initial plant and compensator, the results of the robustness test are identical to those of Table 7-5. For the optimized plant and compensator, the results of the robustness test are identical to the results in Table 7-6. These robustness tests indicate that for this example the robustness of the

initial and the optimized designs are insensitive to the unmodeled modes, which is partially due to well separated natural frequencies of the eleven-mode plant.

In comparing the performance of the initial and the optimized compensators, we use the performance index described in Section 3.1, repeated here for convenience

$$J_p = \int_0^{\infty} [x^T(t)Q_c x(t) + u^T(t)R_c u(t)] dt. \quad (7.27)$$

From (7.27), we see that

$$J_p = J_x + J_u, \quad (7.28)$$

where

$$J_x = \int_0^{\infty} [x^T(t)Q_c x(t)] dt, \quad (7.29)$$

$$J_u = \int_0^{\infty} [u^T(t)R_c u(t)] dt. \quad (7.30)$$

J_x is the quantity we wish to control and J_u is the control effort.

In general, smaller values of J_x for a given initial condition indicate that the initial state converges faster to the origin (zero state). Tables 7-7 through 7-10 show the performances of the initial and the optimized designs for various initial conditions. For the initial plant and compensator, Table 7-7 shows the performance of the four-mode compensator connected to the four-mode plant, and Table 7-8 shows the performance of the four-mode compensator connected to the eleven-mode plant. (In evaluating the performance of a four-mode compensator connected to an eleven-mode plant, the terms in matrix Q_c

corresponding to the additional plant modes are zero.) Note that Tables 7-7 and 7-8 indicate that the performance of the initial compensator is insensitive to the unmodeled modes of the initial plant.

For the optimized plant and compensator, Table 7-9 shows the performance of the four-mode compensator connected to the four-mode plant, and Table 7-10 shows the performance of the four-mode compensator connected to the eleven-mode plant. These tables indicate that the performance of the optimized compensator is insensitive to the unmodeled modes of the optimized plant.

Figures (7-6) - (7-10) show the response of the rigid-body angle $\theta(t)$ and the control $u(t)$ for various initial conditions. (All plots have been scaled so that $\theta(0)=1$.) In each Figure, the dashed lines represent the time histories corresponding to the initial compensator connected to the initial eleven-mode plant, and the solid lines represent the time histories corresponding to the optimized compensator connected to the optimized eleven-mode plant. (For the initial and the optimized designs, the response curves of the four-mode plants connected to the four-mode compensators coincide with those shown in Figures 7-6 through 7-10.) For the initial design, Figure 7-6 shows that the settling time of the rigid-body angle is 10.05 seconds, which is 3.45 times the period of the first flexible open-loop mode ($T_2=2.91$ seconds). For the optimized design, Figure 7-6 shows that the settling time of the rigid-body angle is 9.50 seconds, which is 1.65 times the period of the first flexible open-

loop mode ($T_2=5.74$ seconds). (The settling time is the time required for the response curve to reach and stay within $\pm 5\%$ of its initial value.) Note that the overshoot present in the rigid-body angle response is partially due to the tip mass m_1 which is as heavy as the initial beam; i.e. $m_1 = 1$ slug. Tables 7-8 and 7-10 indicate and Figures 7-6 through 7-10 confirm that there is a significant difference in the performances (value of J_x) of the optimized and the initial designs. This loss of performance is not entirely due to the increased robustness of the closed-loop system but it is mainly due to the significant weight reduction of the structure (46%), and partially due to the more relaxed constraint on the controller eigenvalues, (7.2) and (7.19).

INITIAL CONDITION OF THE STRUCTURE	INITIAL CONDITION OF THE ESTIMATOR	COST $\times 10^{-8}$		
		J_p	J_x	J_u
1st mode	1st mode	2.6922	2.3086	0.3836
1st mode	0	4.8357	3.5515	1.2842
2nd mode	0	0.0601	0.0278	0.0323
3rd mode	0	0.0630	0.0238	0.0392
4th mode	0	0.4174	0.2495	0.1679

Table 7-7. Performance of the 4-Mode Initial Compensator Connected to the 4-Mode Initial Plant for Various Initial Conditions.

INITIAL CONDITION OF THE STRUCTURE	INITIAL CONDITION OF THE ESTIMATOR	COST $\times 10^{-8}$			RESPONSE OF THE RIGID-BODY ANGLE
		J_p	J_x	J_u	
1st mode	1st mode	2.6923	2.3101	0.3822	Fig. 7-6
1st mode	0	4.8333	3.5527	1.2806	Fig. 7-7
2nd mode	0	0.0598	0.0279	0.0319	Fig. 7-8
3rd mode	0	0.0627	0.0239	0.0388	Fig. 7-9
4th mode	0	0.4170	0.2507	0.1663	Fig. 7-10

Table 7-8. Performance of the 4-Mode Initial Compensator Connected to the 11-Mode Initial Plant for Various Initial Conditions.

INITIAL CONDITION OF THE STRUCTURE	INITIAL CONDITION OF THE ESTIMATOR	COST $\times 10^{-8}$		
		J_p	J_x	J_u
1st mode	1st mode	3.6373	3.5626	0.0747
1st mode	0	7.7451	7.3773	0.3678
2nd mode	0	0.0575	0.0337	0.0238
3rd mode	0	0.0561	0.0259	0.0302
4th mode	0	0.3533	0.2504	0.1029

Table 7-9. Performance of the 4-Mode Optimized Compensator Connected to the 4-Mode Optimized Plant for Various Initial Conditions.

INITIAL CONDITION OF THE STRUCTURE	INITIAL CONDITION OF THE ESTIMATOR	COST $\times 10^{-8}$			RESPONSE OF THE RIGID-BODY ANGLE
		J_p	J_x	J_u	
1st mode	1st mode	3.6391	3.5648	0.0743	Fig. 7-6
1st mode	0	7.7373	7.3709	0.3664	Fig. 7-7
2nd mode	0	0.0576	0.0338	0.0238	Fig. 7-8
3rd mode	0	0.0562	0.0260	0.0302	Fig. 7-9
4th mode	0	0.3590	0.2566	0.1024	Fig. 7-10

Table 7-10. Performance of the 4-Mode Optimized Compensator Connected to the 11-Mode Optimized Plant for Various Initial Conditions.

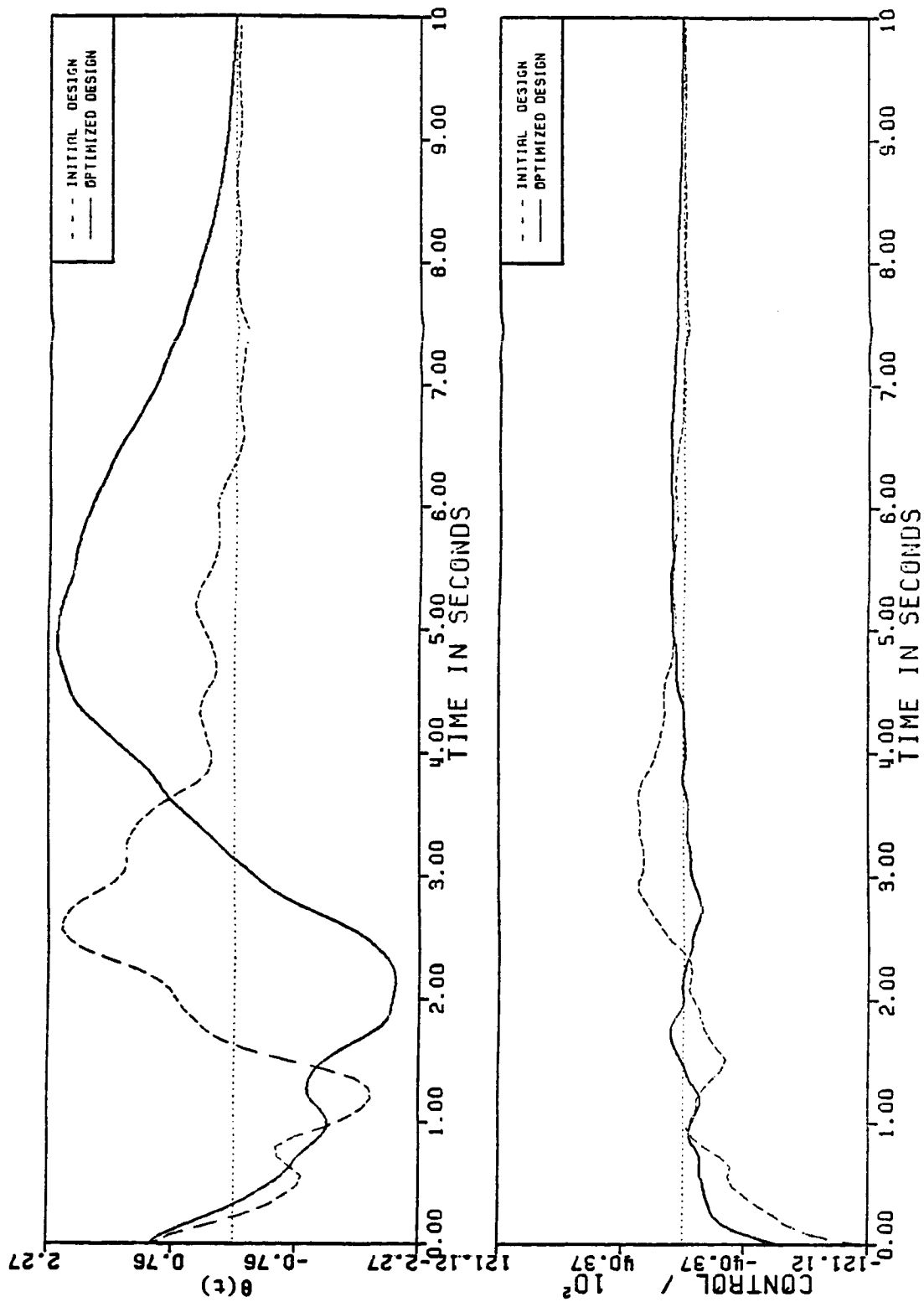


Figure 7-6. Time Histories of the Rigid-Body Angle and the Hub Torque. 11-mode plant, 4-mode compensator, I.C. of the structure = 1st mode, I.C. of the estimator = 1st mode.

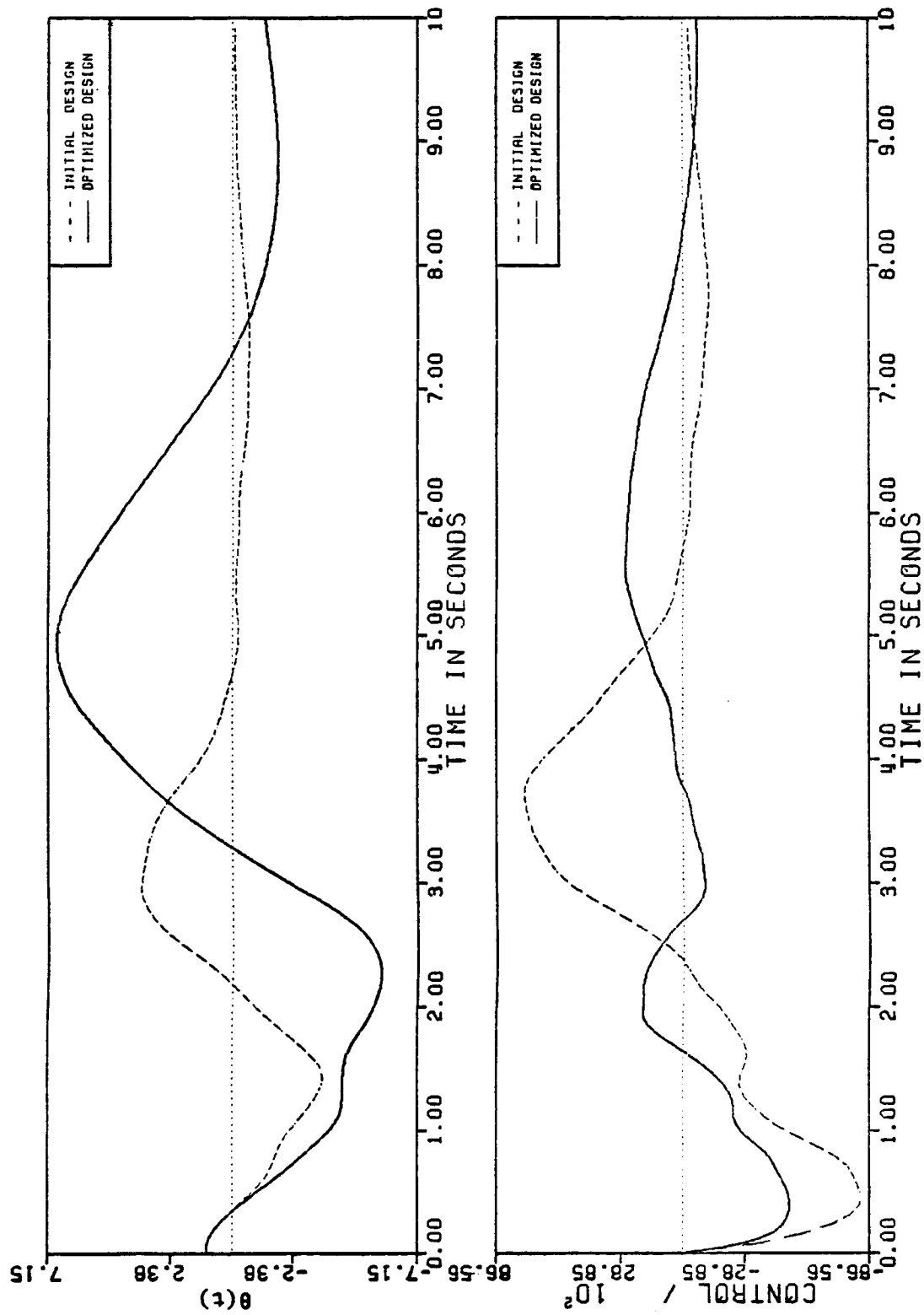


Figure 7-7. Time Histories of the Rigid-Body Angle and the Hub Torque. 11-mode plant, 4-mode compensator, I.C. of the structure = 1st mode, I.C. of the estimator = 0.

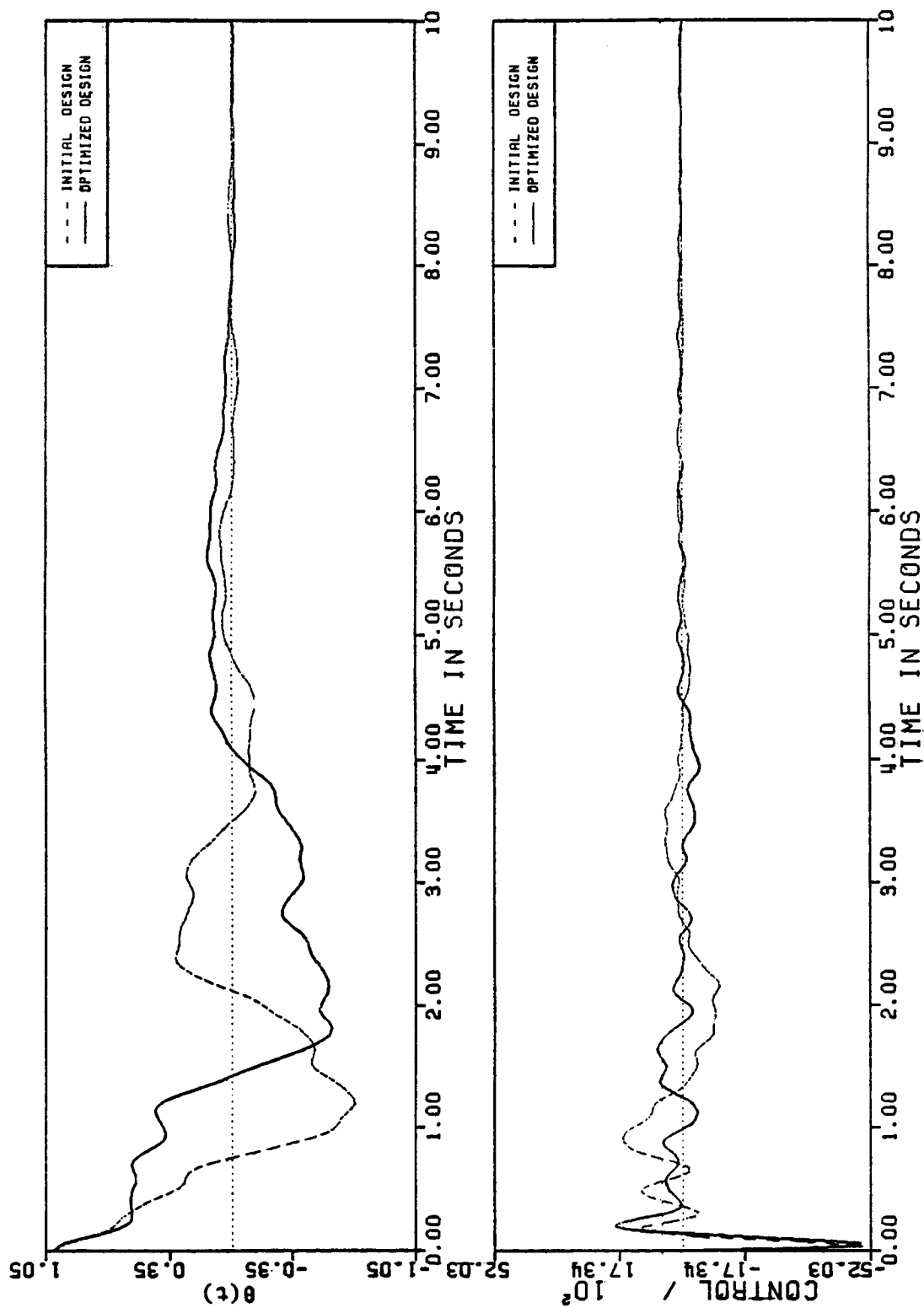


Figure 7-8. Time Histories of the Rigid-Body Angle and the Hub Torque. 11-mode plant, 4-mode compensator, I.C. of the structure = 2nd mode, I.C. of the estimator = 0.

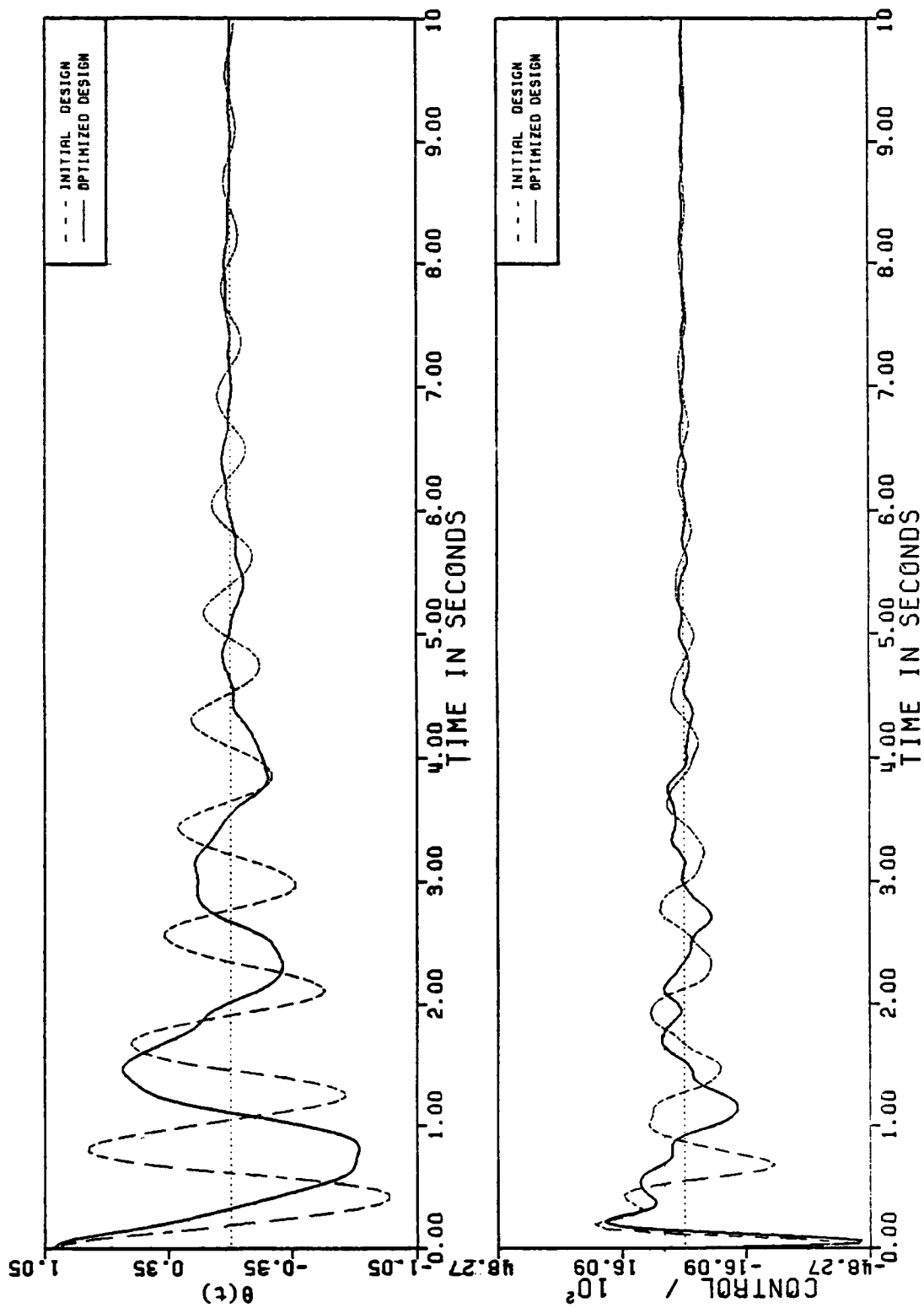


Figure 7-9. Time Histories of the Rigid-Body Angle and the Hub Torque. 11-mode plant, 4-mode compensator, I.C. of the structure = 3rd mode, I.C. of the estimator = 0.

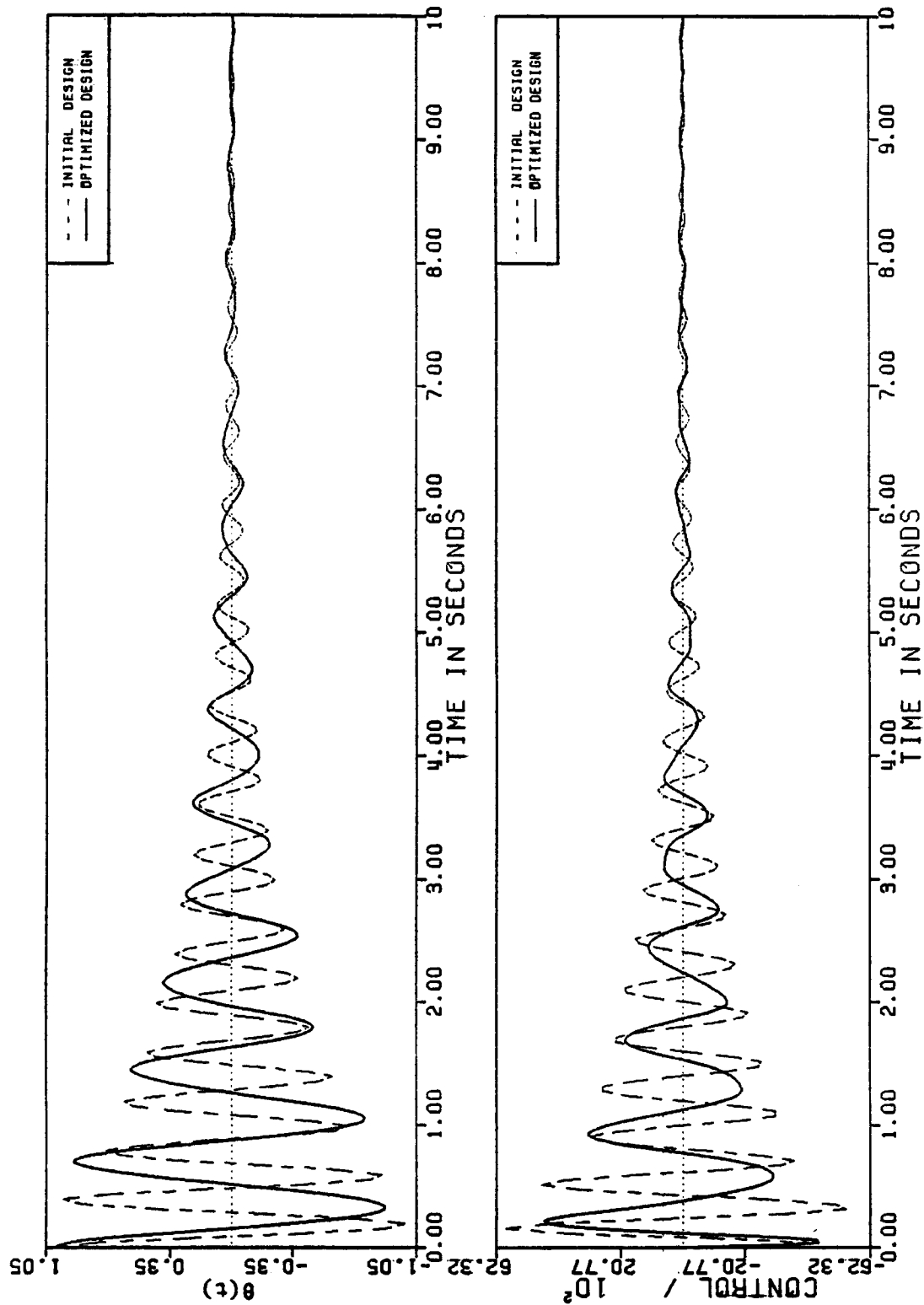


Figure 7-10. Time Histories of the Rigid-Body Angle and the Hub Torque. 11-mode plant, 4-mode compensator, I.C. of the structure = 4th mode, I.C. of the estimator = 0.

7.2.2 Five-Mode Compensator Example

To demonstrate the trade off between the control objective $J_c(F, G, h)$ and the structural weight $W(h)$ minimization, consider the initial design of Sec. 6.3 for three optimization problems where the objective functions are constructed with $\alpha = 2, 4$ and 6 in (7.1). Since we use the ten element model of the structure, we have 11 structural design variables (the heights of the cross sections at the beam nodes). Also, we have the 1×10 control gain matrix F and the 10×2 estimator gain matrix G , so that there are 30 control design variables. Therefore, we have a total of $11 + 30 = 41$ design variables. The scalar weighting factors and lower bounds and upper bounds in (7.1)-(7.6) are

$$\operatorname{Re}(\lambda_c)_i^u = 0.90 \operatorname{Re}[\lambda_c(F_0, h_0)] \quad i = 1, \dots, 2n, \quad (7.31)$$

$$\operatorname{Re}(\lambda_e)_i^u = -0.40 \quad i = 1, \dots, 2n, \quad (7.32)$$

$$\operatorname{Im}(\lambda_c)_i^l = 0.20 \quad i = 1, \dots, 2n, \quad (7.33)$$

$$\operatorname{Im}(\lambda_e)_i^l = 0.20 \quad i = 1, \dots, 2n, \quad (7.34)$$

$$\gamma_i = \max \left[\frac{1}{|\operatorname{Re}(\lambda_{cl})_i|}, \frac{1}{|\operatorname{Im}(\lambda_{cl})_i|} \right] \quad i = 1, \dots, 4n, \quad (7.35)$$

$$h_i^l = 0.25 \quad i = 1, \dots, n_s, \quad (7.36)$$

$$h_i^u = 3.0 \quad i = 1, \dots, n_s. \quad (7.37)$$

Note that (7.31) indicates that the magnitude of the real part of the controller eigenvalues can decrease by 10% only.

Each of the optimized designs were obtained by using the ADS optimizer (Ref. V2), where the sequential unconstrained minimization technique (SUMT) using the exterior penalty function method, and Broydon-Fletcher-Goldfarb-Shanno (BFGS) variable metric method for unconstrained minimization of pseudo-objective function (created by the exterior penalty function method) were selected, see [V1]. Also, the 41 design variables were scaled by the ADS program, and finite difference gradients were used in the optimization problems. Each of the three optimization problems converges in 1 SUMT iteration which includes fewer than 35 unconstrained minimization (BFGS) iterations. The constraint on the real part of the controller eigenvalues (7.31) and the side constraint corresponding to the height of the cross-section at the last beam node (tip end) are active for all three optimized designs. Table 7-11 shows the numerical values of the control objective functions and the structural weights. In general, larger values of α result in more structural weight and less control objective function reduction. However, there are some exceptions due to the complexity of the numerical optimization and nonlinearity of the objective function. Figure 7-11 shows the initial and the three optimized substructures (beams). The initial substructure is drawn in dashed line and an optimized substructure is drawn in solid line. (Only the portion of a beam over the center-line is shown.)

CASE	α	INITIAL DESIGN			OPTIMIZED DESIGN			ITERATION HISTORY FIGURE
		W	J_c	J	W	J_c	J	
A	2	1.000	10.60	3.000	0.664	3.418	1.651	-
B	4	1.000	10.60	5.000	0.658	6.750	3.267	-
C	6	1.000	10.60	7.000	0.651	7.722	4.635	7-12,7-13

Table 7-11. Control Objective and Structural Weighth of the Initial and Three Optimized Designs with 5-Mode Compensators.

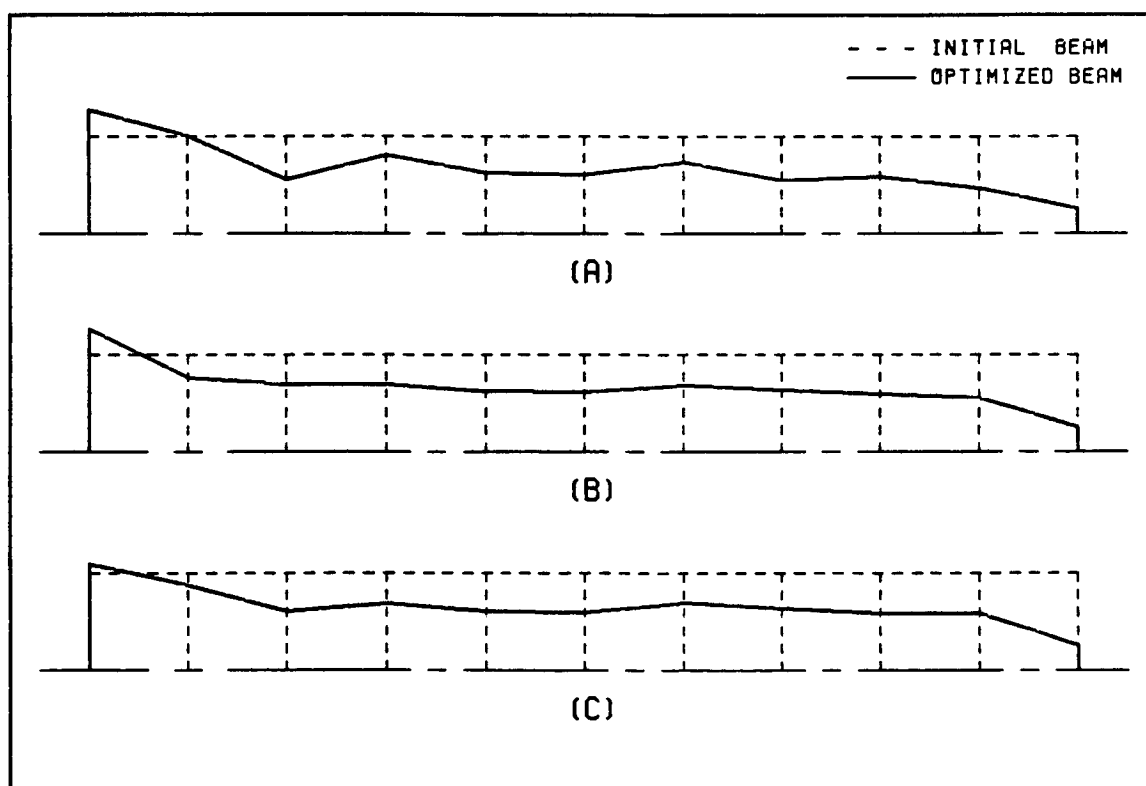


Figure 7-11. The Initial and Three Optimized substructures (Beams). (A) $\alpha = 2$, (B) $\alpha = 4$, (C) $\alpha = 6$. (5-mode compensators.)

To see the effect of first-order closed-loop eigenvalue sensitivity and structural weight optimization on robustness, consider for example Case C ($\alpha=6$) of the three optimized designs. For this case, the optimization converges in 1 SUMT iteration which includes 27 unconstrained minimization (BFGS) iterations. Figure (7-12) shows the unconstrained minimization (BFGS) iteration history of the objective function where $J(F,G,h)$ (normalized with respect to its initial value 7.0) is reduced by 34%. Figure (7-13) shows the unconstrained minimization (BFGS) iteration histories of the control objective function and the structural weight, where $J_c(F,G,h)$ (normalized with respect to its initial value 10.60) is reduced by 27% and $W(h)$ (normalized with respect to its initial value 1.0) is reduced by 35%. Table 7-12 lists the natural frequencies and the structural design variables of the initial and the optimized structures, Table 7-13 lists the control design variables of the initial and the optimized compensators. Figure 7-14 shows the first three flexible mode-shapes of the initial and the optimized structures. In this figure, nodes of the initial structure are marked with squares and nodes of the optimized structure are marked with circles. Note that Fig. 7-12 also shows the increased flexibility of the optimized design due to its significant weight reduction. Table 7-14 and Figure 7-15 show the open-loop and the closed-loop eigenvalues of the initial and the optimized designs. In Figure 7-15, the dashed lines connect the eigenvalues of the initial design and the solid lines connect the eigenvalues of the optimized design. (Only eigenvalues with positive

imaginary parts are plotted.)

Our measure of robustness for a compensator is how much the plant natural frequencies can vary, from their nominal values, before the closed-loop system becomes unstable; i.e., before some eigenvalue of A_{cl} has nonnegative real part. The robustness of the closed-loop eigenvalues was tested by varying the natural frequencies of the plant by a constant percentage times a variation factor (1,0 or -1 for each natural frequency), while maintaining the original damping of the plant and the original natural frequencies in the compensator. Tables 6-6 and 7-15 present the robustness test results of the initial and the optimized closed-loop designs. In each of the robustness tables, each row represents nine closed-loop designs where the natural frequencies of the plant were perturbed by a percentage (indicated by a percentage sign %) times a variation factor for each natural frequency (listed in the left portion of the tables). In these tables, "." indicates a stable design and "x" indicates an unstable design. For the initial plant and compensator, Table 6-6 shows that the closed-loop design becomes unstable for 20% variations in plant frequencies. For the optimized plant and compensator, Table 7-15 shows that the closed-loop design becomes unstable for 60% variations in plant frequencies. Note that we have improved the robustness of the closed-loop system by factor of three and at the same time reduced the weight of the structure by 35%. Note also that the optimized compensator results in an unstable closed-loop system only when the variations in plant natural frequencies are such that the first and

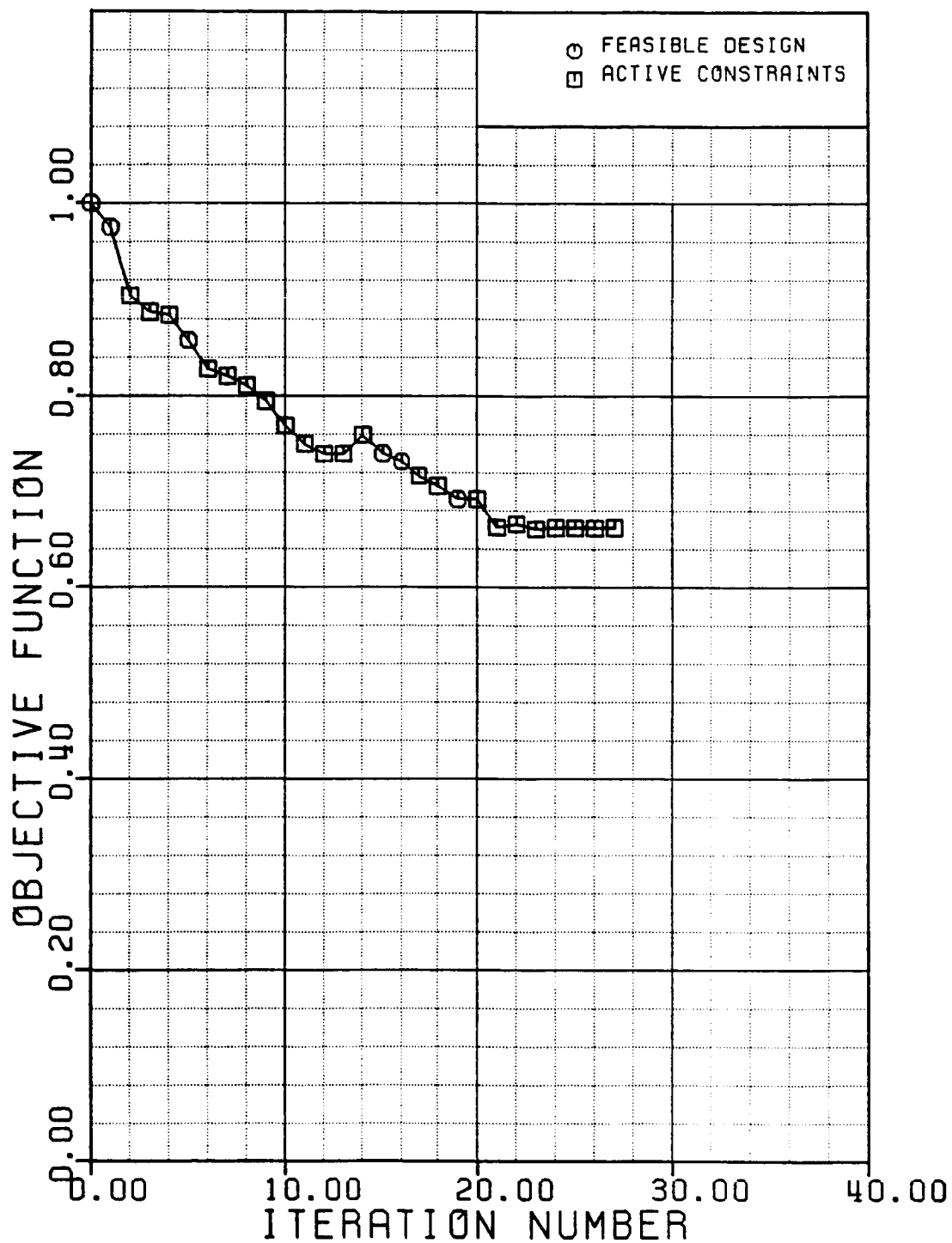


Figure 7-12 Unconstrained Minimization (BFGS) Iteration History of the Objective Function. (5-mode compensator.)

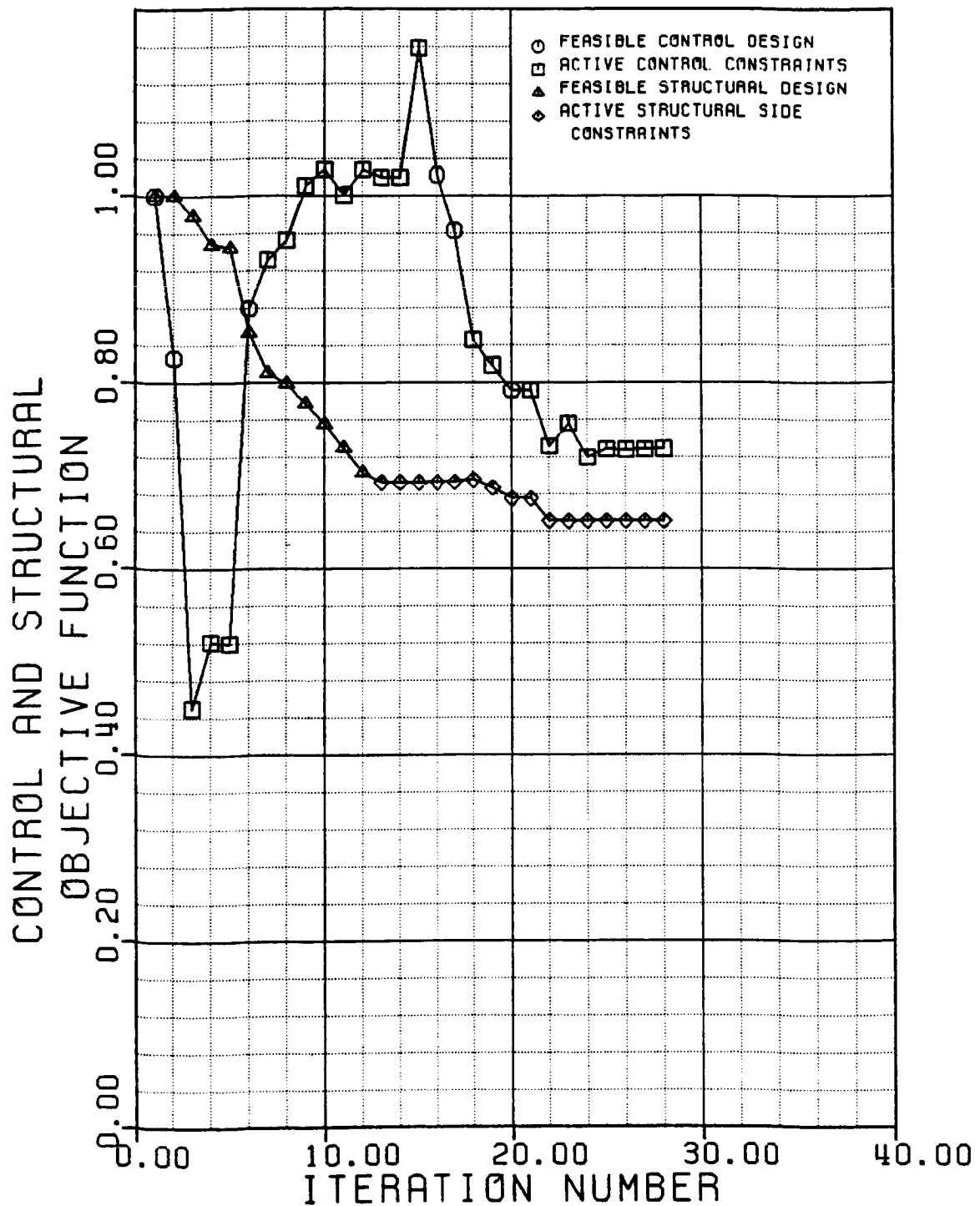


Figure 7-13. Unconstrained Minimization (BFGS) Iteration Histories of the Control and the Structural Objective Functions. (5-mode compensator.)

	INITIAL DESIGN		OPTIMIZED DESIGN	
j	ω_j	h_j	ω_j	h_j
1	0.0	1.0000	0.0	1.0910
2	2.1583	1.0000	1.3080	0.8750
3	7.1826	1.0000	4.7698	0.5979
4	15.568	1.0000	10.739	0.6823
5	29.010	1.0000	20.427	0.6038
6	47.901	1.0000	32.388	0.5889
7	72.399	1.0000	48.014	0.6946
8	103.14	1.0000	69.172	0.6335
9	141.47	1.0000	95.028	0.5796
10	188.23	1.0000	132.00	0.5842
11	235.33	1.0000	166.16	0.2500

Table 7-12 Natural Frequencies and Structural Design Variables of the Initial and the Optimized Structures. (5-mode compensators.)

the second, or the first and the third natural frequencies cross over. For each of the above robustness tests, there are 720 variations (see Eqn. 6.32). For the initial plant and compensator, 226 variations out of 720 result in unstable designs and for the optimized plant and compensator, 59 variations out of 720 result in unstable designs.

In investigating robustness with respect to unmodeled modes, we connected the initial five-mode compensator to the initial eleven-mode

	INITIAL DESIGN			OPTIMIZED DESIGN		
j	F_{1j}	G_{j1}	G_{j2}	F_{1j}	G_{j1}	G_{j2}
1	89.443	247.57	0.7453	86.638	247.34	0.8082
2	-47.212	-0.0360	9.9207	-22.927	-0.0360	9.8931
3	-32.144	-0.0251	-0.3027	-99.311	-0.0253	-0.3135
4	-56.023	-0.0028	0.0944	-11.910	-0.0041	0.0265
5	-90.007	-0.0131	0.7929	-316.34	-0.0111	0.7235
6	181.06	163.33	0.5014	180.42	163.22	0.3514
7	-24.205	-0.0593	27.796	-23.557	-0.0542	27.792
8	-12.242	-0.3045	35.710	-12.146	-0.3023	35.704
9	-15.444	-0.3024	34.285	-19.401	-0.3005	34.285
10	-17.147	-1.2148	136.14	-26.571	-1.2141	136.14

Table 7-13. Controller and Observer Gains of the Initial and the Optimized 5-Mode Compensators.

plant and the optimized five-mode compensator to the optimized eleven-mode plant, and performed the robustness test by varying first three natural frequencies of the plants by a constant percentage times a variation factor (1,0 or -1 for each natural frequency), while maintaining the original damping of each plant and the original natural frequencies in each compensator. For the initial plant and compensator, the results of the robustness test are identical to those of Table 6-6. For the optimized plant and compensator, the results of

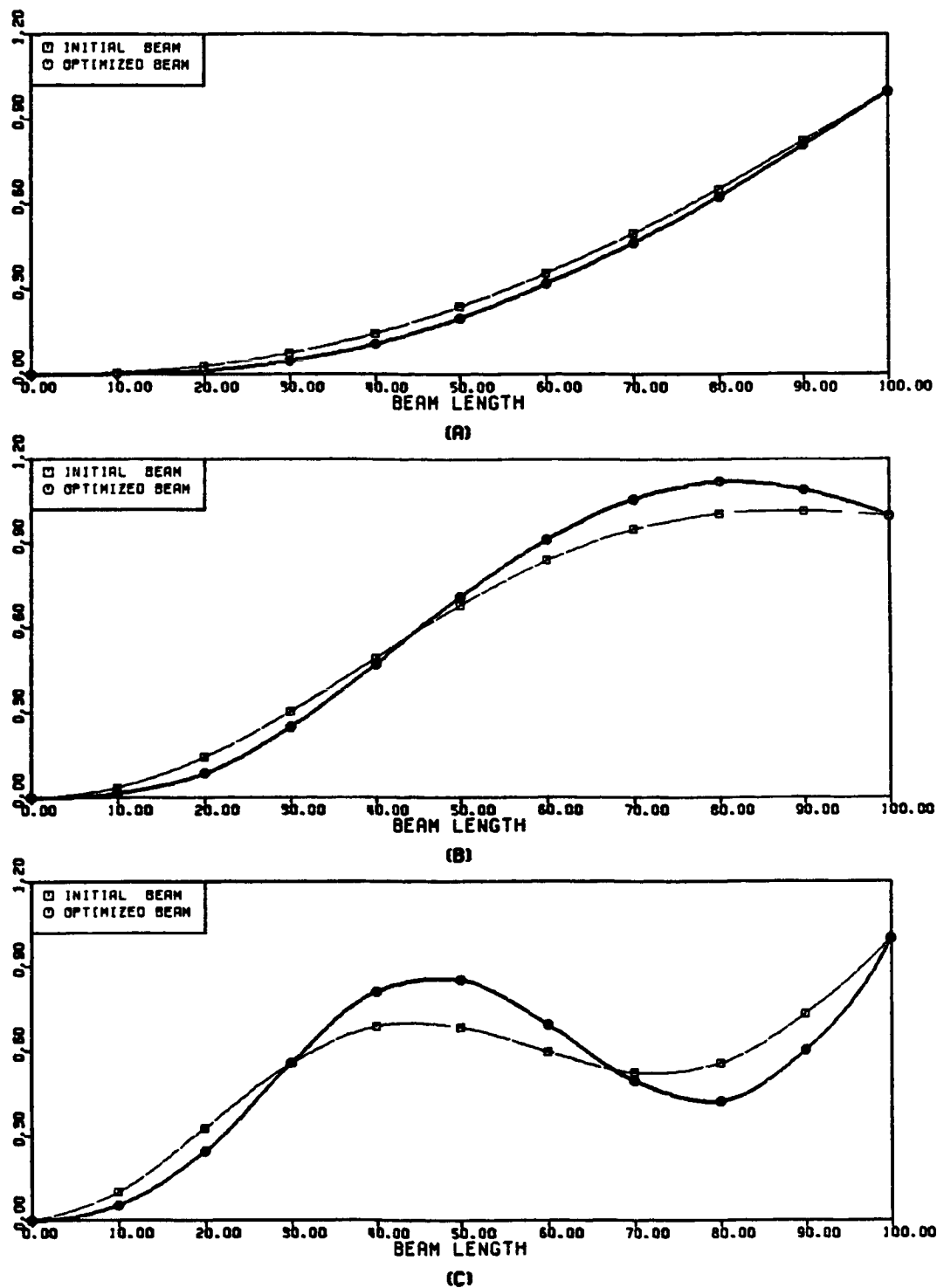


Figure 7-14. First Three Flexible Mode-Shapes of the Initial and The Optimized structures. (A) 1st Mode, (B) 2nd Mode, (C) 3rd Mode. (5-mode compensator.)

OPEN-LOOP EIGENVALUES	CLOSED-LOOP EIGENVALUES	
	CONTROLLER	ESTIMATOR
0.0	-0.5415±i0.5580	-0.9598±i0.5876
0.0		
-0.0023±i2.1583	-0.5721±i2.2293	-2.5932±i5.0472
-0.0258±i7.1826	-0.3937±i7.1932	-8.0933±i12.011
-0.1212±i15.567	-0.5001±i15.575	-3.9348±i15.290
-0.4208±i29.007	-0.7097±i29.012	-8.5054±i29.711

a) Initial Design.

OPEN-LOOP EIGENVALUES	CLOSED-LOOP EIGENVALUES	
	CONTROLLER	ESTIMATOR
0.0	-0.4874±i0.7234	-1.0192±i0.5535
0.0		
-0.0009±i1.3080	-0.5269±i1.0556	-1.0520±i3.2532
-0.0114±i4.7698	-0.4824±i5.0990	-1.9676±i9.1562
-0.0577±i10.739	-0.4638±i10.642	-4.1895±i14.508
-0.2086±i20.426	-0.7197±i20.586	-16.985±i20.570

b) Optimized Design.

Table 7-14. Open-Loop and Closed-Loop Eigenvalues of the Initial and the Optimized Designs of 5-Mode Compensators.

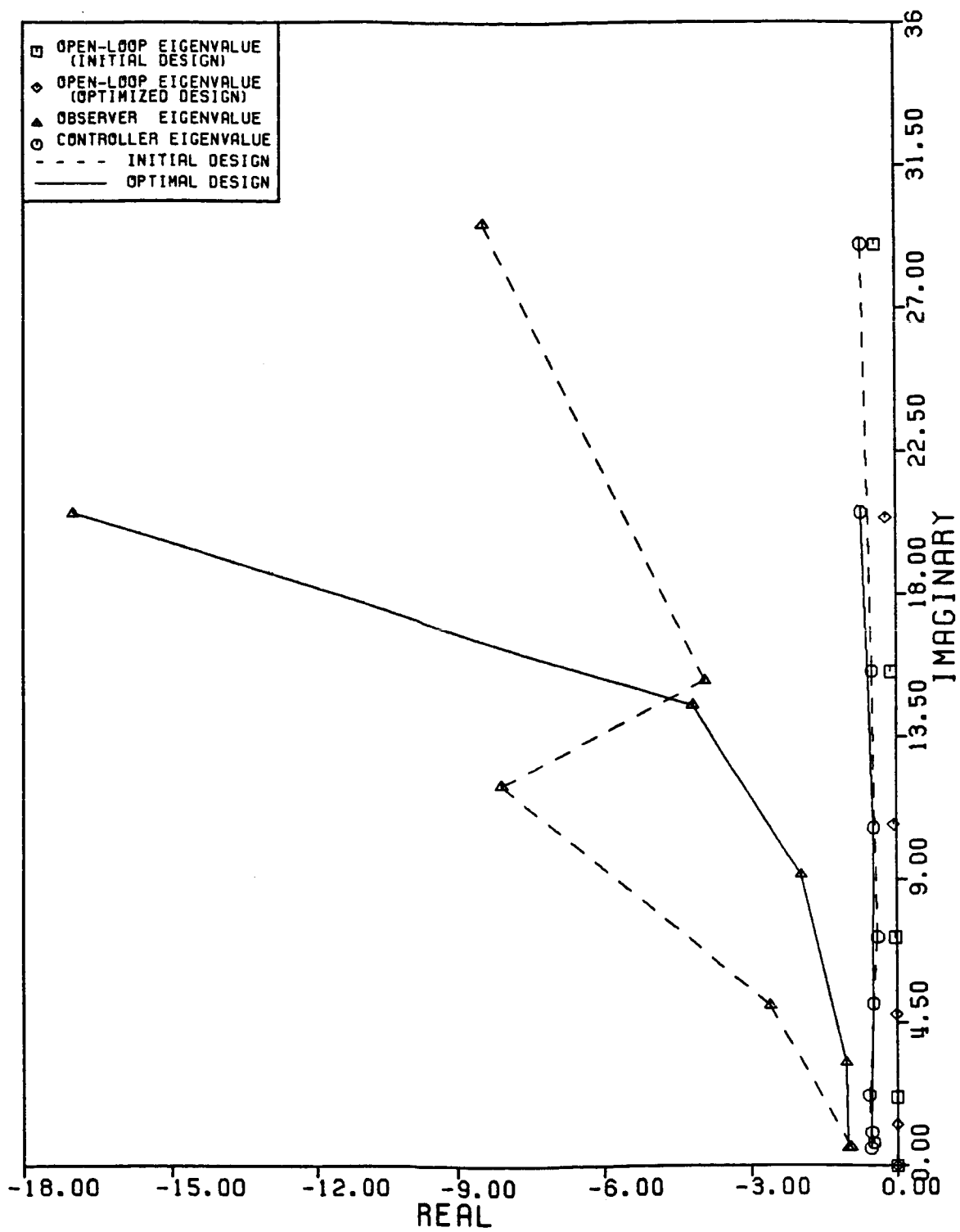


Figure 7-15. Open-Loop and Closed-Loop Eigenvalues of the Initial and the Optimized Designs of 5-Mode Compensators.

NATURAL FREQUENCY VARIATION FACTORS				VARIATION PERCENTAGE								
ω_2	ω_3	ω_4	ω_5	10%	20%	30%	40%	50%	60%	70%	80%	90%
1	1	1	1
-1	1	1	1
1	-1	1	1	x	x	x	x
1	1	-1	1
1	1	1	-1
1	1	-1	-1
1	-1	1	-1	x	x	x	x
1	-1	-1	1	x	x	x	x
-1	-1	1	1
-1	1	-1	1
-1	1	1	-1
-1	-1	-1	-1
1	-1	-1	-1	x	x	x	x
-1	1	-1	-1
-1	-1	1	-1
-1	-1	-1	1
0	1	1	1
0	-1	1	1	x	x
0	1	-1	1	x
0	1	1	-1
0	-1	-1	-1	x	x
0	1	-1	-1	x
0	-1	1	-1	x	x
0	-1	-1	1	x	x
1	0	1	1
-1	0	1	1
1	0	-1	1
1	0	1	-1
-1	0	-1	-1
1	0	-1	-1
-1	0	1	-1
-1	0	-1	1
1	1	0	1
-1	1	0	1
1	-1	0	1	x	x	x	x
1	1	0	-1
-1	-1	0	-1
1	-1	0	-1	x	x	x	x
-1	1	0	-1
-1	-1	0	1

Table 7-15. Robustness Test Results of the Optimized 5-Mode Compensator.

NATURAL FREQUENCY VARIATION FACTORS				VARIATION PERCENTAGE								
ω_2	ω_3	ω_4	ω_5	10%	20%	30%	40%	50%	60%	70%	80%	90%
1	1	1	0
-1	1	1	0
1	-1	1	0	x	x	x	x
1	1	-1	0
-1	-1	-1	0
1	-1	-1	0	x	x	x	x
-1	1	-1	0
-1	-1	1	0
0	0	1	1
0	0	1	-1
0	0	-1	-1
0	0	-1	1	x
0	1	0	1
0	1	0	-1
0	-1	0	-1	x	x
0	-1	0	1	x	x
0	1	1	0
0	1	-1	0	x
0	-1	-1	0	x	x
0	-1	1	0	x	x
1	0	1	0
1	0	-1	0
-1	0	-1	0
-1	0	1	0
1	0	0	1
1	0	0	-1
-1	0	0	-1
-1	0	0	1
1	1	0	0
1	-1	0	0	x	x	x	x
-1	-1	0	0
-1	1	0	0
1	0	0	0
0	1	0	0
0	0	1	0
0	0	0	1
-1	0	0	0
0	-1	0	0	x	x
0	0	-1	0	x
0	0	0	-1

Table 7-15. (Cont.) Robustness Test Results of the Optimized 5-Mode Compensator.

the robustness test are identical to the results in Table 7-15. These robustness tests indicate that for this example the robustness of the initial and the optimized designs are insensitive to the unmodeled modes, which is partially due to well separated natural frequencies of the eleven-mode plant.

In comparing the performance of the initial and the optimized compensators, we use the performance index in (6.33) where

$$J_p = J_x + J_u. \quad (7.38)$$

For the initial plant and compensator, Table 6-9 shows the performance of the five-mode compensator connected to the five-mode plant, and Table 6-10 shows the performance of the five-mode compensator connected to the eleven-mode plant. These tables indicate that the performance of the initial compensator is insensitive to the unmodeled modes of the initial plant.

For the optimized plant and compensator, Table 7-16 shows the performance of the five-mode compensator connected to the five-mode plant, and Table 7-17 shows the performance of the five-mode compensator connected to the eleven-mode plant. These tables indicate that the performance of the optimized compensator is insensitive to the unmodeled modes of the optimized plant.

Figures (7-16) - (7-21) show the response of the rigid-body angle $\theta(t)$ and the control $u(t)$ for various initial conditions. (All plots have been scaled such that $\theta(0)=1$.) In each Figure, the dashed lines represent the time histories corresponding to the initial compensator connected to the initial eleven-mode plant, and the solid lines

represent the time histories corresponding to the optimized compensator connected to the optimized eleven-mode plant. (For the initial and the optimized designs, the response curves of the five-mode plants connected to the five-mode compensators coincide with those shown in Figures 7-16 through 7-21.) For the initial design, Figure 7-16 shows that the settling time of the rigid-body angle is 10.05 seconds, which is 3.45 times the period of the first flexible open-loop mode ($T_2=2.91$ seconds). For the optimized design, Figure 7-16 shows that the settling time of the rigid-body angle is 13.15 seconds, which is 2.74 times the period of the first flexible open-loop mode ($T_2=4.80$ seconds). (The settling time is the time required for the response curve to reach and stay within $\pm 5\%$ of its initial value.) Note that the overshoot present in the rigid-body angle response is partially due to the tip mass m_1 which is as heavy as the initial beam; i.e. $m_1 = 1$ slug. Tables 6-10 and 7-17 indicate and Figures 7-16 through 7-21 confirm that there is a significant difference in the performances (value of J_x) of the optimized and the initial designs. This loss of performance is not entirely due to the increased robustness of the closed-loop system but it is mainly due to the significant weight reduction of the structure (35%), and partially due to the more relaxed constraint on the controller eigenvalues, (7.2) and (7.31). In comparing this optimized compensator/structure design with Case C of Section 7.2.1, we see that both designs can tolerate at least 50% variations in their plant natural frequencies.

Also, due to significantly different performance of the 5-mode compensators, we obtain less weight reduction here compared to the 46% structural weight reduction in section 7.2.1

INITIAL CONDITION OF THE STRUCTURE	INITIAL CONDITION OF THE ESTIMATOR	COST $\times 10^{-8}$		
		J_p	J_x	J_u
1st mode	1st mode	3.7502	3.4771	0.2731
1st mode	0	10.6536	9.7981	0.8555
2nd mode	0	0.0938	0.0363	0.0575
3rd mode	0	0.1028	0.0356	0.0672
4th mode	0	0.5475	0.3777	0.1698
5th mode	0	4.2898	3.2714	1.0184

Table 7-16. Performance of the 5-Mode Optimized Compensator Connected to the 5-Mode Optimized Plant for Various Initial Conditions.

INITIAL CONDITION OF THE STRUCTURE	INITIAL CONDITION OF THE ESTIMATOR	COST $\times 10^{-8}$			RESPONSE OF THE RIGID-BODY ANGLE
		J_p	J_x	J_u	
1st mode	1st mode	3.7495	3.4768	0.2727	Fig. 7-16
1st mode	0	10.6481	9.7931	0.8550	Fig. 7-17
2nd mode	0	0.0925	0.0363	0.0562	Fig. 7-18
3rd mode	0	0.1017	0.0356	0.0661	Fig. 7-19
4th mode	0	0.5453	0.3772	0.1681	Fig. 7-20
5th mode	0	4.3171	3.3106	1.0065	Fig. 7-21

Table 7-17. Performance of the 5-Mode Optimized Compensator Connected to the 11-Mode Optimized Plant for Various Initial Conditions.

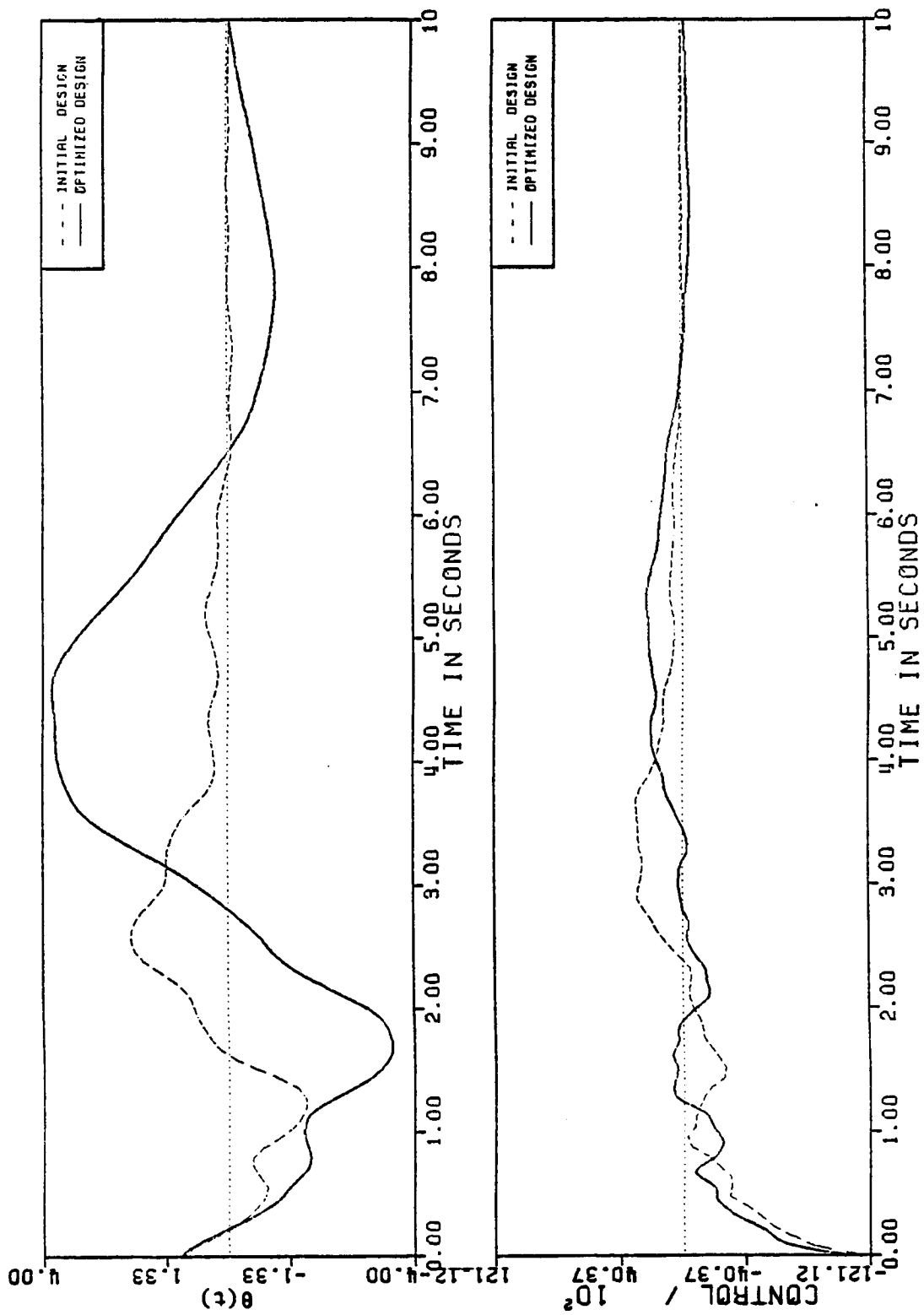


Figure 7-16. Time Histories of the Rigid-Body Angle and the Hub Torque. 11-mode plant, 5-mode compensator, I.C. of the structure = 1st mode, I.C. of the estimator = 1st mode.

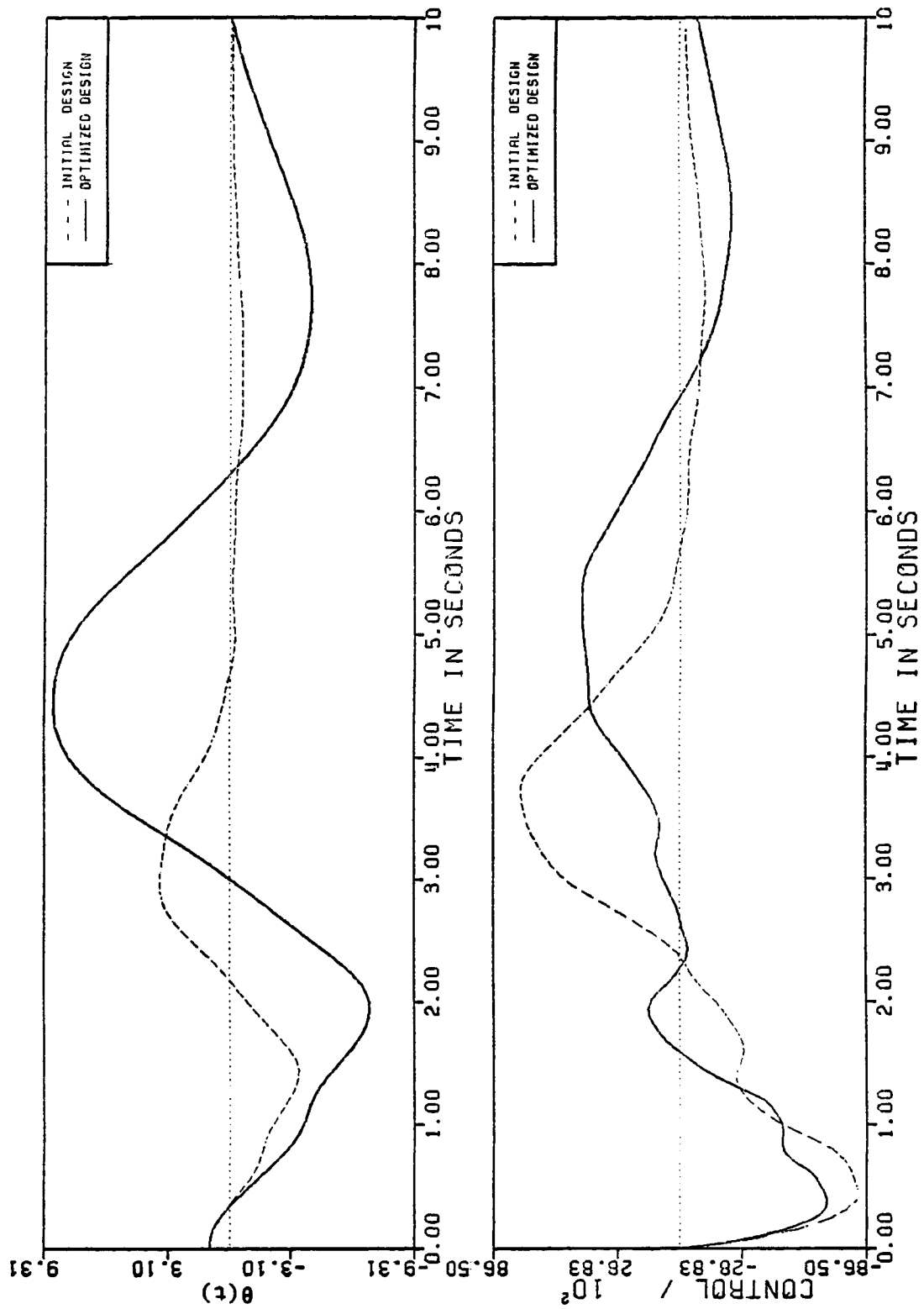


Figure 7-17. Time Histories of the Rigid-Body Angle and the Hub Torque. 11-mode plant, 5-mode compensator, I.C. of the structure = 1st mode, I.C. of the estimator = 0.

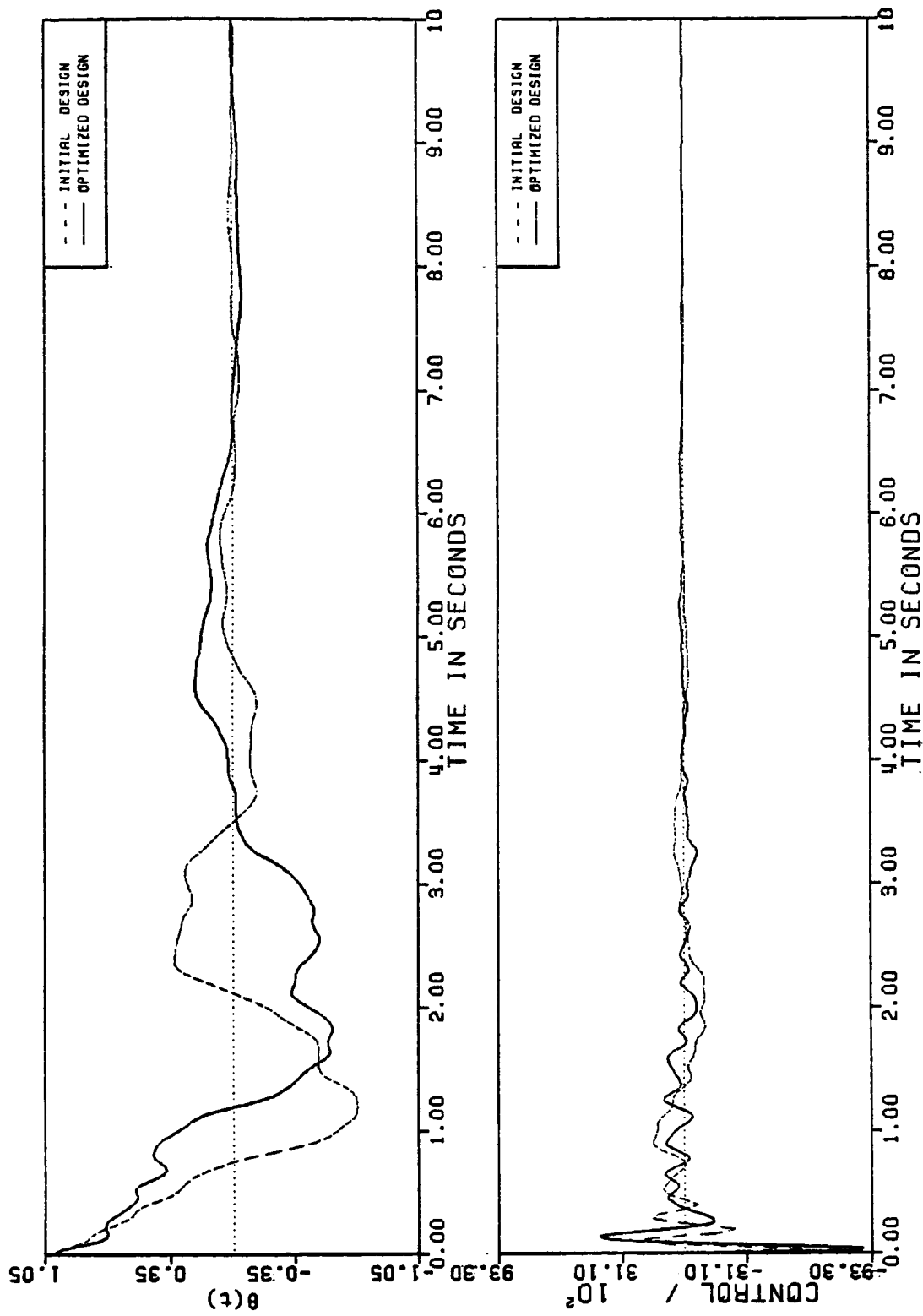


Figure 7-18. Time Histories of the Rigid-Body Angle and the Hub Torque. 11-mode plant, 5-mode compensator, I.C. of the structure = 2nd mode, I.C. of the estimator = 0.

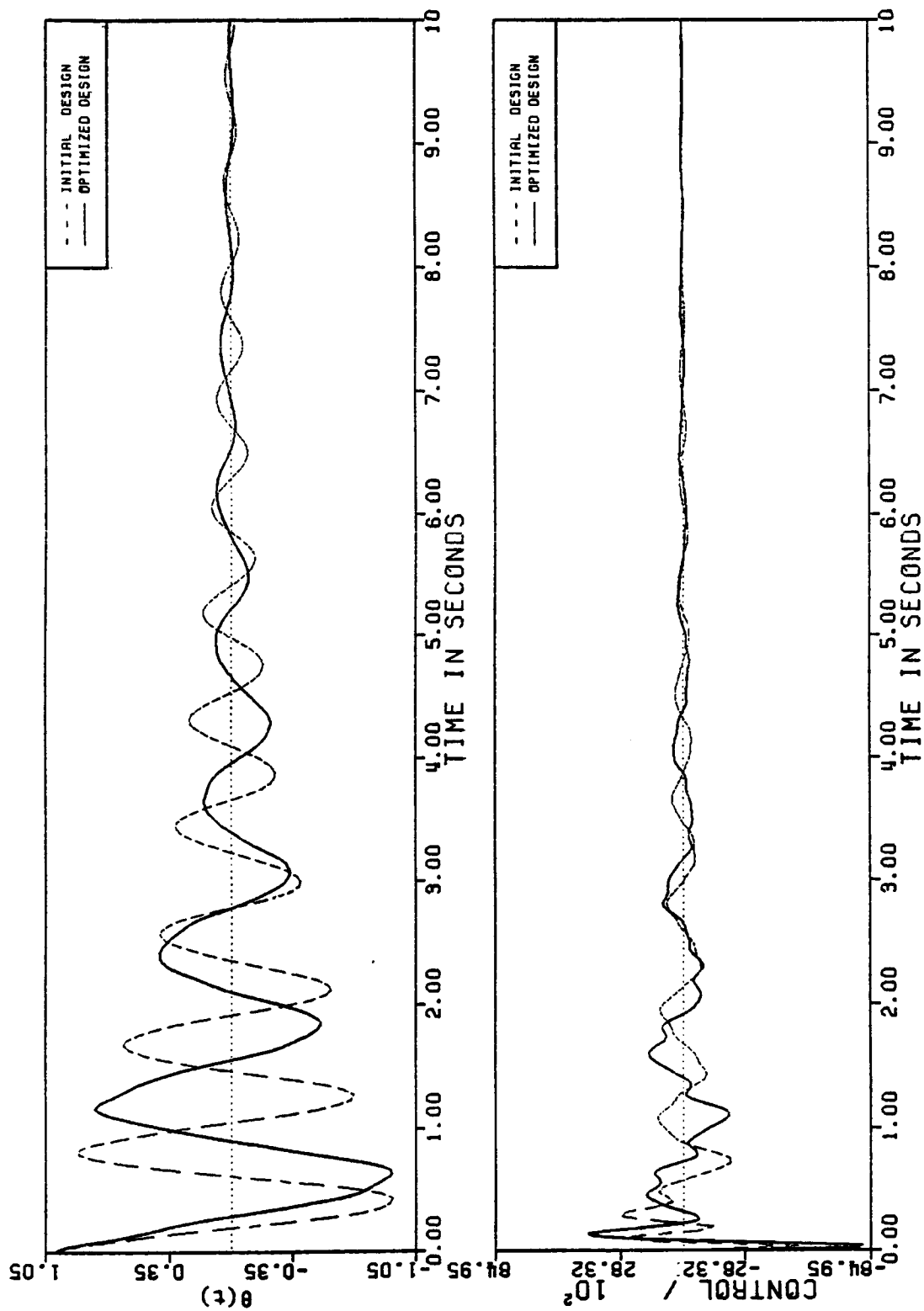


Figure 7-19. Time Histories of the Rigid-Body Angle and the Hub Torque. 11-mode plant, 5-mode compensator, I.C. of the structure = 3rd mode, I.C. of the estimator = 0.

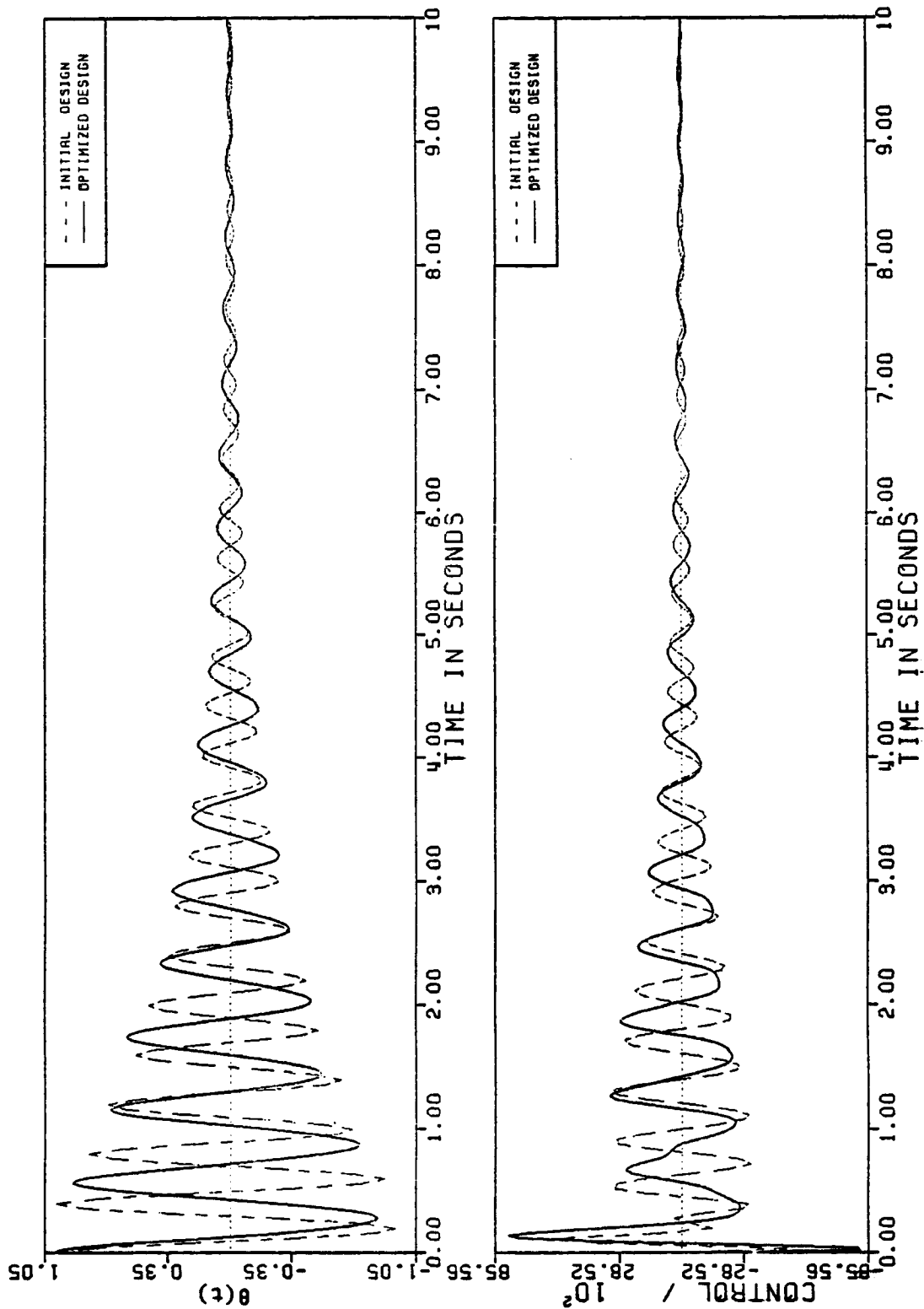


Figure 7-20. Time Histories of the Rigid-Body Angle and the Hub Torque. 11-mode plant, 5-mode compensator, I.C. of the structure = 4th mode, I.C. of the estimator = 0.

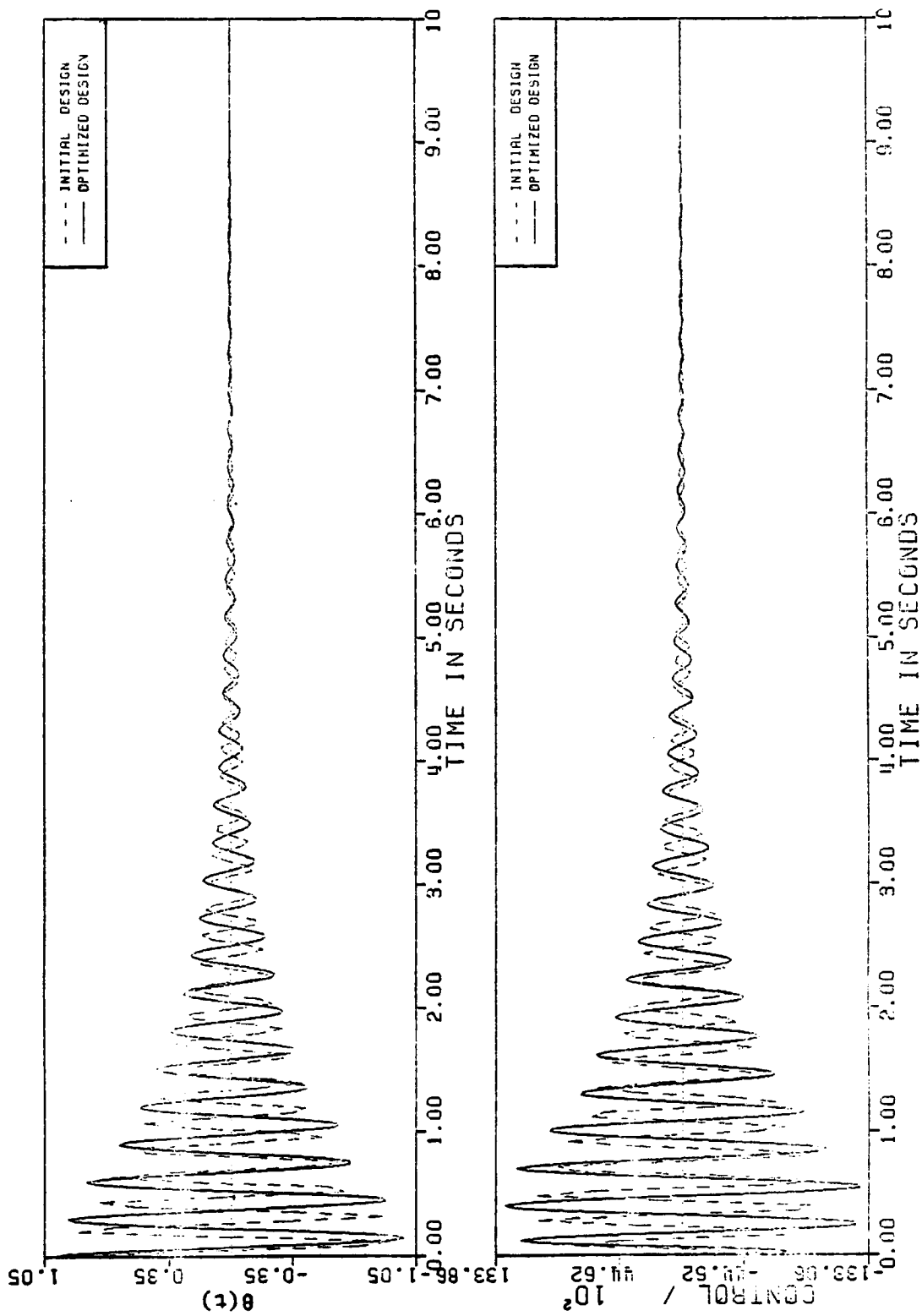


Figure 7-21. Time Histories of the Rigid-Body Angle and the Hub Torque. 11-mode plant, 5-mode compensator, I.C. of the structure = 5th mode, I.C. of the estimator = 0.

Chapter VIII

CONCLUSIONS

The numerical results for the example of Chapter 5 illustrate the significant effect that the closed-loop eigenvalue sensitivity derived in Section 5.1 has on robustness with respect to modeling errors. The results in Section 5.2 suggest and the example confirms that controller and estimator eigenvalues should be separated for a robust design. Almost linearly dependent estimator eigenvectors or controller eigenvectors diminish robustness also.

In the example, we chose to move the estimator eigenvalues to the left of the controller eigenvalues. While such relative placement of controller and estimator eigenvalues is used frequently in compensator design so that the faster decaying estimator error will make the compensator approximate full-state feedback, we have seen no mention in the literature of the relationship demonstrated here between controller/estimator eigenvalue location and robustness. We have found that, to improve robustness by reducing closed-loop eigenvalue sensitivity, the eigenvalue separation may be achieved as well by placing some or all of the controller eigenvalues sufficiently to the left of nearby estimator eigenvalues or, not surprisingly, by separating imaginary parts of eigenvalues. This is important in controlling complex flexible structures, which often have lightly

damped modes along with heavily damped modes, making it impractical to place all estimator eigenvalues to the left of all controller eigenvalues.

For a fixed structure, the numerical results for the example of Chapter 6 demonstrate that first-order sensitivity optimization of the closed-loop eigenvalues can significantly increase the robustness of the initial closed-loop design (LQG). In the example, the robustness of the optimized design is better than the robustness of the full-state feedback initial and optimized designs, and the optimized compensator results in an unstable closed-loop system only when the variations in natural frequencies are such that the first and the second natural frequencies cross over. Although we have improved the robustness of the initial design by a factor of three, there is no significant difference in the performances of the optimized and the initial compensators for the nominal plant parameters.

The numerical results of Sections 7.2.1 and 7.2.2 demonstrate the effectiveness of the first-order sensitivity and structural weight optimization for simultaneously reducing the structural weight and increasing the robustness of the initial LQG compensator/structure designs. For each of these examples, the robustness of the optimized compensator/structure design is better than the robustness of the full-state feedback initial and optimized designs, and the optimized compensator/structure design result in an unstable closed-loop system only when the variations in the plant natural frequencies are such that the first and the second, or the first and the third natural frequencies cross over. As illustrated by these examples, the amount of structural

weight reduction is a strong function of desired performance. In addition, the loss of performance in the optimized compensator/structure designs is not entirely due to the increased robustness (factor of 3), but it is mainly due to the significant weight reduction of the structures. To maintain the high-performance of the initial compensator/structure design, we recommend inclusion of a quadratic performance measure in the objective function of Chapter 7.

REFERENCES

- B1 Bodden, D.S., and Junkins, J.L., "Eigenvalue Optimization Algorithms for Structural/Control Design Iterations," presented in the 1984 American Control Conference, June 6-8, 1984, San Diego, CA, USA.
- G1 Gibson, J.S., Mingori, D.L., Adamian, A. and Jabbari, F., "Approximation of Optimal Infinite Dimensional Compensators For Flexible Structures," Presented at the "Workshop on Identification and Control of Flexible Structures", San Diego, CA, June 4-6, 1984.
- G2 Gibson, J.S., Mingori, D.L., et al, HR Textron Report # 956541 - Final, to JPL, September, 1984.
- G3 Gibson, J.S, and Adamian, A., "A Comparison of Three Approximation Schemes for Optimal Control of Flexible Structures," to appear.
- G4 Gibson, J.S, and Adamian, A., "Approximation Theory for LQG Optimal Control of Flexible Structures," Submitted to SIAM J. Contr. Opt.
- G5 Gibson, J.S, "An Analysis of Optimal Modal Regulation: Convergence and Stability," Vol. 19, No. 5, September 1981, pp. 686-707.

- J1 Junkins, J.L., Bodden, D.S., and Turner, D.J., "A Unified Approach to Structure and Control System Design Iterations," Fourth International Conference on Applied Numerical Modeling, Tainan, Taiwan, Dec. 27-29, 1984.
- K1 Kawakernaak, H. and Sivan, R., "Linear Optimal Control Systems", Wiley Interscience, 1972.
- L1 Lust, R.V., "Control Augmented Structural Synthesis," Ph.D. dissertation, UCLA, 1985.
- L2 Lancaster, P., "On Eigenvalues Of Matrices Dependent on a Parameter," Numerische Mathematik, Vol. 6, No. 5, Dec. 1964, pp. 377-387.,"
- M1 Mingori, D.L., Gibson, J.S., Blelloch, P., and Adamian, A., "Control of a Flexible Space Antenna: A Finite Dimensional Perspective Based on Distributed Parameter Theory," Presented at the "Workshop on Identification and Control of Flexible Structures", San Diego, CA, June 4-6, 1984.
- M2 Meditch, J.S., "Stochastic Optimal Linear Estimation and Control", McGraw-Hill, 1969.
- M3 Manning, R.A., "Control Augmented Structural Synthesis with Transient Response Constraints," Ph.D. dissertation, UCLA, 1986.

- M4 Messac, A., Turner, J., and Soosaar, K., "An Integrated Control and Minimum Mass Structural Optimization Algorithm For Large Space Structures," Presented at the "Workshop on Identification and Control of Flexible Structures", San Diego, CA, June 4-6, 1984.
- N1 Navid, M., "Integrated Structural and Control System Design Optimization for Structures Under Dynamic Loading", Ph.D. dissertation, UCLA, 1986.
- N2 Nelson, R.B., "Simplified Calculation of Eigenvector Derivatives," AIAA Journal, September, 1976.
- P1 Plaut, R.H., and Huseyin, K., "Derivatives of Eigenvalues and Eigenvectors in Non-Self-Adjoint Systems," AIAA Journal, Vol. 11, No. 2, pp. 250-251, Feb. 1973.
- R1 Rosen, I.G., "Spline-based Rayleigh-Ritz Methods for the Approximation of the Natural Modes of Vibration for Flexible Beams with Tip Bodies," to appear in Quarterly of Applied Mathematics.
- S1 Strang, G. and Fix, G.J., "An Analysis of the Finite Element Method", Prentice-Hall, 1973.
- S2 Salama, M., Hamidi, M., and Demsetz, L., "Optimization of Controlled Structures," JPL Workshop on Identification and Control of Space Structures, San Diego, CA, June 1984.

- V1 Vanderplaats, G.N., "Numerical Optimization Techniques For Engineering Design: With Applications", McGraw-hill, 1984.
- V2 Vanderplaats, G.N., "ADS- A Fortran Program for Automated Design Synthesis - User's Manual", Version 1.00, May 1984.
- Z1 Zienkiewicz, O.C., "The Finite Element Method", 3rd Edn., McGraw-hill, 1977.

Appendix A

DERIVATIVES OF EIGENVALUES AND EIGENVECTORS WITH RESPECT TO A PARAMETER

Here we summarize some standard results involving derivatives of the eigenvalues and eigenvectors of a matrix with respect to a parameter. To simplify the discussion while covering almost all applications that interest us, we assume that all eigenvalues are simple. We use the following notation:

A = an $n \times n$ matrix

λ_j ($j = 1, \dots, n$) = an eigenvalue of A

x_j = an eigenvector corresponding to λ_j

y_j = a left eigenvector corresponding to λ_j

Λ = the $n \times n$ diagonal matrix containing the eigenvalues λ_j

X = the $n \times n$ matrix whose j^{th} column is x_j ($j = 1, \dots, n$)

Y = the $n \times n$ matrix whose j^{th} column is y_j ($j = 1, \dots, n$)

A_β = the derivative of A with respect to a parameter β

$\lambda_{j\beta}$ = the derivative of λ_j with respect to β

Λ_β = the $n \times n$ diagonal matrix containing $\lambda_{j\beta}$ ($j = 1, \dots, n$)

$x_{j\beta}$ = the derivative of x_j with respect to β

$\lambda_{j\beta\beta}$ = the second derivative of λ_j with respect to β

I = the $n \times n$ identity matrix

We have then

$$Ax_j = \lambda_j x_j, \quad (A.1)$$

and

$$y_j^T A = \lambda_j y_j^T. \quad (A.2)$$

Also, we assume that the eigenvectors are normalized so that

$$x_j^T x_j = y_j^T x_j = 1. \quad (A.3)$$

From (A.1) - (A.3), it follows that

$$Y^T = X^{-1}. \quad (A.4)$$

The First Derivatives of the Eigenvalues

In the standard way, we differentiate (A.1) with respect to β to obtain

$$A_\beta x_j + [A - I\lambda_j]x_{j\beta} = \lambda_{j\beta} x_j, \quad (A.5)$$

and multiply this equation on the left by y_j^T to obtain

$$\lambda_{j\beta} = y_j^T A_\beta x_j, \quad j = 1, \dots, n. \quad (A.6)$$

In matrix form,

$$\Lambda_\beta = \text{diag}[Y^T A_\beta X]; \quad (A.7)$$

i.e., Λ_β is the diagonal matrix whose diagonal terms are equal to the diagonal terms of $[Y^T A_\beta X]$.

The First Derivatives of the Eigenvectors

From here on, we assume that the eigenvalues are distinct. We move the first term on the right side of (A.5) to the left side and then multiply the equation on the left by X^{-1} to obtain

$$X^{-1}[A - I\lambda_j]XX^{-1}x_{j\beta} = -X^{-1}[A_\beta - I\lambda_{j\beta}]x_j. \quad (\text{A.8})$$

Since

$$X^{-1}AX = \Lambda, \quad (\text{A.9})$$

(A.8) becomes

$$[A - I\lambda_j]X^{-1}x_{j\beta} = -X^{-1}[A_\beta - I\lambda_{j\beta}]x_j. \quad (\text{A.10})$$

Next, we define the n -vector

$$q_{j\beta} = [q_{1j\beta} \ q_{2j\beta} \ \dots \ q_{nj\beta}]^T \quad (\text{A.11})$$

so that

$$x_{j\beta} = Xq_{j\beta}. \quad (\text{A.12})$$

From (A.4), (A.6) and (A.10), we see

$$q_{ij\beta} = \frac{y_i^T A_\beta x_j}{[\lambda_i - \lambda_j]}, \quad i \neq j, \quad (\text{A.13})$$

and, in view of (A.3), we must choose $q_{jj\beta}$ so that

$$x_j^T x_{j\beta} = x_j^T X q_{j\beta} = 0. \quad (\text{A.14})$$

The Second Derivatives of the Eigenvalues

Here, we assume that A is linear in β . Hence,

$$A_{\beta\beta} = 0. \quad (A.15)$$

Differentiating (A.5) with respect to β and multiplying the resulting equation by y_j^T on the left yields

$$\lambda_{j\beta\beta} = 2y_j^T [A_{\beta} - I\lambda_{j\beta}] x_{j\beta} = 2y_j^T [A_{\beta} - I\lambda_{j\beta}] X q_{j\beta}. \quad (A.16)$$

(Recall (A.2), (A.3) and (A.12).) In view of (A.4), (A.6) and (A.13), (A.16) yields

$$\lambda_{j\beta\beta} = 2 \sum_{\substack{i=1 \\ i \neq j}}^n \frac{[y_j^T A_{\beta} x_i][y_i^T A_{\beta} x_j]}{[\lambda_i - \lambda_j]}, \quad j = 1, \dots, n. \quad (A.17)$$

Appendix B

COMPARISON OF ANALYTIC AND FINITE DIFFERENCE GRADIENTS

Here we compare the analytic and the first forward finite difference gradients of the initial design of Section 6.3. For the gradient of the objective function (6.9), Tables B-1 list the partial derivatives with respect to the elements of the 1×10 control gain matrix F and 10×2 estimator gain matrix G . For the gradients of the constraint equations (6.9) - (6.12), Tables B-2 and B-4 list the partial derivatives with respect to the elements of the control gain matrix F only since the controller eigenvalues are independent of the estimator gain matrix G . Tables B-3 and B-5 list the partial derivatives with respect to the elements of the estimator gain matrix G only since the estimator eigenvalues are independent of the control gain matrix F . In these tables, design variables 1-10 correspond to the elements of the control gain matrix F ($F(1,1)=\text{D.V. number 1}$, $F(1,10)=\text{D.V. number 10}$), design variables 11-20 correspond to the first column of the estimator gain matrix G which are related to the rigid-body angle $\theta(t)$ measurement ($G(1,1)=\text{D.V. number 11}$, $G(10,1)=\text{D.V. number 20}$), and design variables 21-30 correspond to the second column of the estimator gain matrix G which are related to the displacement of the point mass m_1 , $w(t,l)$ measurement ($G(1,2)=\text{D.V. number 21}$, $G(10,2)=\text{D.V. number 30}$). Also, FDCH indicates the relative finite difference step when calculating gradients, and 0.0 indicates less than 10^{-6} , see [V2].

When we use the unscaled design variables in the optimization problem of Sec. 6.3 (with Method of Feasible Directions), analytic and finite difference gradients yield similar optimized designs. However, when we use the scaled design variables in the optimization problem of Sec. 6.3 (with Method of Feasible Directions), analytic gradients cause the violation of the constraint equations (6.10) and (6.12) due to the truncation errors shown in Tables B-3 and B-5.

DESIGN VARIABLE NUMBER	FINITE DIFFERENCE GRADIENT		ANALYTIC GRADIENT
	FDCH = 0.01	FDCH = 0.001	
1	0.02284	0.02297	0.02300
2	-0.06532	-0.06541	-0.06540
3	0.06289	0.06275	0.06281
4	0.01945	0.01936	0.01942
5	0.00487	0.00480	0.00487
6	0.01201	0.01244	0.01250
7	-0.21456	-0.21475	-0.21465
8	0.04299	0.04026	0.04057
9	0.03427	0.03388	0.03407
10	0.11104	0.11055	0.11079
11	0.01186	0.01167	0.00737
12	-0.00332	-0.00474	-0.00285
13	0.00758	0.0	0.01028
14	0.00758	0.0	0.01239
15	0.0	0.0	0.00106
16	0.00253	0.00227	0.00678
17	-0.00047	-0.00474	-0.00037
18	0.0	0.0	0.00112
19	0.0	0.0	0.00037
20	0.0	0.0	0.00010
21	-0.44261	-0.44318	-0.44267
22	0.53198	0.52815	0.52885
23	-0.11977	-0.11743	-0.11649
24	-0.99714	-1.00000	-0.99642
25	0.27351	0.26777	0.27352
26	-0.65388	-0.65501	-0.65491
27	0.06828	0.06684	0.06679
28	-0.16013	-0.16642	-0.16711
29	-0.05191	-0.05247	-0.05256
30	-0.01320	-0.01300	-0.01298

Table B-1. Analytic and Finite Difference Gradients of the Objective Function (6.8).

DESIGN VARIABLE NUMBER	FINITE DIFFERENCE GRADIENT		ANALYTIC GRADIENT
	FDCH = 0.01	FDCH = 0.001	
1	-0.00203	-0.00196	-0.00202
2	0.01045	0.01037	0.01048
3	0.04233	0.04244	0.04229
4	-0.00331	-0.00312	-0.00328
5	-0.00054	0.0	-0.00055
6	0.00344	0.00348	0.00341
7	-0.01676	-0.01734	-0.01693
8	0.99857	1.00000	0.99864
9	0.00883	0.00906	0.00881
10	0.00143	0.0	0.00139

Table B-2. Analytic and Finite Difference Gradients of the Constraint Equation (6.9).

DESIGN VARIABLE NUMBER	FINITE DIFFERENCE GRADIENT		ANALYTIC GRADIENT
	FDCH = 0.01	FDCH = 0.001	
11	-1.00000	-0.99961	-0.99997
12	0.0	0.0	-0.00219
13	0.0	0.0	0.03735
14	0.0	0.0	0.00279
15	0.0	0.0	0.00047
16	0.0	0.0	0.00000
17	0.0	0.0	0.00177
18	0.0	0.0	-0.03048
19	0.0	0.0	-0.00273
20	0.0	0.0	-0.00112
21	0.0	0.0	-0.00301
22	0.0	0.0	-0.00001
23	0.0	0.0	0.00011
24	0.0	0.0	0.00001
25	0.0	0.0	0.00000
26	0.0	0.0	0.00000
27	0.0	0.0	0.00001
28	0.0	0.0	-0.00009
29	0.0	0.0	-0.00001
30	0.0	0.0	-0.00000

Table B-3. Analytic and Finite Difference Gradients of the Constraint Equation (6.10).

DESIGN VARIABLE NUMBER	FINITE DIFFERENCE GRADIENT		ANALYTIC GRADIENT
	FDCH = 0.01	FDCH = 0.001	
1	-0.99434	-0.99881	-1.00000
2	-0.02778	-0.02925	-0.02918
3	-0.01418	-0.01289	-0.01429
4	-0.00271	0.0	-0.00270
5	-0.00046	0.0	-0.00054
6	0.46823	0.45985	0.45924
7	0.35882	0.35938	0.35966
8	0.05527	0.05640	0.05556
9	0.00983	0.0	0.01003
10	0.00242	0.0	0.00200

Table B-4. Analytic and Finite Difference Gradients of the Constraint Equation (6.11).

DESIGN VARIABLE NUMBER	FINITE DIFFERENCE GRADIENT		ANALYTIC GRADIENT
	FDCH = 0.01	FDCH = 0.001	
11	0.97789	0.96165	0.95976
12	0.0	0.0	-0.00014
13	0.0	0.0	0.00174
14	0.0	0.0	0.00034
15	0.0	0.0	0.00035
16	-0.99094	-0.99917	-1.00000
17	0.0	0.0	-0.00050
18	0.0	0.0	0.00967
19	0.0	0.0	0.00084
20	0.0	0.0	0.00034
21	0.0	0.0	0.00288
22	0.0	0.0	-0.00000
23	0.0	0.0	0.00001
24	0.0	0.0	0.00000
25	0.0	0.0	0.00000
26	0.0	0.0	-0.00301
27	0.0	0.0	-0.00000
28	0.0	0.0	0.00003
29	0.0	0.0	0.00000
30	0.0	0.0	0.00000

Table B-5. Analytic and Finite Difference Gradients of the Constraint Equation (6.12).